CHEMICAL REVIEWS

REVIEW

pubs.acs.org/CR

Luminescent Functional Metal–Organic Frameworks

Yuanjing Cui,[†,‡] Yanfeng Yue,[‡] Guodong Qian,[*,†] and Banglin Chen[*,‡]

[†]State Key Laboratory of Silicon Materials, Department of Materials Science and Engineering, Zhejiang University, Hangzhou 310027, China

[‡]Department of Chemistry, University of Texas at San Antonio, San Antonio, Texas 78249-0698, United States

CONTENTS

1. INTRODUCTION

Traditional inorganic and organic luminescent materials have been extensively explored and realized for their diverse functionalities and applications in lighting, display, sensing, and optical devices.[1−4] In fact, some inorganic luminescent materials, for example, $BaMgAl_{10}O_{17}:Eu^{2+}$ and $GdMgB_5O_{10}:Ce^{3+}$, Tb^{3+}, have been commercially utilized for blue and green luminescent lamps, respectively. Their unique functionalities are attributed to the narrow emission and high color purity generated from the rare-earth ions. A number of factors such as the atomic structure, homogeneity in composition, particle size, defect, microstructure, and interface might affect the luminescent properties of inorganic luminescent materials. One of the most famous examples is the particle size-dependent luminescence of CdS nanoparticles whose emitted light can be tuned from green to red simply by tuning the particle size. The interest in organic luminescent materials has been mainly motivated by their applications in organic light emitting diodes (OLEDs) in which a thin film of a luminescent organic material needs to be incorporated between two conductors for such electronic devices.[5−7] Since the invention of OLED device in 1980, thousands of different n-type and p-type organic luminescent materials have been emerging for this very important application.

To assemble both inorganic and organic components into metal–organic frameworks (MOFs), also known as coordination polymers (CPs) or coordination networks, the new type of organic–inorganic hybrid materials is certainly very promising as a multifunctional luminescent material,[8−20] because both the inorganic and the organic moieties can provide the platforms to generate luminescence, while metal–ligand charge transfer related luminescence within MOFs can add another dimensional luminescent functionalities. Furthermore, some guest molecules within MOFs can also emit and/or induce luminescence. Based on the ISI Web of Science (retrieved March, 2011), 12 717 MOFs (CPs were also included in this case) have been reported in which 1337 of them are luminescent (about 10%). There is an increasing trend in the exploration and discovery of functional luminescent MOFs. Studies on luminescent MOFs up to now mainly include investigating the fundamental syntheses and luminescent properties of MOFs; creating MOFs with tunable luminescence for application in light-emitting and display devices; using luminescence of MOFs to probe local environment, structure, and guest species; and developing multifunctional MOFs combining luminescence, magnetism, and biocompatibility for biomedical application. The permanent porosity with some luminescent MOFs has enabled their reversible storage and release of guest substrates and provided the hosts for their differential recognitions with sensing species, thus distinguishing porous luminescent

Special Issue: 2012 Metal-Organic Frameworks

Received: March 30, 2011
Published: June 21, 2011

MOFs from the traditional inorganic and organic luminescent materials in terms of their multifunctionalities. The MOF approach can also offer a variety of other attractive characteristics such as the straightforward syntheses, predictable structures and porosities, nanoscale processability, and collaborative properties to develop luminescent functional MOF materials.

The aim of this Review is to give a comprehensive overview of the different types of luminescent MOFs, particularly those with interesting and important applications. The definition of MOFs is interpreted rather broadly in this Review, so some nonporous coordination polymers will be also included. The literature has been updated to March 2011.

2. ATTRACTIVE CHARACTERISTICS OF THE MOF APPROACH TO CONSTRUCT LUMINESCENT MATERIALS

2.1. Straightforward Syntheses

Initial syntheses of coordination polymers/metal−organic frameworks were realized by the diffusion technique in which the solution containing metal salts was slowly diffused into the solution containing organic linkers such as 4,4-bipyridyl and/or the weak bases such as triethylamine were slowly diffused into the solution containing metal salt and bridging organic carboxylic acid.[21] Such a synthesis approach is very time-consuming while the yield is typically low. In fact, the yield to synthesize MOF-5 in the first published paper is only about 5%.[21] Hydrothermal syntheses of MOFs have been feasible to those reaction systems in which organic linkers can be partially soluble in water at higher temperature. The implementation of solvothermal syntheses by making use of organic solvents to readily dissolve organic linkers, as exemplified in the synthesis of MOF-14 in 2001, has facilitated the syntheses of crystalline MOF materials significantly.[22] Generally speaking, heating the mixture containing inorganic salts and organic linkers in certain types of solvents (DMF is the most popular solvent) at a certain temperature (60−120 °C) for several hours to 2 days can readily lead to crystalline MOFs for structure characterization and property exploration. The simple and straightforward syntheses of MOFs, to some of the extent, have allowed many chemists and materials scientists readily to start their research programs in such a very active research field.[23−27] The solvothermal synthesis approach has also enabled the exploration of a combinatorial approach to screen and discover new MOF materials within a very short period of time, as exemplified in the combinatorial syntheses of a series of zeolitic imidazole frameworks (ZIFs, a special subclass of MOFs).[28−33] BASF has even been able to produce and commercialize some prototypical MOFs in large scale.

Recently, some alternative while still straightforward syntheses of MOFs have been realized, including mechanochemical solid-state grinding and liquid-assisted grinding, and sonochemical and microwave-assisted syntheses. In mechanochemical syntheses, a mixture of organic linkers and metal salts is ground together in a mechanical ball mill to yield the MOFs. As compared to solvothermal syntheses, the obvious advantage of mechanochemical syntheses is the possibility for us not to use organic solvents. In addition, large amounts of MOF materials can be easily produced. For example, Klimakow et al. carried out the mechanochemical syntheses of the intensively studied MOFs HKUST-1 ($Cu_3(BTC)_2$, BTC = 1,3,5-benzenetricarboxylate) and MOF-14 ($Cu_3(BTB)_2$, BTB = 4,4′,4″-benzenetribenzoate).[34] The obtained MOFs by such mechanochemical syntheses exhibit high surface areas, which are comparable to the highest given values in the literature for the respective MOFs. Grinding of the copper iodide with 1,4-diazabicyclo[2.2.2]octane (DABCO) or piperazine in the presence of a catalytic amount of different solvents produced luminescent MOFs $Cu_2I_2(DABCO)_2$, $Cu_2I_2(piperazine)_2$, and several others.[35] Yuan et al. demonstrated the ability of liquid-assisted grinding (LAG) to construct different MOFs from the same set of reactants.[36] By grinding 1,4-benzenedicarboxylic acid with ZnO or basic zinc carbonate $[ZnCO_3]_2\cdot[Zn(OH)_2]_3$ in the presence of a small amount of solvent (H_2O, MeOH, or DMF), three MOFs $Zn(1,4\text{-BDC})(H_2O)_2$, $Zn(1,4\text{-BDC})(H_2O)\cdot DMF$, and $Zn(1,4\text{-BDC})(H_2O)$ with one-, two-, and three-dimensional connectivity are prepared, respectively. Friščić et al. introduced an improved mechanochemical approach, denoted as ion- and liquid-assisted grinding (ILAG) syntheses, to synthesize MOFs.[37] The construction of MOFs is accelerated and directed by small amounts of accessory salts in which nitrate and sulfate salts induce the formation of MOFs with tetragonal and hexagonal structure, respectively.[37]

Sonochemistry has been recently explored by Son et al. in the synthesis of the MOF-5 from solution of zinc nitrate and terephthalic acid.[38] As compared to conventional solvothermal syntheses, the sonochemistry method can lead to homogeneous nucleation and short crystallization time. Sonochemical syntheses in 1-methyl-2-pyrrolidone (NMP) produced high-quality MOF-5 crystals (5−25 μm) whose physicochemical properties are comparable to those prepared by conventional solvothermal syntheses. Similarly, high-quality MOF-177 crystals, $Zn_4O(BTB)_2$ (BTB = 4,4′,4″-benzenetribenzoate), are also synthesized via a sonochemical route in the presence of NMP.[39] The synthesis time is dramatically shortened from 48 h to ca. 0.5 h, while the crystal size is substantially reduced to 5−20 μm. The obtained MOFs of significantly high yield of 95.6% exhibit even higher CO_2 adsorption capacities than does solvothermally synthesized MOF-177 up to 30 bar.

Microwave-assisted solvothermal syntheses make use of microwaves to produce nanosized crystals, which have enabled instant syntheses of high-quality MOF crystals within a minute. The application of microwave radiation to conduct MOF materials has been investigated by Ni et al. in the construction of three well-known MOFs IRMOF-1 (MOF-5), IRMOF-2, and IRMOF-3.[40] The resulting MOF crystals exhibit identical cubic morphology and a very uniform distribution of particle sizes in the range of micrometer to nanometer, which are attributed to controllable nucleation process by such a new synthesis methodology. The microwave-assisted syntheses of MIL-47 and six other new vanadium MOFs have also been recently reported by Centrone et al.[41]

2.2. Predictable Structures

Luminescent properties of materials are not only related to the composition of the materials, but also are heavily dependent on the structure and intermolecular packing of the compounds for their energy transfer; it is thus very important to control the three-dimensional structure and intermolecular packing at the molecular level. However, the chemical driving force of ionic bonding to construct solid-state inorganic luminescent materials is very strong, and thus the solid-state syntheses of inorganic materials at extremely high temperatures up to several thousand °C have generally led to the formation of inorganic solid-state materials without predictable three-dimensional structures and have been criticized by the community as the "shake and bake", "mix and wait", and "heat and beat" methodology.[42] On the other hand, although the chemical bonding connectivity

within organic molecules and/or metal−organic complexes is predictable, the overall three-dimensional packing structures of such molecular compounds are still not predictable because of weak intermolecular interactions such as van der Waals interactions, hydrogen bonding, and aromatic $\pi-\pi$ interactions to control the 3D molecular packing.[43] The bonding energy of the coordination bonds for the construction of metal−organic framework materials is moderate, which has allowed the reversible bonding formation and breaking possible during the MOF syntheses, eventually leading to the construction of thermodynamically stable MOFs. Because the metal ions, particularly some in situ formed metal-containing clusters (generally termed as secondary building units (SBUs)), have some preferential coordination geometries, the three-dimensional connectivity of these metal ions and/or metal-containing clusters (as the nodes) with organic linkers of predetermined shapes such as linear and triangular has led to the construction of MOFs with a much higher degree of predictable structures. For example, the connectivity of $Zn_4O(COO)_6$ nodes (octahedral nodes) with a large number of bicarboxylate (linear bridging linkers) has led to the formation of a series of so-called isoreticular MOFs (IRMOFs) with the default cubic structures (Figure 1).[44] Another well-known example of isoreticular MOFs is those assembled from paddle-wheel $M_2(COO)_4$ (M = Cu^{2+}, Zn^{2+}, Co^{2+}, and Ni^{2+}) with bicarboxylate ($R(COO)_2$) and pillar organic linker (L) to form distorted primitive cubic nets of $M_2(ROO)_2L$.[45,46] Systematical studies on those structurally characterized MOFs deposited in CCDC have revealed that most of the MOFs have preferred default structural topologies such as diamond (dia) and extended body-centered cubic (bcu-x).[47]

2.3. Nanoscale Processability

Nanoscale processability of MOFs will definitely facilitate the wide applications of luminescent MOFs, particularly in the fields of biology, drug delivery, and biomedical imaging in which the nanoscale materials are essential for their internalization into cells.[48−50] Nanoscale MOFs were initially realized back in 2005. Such an exciting new class of MOF materials (typically known as nano-MOFs (NMOFs)) not only exhibit their rich diversity of compositions, structures, and properties, but also demonstrate their high dispersity in solutions and thus for their biocompatibility. In addition, the NMOFs may display higher surface areas than their macroscopic counterparts and unique size-dependent optical, electrical, and magnetic properties.

Usually, NMOFs can be produced through two strategies.[48] One is the controlled precipitation of self-assembled MOFs by microwave-assisted or sonochemical syntheses. The microwave radiation and ultrasounds can accelerate the nucleation and increase the seed number, thus inhibiting the MOF crystal growth. The other is the confined assembly process within specific nanoscale spheres. For example, self-assembly of NMOFs can be confined into droplets by microemulsion and/or controlled on the surface of substrates by templates.

2.4. Collaborative Multifunctionalities

Luminescent MOF materials also distinguish themselves from other inorganic and organic luminescent materials because of their potentially collaborative multifunctionalities. As we mentioned before, the metal centers, organic moieties, metal−organic charge transfer, and guest molecules within porous MOFs all can potentially generate luminescence. Such attractive characteristics can allow us to generate luminescent MOF materials with systematically varied emission wavelengths, which

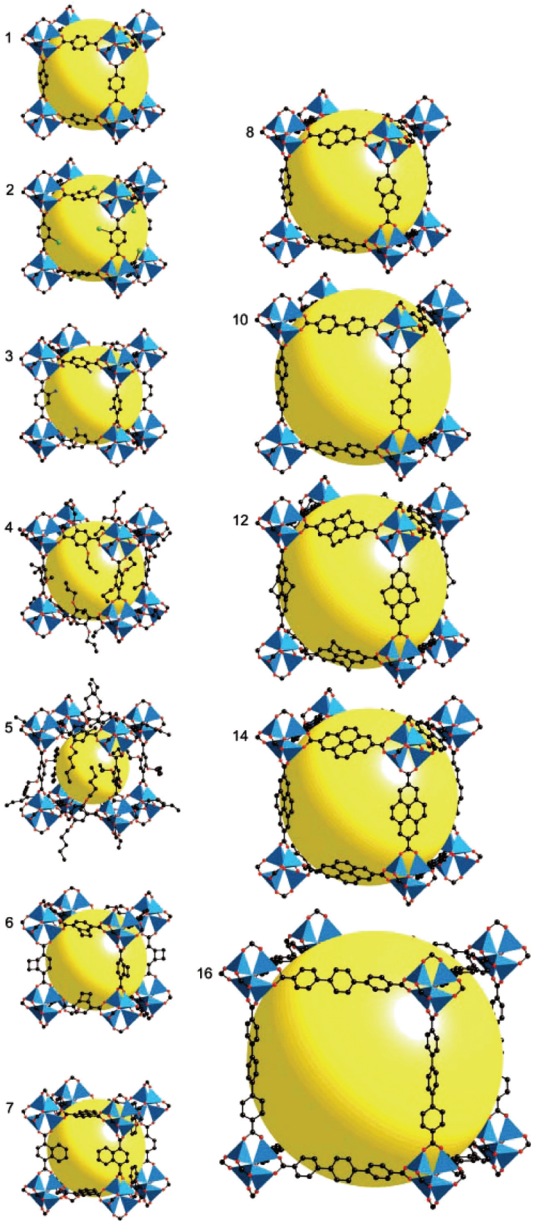

Figure 1. Crystal structures of IRMOF-*n* (*n* = 1−7, 8, 10, 12, 14, and 16). Reprinted with permission from ref 44. Copyright 2002 American Association for the Advancement of Science.

are crucial for lighting, display, and optical devices. The permanent porosities and collaborative luminescent properties of some MOFs are particularly useful to develop luminescent sensing materials. In fact, to make use of the pores within luminescent MOFs for their differential recognition of sensing substrates, a number of porous luminescent sensing MOFs have been fulfilled.[51−59] Several examples of luminescent and nanoscale MOFs have been implemented into their sensing and bioimaging applications.[60−64] Although only a few luminescent MOFs have been reported to exhibit collaborative multifunctionalities, it is foreseen that the collaborative functionalities of luminescence, magnetism, and nanoscale processability of MOF materials will enable MOFs as very practically useful materials for their diverse biomedical applications, while nanoscale processability, luminescent properties, and permanent

porosity will make the fabrication of luminescent thin films of MOFs feasible for sensing devices.

3. ORIGIN OF MOF LUMINESCENCE

Luminescence is the term used to describe the process in which light is produced by the absorption of energy. Luminescence contains two basic forms, fluorescence and phosphorescence, depending on multiple spin state during the radiative relaxation process. Fluorescence refers to the emitting of light between energy states of the same spin multiplicity, and the process generally lasts no more than about 10 ns. However, phosphorescence refers to the emitting of light between states with difference spin multiplicity, and the process lasts a microsecond to seconds.

So far, hundreds of luminescent MOFs have been reported, and the luminescence can exist in several forms.[65−154] Luminescence can arise from direct organic ligands excitation (particularly from the highly conjugated ligands), metal-centered emission (widely observed in lanthanide MOFs through the so-called antenna effect), and charge-transfer such as ligand-to-metal charge transfer (LMCT) and metal-to-ligand charge transfer (MLCT). Furthermore, the guest molecules can also result in luminescence onto MOFs.

3.1. Ligand-Based Luminescence

Generally, when an organic molecule absorbs a photon of appropriate energy, a chain of photophysical events occur, including internal conversion or vibrational relaxation, fluorescence, intersystem crossing, and phosphorescence (Figure 2). The fluorescence of organic molecules corresponds to the radiative transition from its first singlet state S_1 to the ground singlet state S_0. Such a transition, $S_1 \rightarrow S_0$, is termed molecular fluorescence, which is spin-allowed. Phosphorescence corresponds to the radiative transition from triplet state T_1 to S_0, which is spin-forbidden and has a lifetime on the order of several microseconds to seconds. The luminescence properties can be characterized by the following parameters: (1) luminescence spectra, defined as fluorescence intensity as a function of a wavelength, (2) quantum yield, which gives the efficiency of the fluorescence process and is defined as the ratio of the number of emitted photons released in the process of fluorescence to the number of photons absorbed, and (3) lifetime, which refers to the average time the molecule stays in its excited state before emitting a photon and is determined as being inversely proportional to the sum rate constants of a radiative process and the nonradiative processes:

$$\tau = \frac{1}{k_f + k_{nr}} \quad (1)$$

where k_f is the rate constant of a radiative process and k_{nr} is the rate constant of a nonradiative process.[155]

In MOFs, a wide range of π-conjugated organic molecules are commonly used as linkers due to their rigidity, and the majority of them are based on rigid backbones functionalized with multicarboxylate groups or heterocyclic groups for metal−ligand coordination. Usually, the fluorescence emission from organic ligands is similar to their emission behavior in solution, corresponding to the transition from the lowest excited singlet state to the singlet ground state, and the transitions are either $\pi \rightarrow \pi^*$ or $n \rightarrow \pi^*$ in nature. However, the fluorescence properties such as maximum emission wavelength and lifetime of organic linkers in solid MOFs are often different from those of the free molecules.

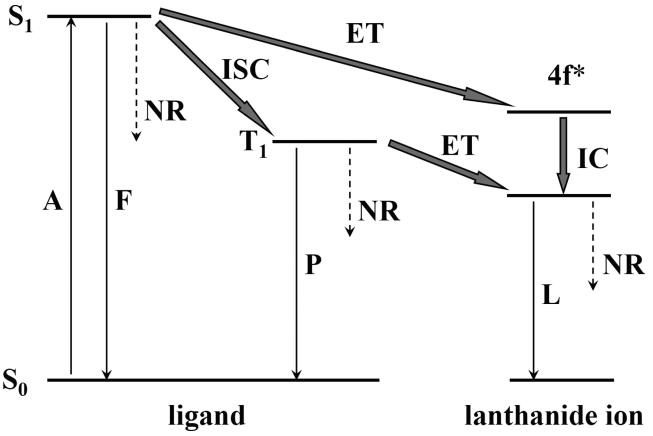

Figure 2. Schematic representation of energy absorption, migration, emission, and processes in MOFs. Abbreviations: A = absorption; F = fluorescence; P = phosphorescence; L = lanthanide-centered luminescence; ISC = intersystem crossing; ET = energy transfer; IC = internal conversion; S = singlet; T = triplet. Plain arrows indicate radiative transitions; dotted arrows indicate nonradiative transitions.

This is because the organic linkers are stabilized within MOFs, which reduces the nonradiative decay rate and leads to increased fluorescence intensity, lifetimes, and quantum efficiencies. In the solid state, molecular interactions make the molecules close together, which enable charge transfer among the organic ligands/linkers, resulting in shift of spectra, broadening of the emission, and loss of fine structure. In addition, the size and nature of metal ions, the orientation and arrangement of linkers, and the coordination environment within MOF can affect the fluorescence properties of the organic linkers because these factors will induce their different intramolecular or intermolecular interactions among organic linkers. Therefore, controlling these interactions is crucial to tuning the luminescence properties of MOFs for a particular application. The following examples show how intramolecular/intermolecular interactions of organic linkers have played the important roles in the luminescence properties of the resulting MOFs.

The strong luminescence of MOF $Zn_3(\mu_5\text{-pta})_2(\mu_2\text{-}H_2O)_2$ (pta = 2,4,6-pyridinetricarboxylate)[96] is observed at 467 nm, while the free ligand molecule displays a weak luminescence at 415 nm when excited at 338 nm at room temperature. The fluorescent enhancement and red-shift of organic linkers within this MOF are attributed to the formation of the framework structure, which has enabled the rigidity of the aromatic backbones and maximized the intramolecular/intermoleculear interactions among the organic linkers for their energy transfer, and decreased the intraligand HOMO−LUMO energy gap.

Coordination-perturbed ligand-centered luminescence was reported in MOFs $Zn_3(BTC)_2(DMF)_3(H_2O)\cdot(DMF)(H_2O)$ and $Cd_4(BTC)_3(DMF)_2(H_2O)_2\cdot 6H_2O$ (BTC = 1,3,5-benzenetricarboxylate).[68] The strongest emission at 370 nm of the free BTC when excited at 334 nm, attributed to the $\pi^* \rightarrow$ n transitions, was shifted to 410 and 405 nm in these two MOFs, respectively, when excited at 341 and 319 nm. Bauer et al. demonstrated that the luminescence properties of MOFs can be modified by different local ligand environments.[66] The 2D MOF $Zn_3L_3(DMF)_2$ and 3D MOF $Zn_4OL_3(DMF)(CHCl_3)$ (H_2L = *trans*-4,4′-stilbene dicarboxylic acid) display very different bright luminescence under UV light: the 2D MOF exhibits blue emission, while the 3D MOF shows purple/blue emission,

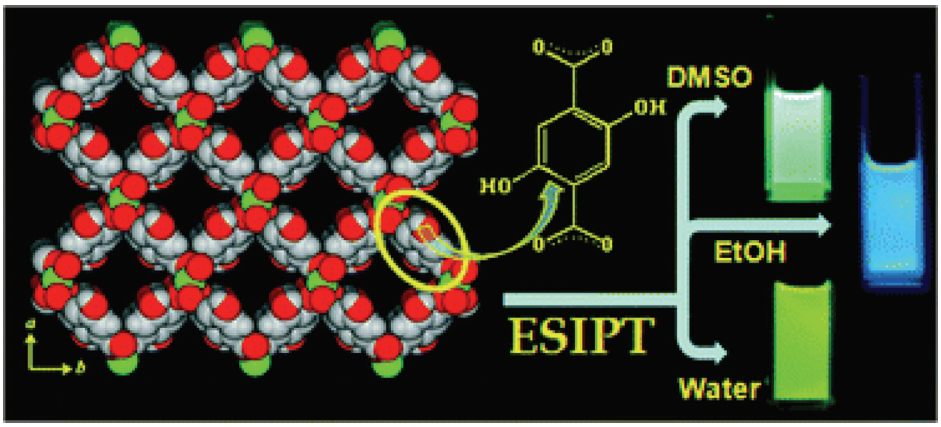

Figure 3. The ESIPT induced luminescence changes of MOF $Mg(DHT)(DMF)_2$ in different solvents. Reprinted with permission from ref 156. Copyright 2010 The Royal Society of Chemistry.

apparently because of their different ligand environments within these two MOFs.

Fluorescence of organic ligands could also be affected by reversible changes in electron distribution occurring in the excited state. The two important processes are excited-state electron transfer (ESET) and proton transfer (ESPT). The electrons in the excited state travel from the electron-rich donor to the electron acceptor upon excitation in ESET process, while in ESPT the protons in the excited state depart or join the molecule at rates different from those in the ground state. ESPT is a fast process as compared to fluorescence emission, and the intramolecular proton transfer is faster than intermolecular.[155] The luminescence change induced by excited-state intramolecular proton transfer (ESIPT) of the organic linker has been observed in both the free H_2DHT organic linker and the resulting MOF $Mg(DHT)(DMF)_2$ (DHT = 2,5-dihydroxyterephthalate) by Jayaramulu et al.[156] The DHT is a multifunctional organic linker that has constitutional stiffness, with four pH-dependent abstractable protons that can be used for generating stable and rigid high dimensional MOFs. H_2DHT exhibits absorption bands in the UV region at about 360 nm in different solvents. Significant emission changes are observed when the free H_2DHT are dissolved in different solvents. The free H_2DHT shows a green emission at 510 nm in polar solvents DMSO and DMF, while it displays a high-energy blue emission around 440 nm in protic solvents such as ethanol, which are attributed to the keto and enol form of this unique organic linker. Because of the ESIPT-induced fluorescence changes of the organic linker DHT, MOF $Mg(DHT)(DMF)_2$ also exhibits a tunable emission from blue to yellow, which are dependent the solvents. This MOF exhibits a blue emission at 404 and 429 nm in ethanol, a significantly red-shifted green emission at 508 nm in DMSO, and a further red-shifted emission at 532 nm in H_2O. The ligand-centered luminescence of $Mg(DHT)(DMF)_2$ was blue-shifted upon the addition of trifluoroacetic acid (TFA) in which the TFA blocks the ESIPT process throught its formation of intermolecular H-bonds with the organic linker DHT. Interestingly and importantly, the ESIPT-induced fluorescence changes have been also observed in the solid state of MOFs $Mg(DHT)(G)_x$ (G = guest molecules) (Figure 3). The powders of three MOFs $Mg(DHT)(TFA)_x$, $Mg(DHT)(DMSO)_x$, and $Mg(DHT)(H_2O)_x$ show blue (λ_{max} = 454 nm), green (λ_{max} = 483 nm), and yellow (λ_{max} = 535 nm) emission, respectively.

3.2. Lanthanide Luminescence

Lanthanide ions (Ln^{3+}) are characterized by a gradual filling of the 4f orbitals, from $4f^0$ (for La^{3+}) to $4f^{14}$ (for Lu^{3+}). These electronic $[Xe]4f^n$ configurations (n = 0−14) generate a variety of electronic energy levels (Figure 4),[157] resulting in the intricate optical properties.[2,158−160] Such electronic energy levels are well-defined due to the shielding of the 4f orbitals by the filled $5s^25p^6$ subshells, and they are less sensitive to the chemical environments around lanthanide ions. Consequently, each lanthanide ion exhibits narrow and characteristic 4f−4f transitions. All Ln^{3+} ions except La^{3+} and Lu^{3+} can generate luminescent f−f emissions from ultraviolet (UV) to visible and near-infrared (NIR) ranges. The Eu^{3+}, Tb^{3+}, Sm^{3+}, and Tm^{3+} emit red, green, orange, and blue light, respectively, while the Yb^{3+}, Nd^{3+}, and Er^{3+} display the well-known near-infrared luminescence.

The lanthanide ions suffer from weak light absorption due to the forbidden f−f transitions, making the direct excitation of the metals very inefficient unless high-power laser excitation is utilized. This problem can be overcome by coupling species that can participate in energy transfer processes, known as "luminescence sensitization" or "antenna effect".[2,157,161,162] The mechanism of antenna sensitization within MOFs is comprised of three steps: light is absorbed by the organic ligands around the lanthanide ions, energy is transferred to the lanthanide ions from organic ligands, and then luminescence is generated from the lanthanide ions. One of the main energy migration paths is ligand-centered absorptions followed by intersystem crossing $S_1 \rightarrow T_1$, $T_1 \rightarrow Ln^{3+}$ transfer, and metal-centered emission. This phenomenon can be modeled using Jablonsky's diagram as shown in Figure 2. Another possible path is the direct transfer of energy from the excited singlet state S_1 to the energy levels of the lanthanide ion, which is known for Eu^{3+} and Tb^{3+}.[2,159] Because of the energy transfer of the organic ligands to the lanthanide ion, the fluorescence and phosphorescence of the ligands is not observed. If such energy transfer is not very efficient, both remaining ligand fluorescence and the lanthanide-centered luminescence could be observed.

Furthermore, ligand-to-metal charge transfer (LMCT), metal-to-ligand charge transfer (MLCT), and 4f−5d transitions may also funnel energy onto the lanthanide ions. For trivalent lanthanide ions such as Sm^{3+}, Eu^{3+}, and Yb^{3+} that can easily be reduced to the divalent ions, the excitation energy can be transferred from an LMCT state to the 4f levels of the lanthanide ions when the LMCT state lies at high-enough energy.[2] Usually,

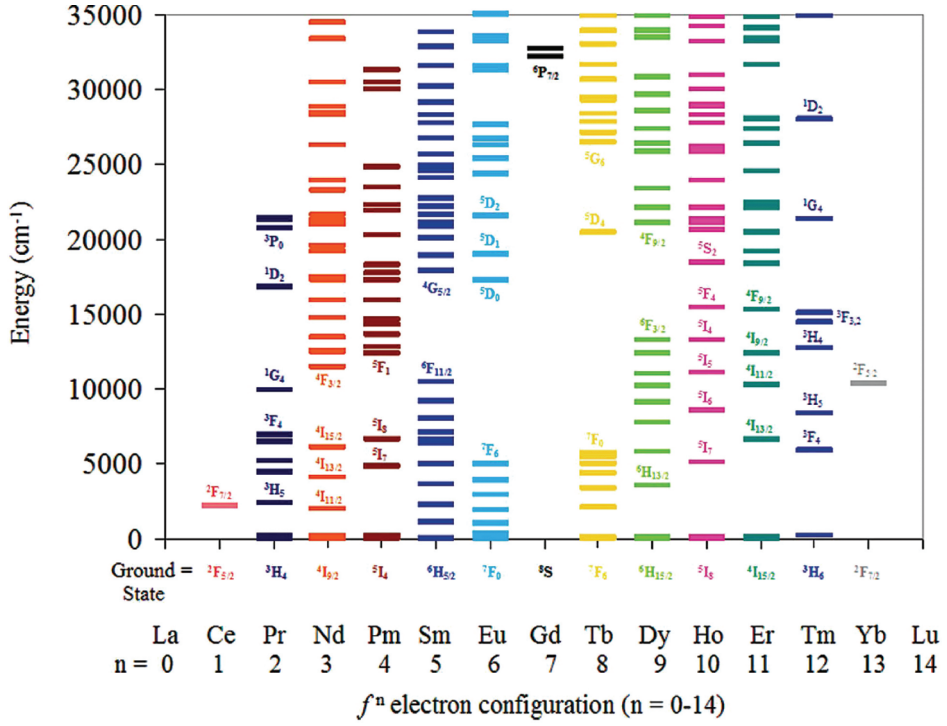

Figure 4. A summary of electronic excited-state energy levels for Ln^{3+} ions. Reprinted with permission from ref 157. Copyright 2009 American Chemical Society.

energy is transferred onto Ln^{3+} levels with higher energy than the emissive level; otherwise, back energy transfer can occur, resulting in poor luminescence properties. A detailed investigation on the numerous energy transfers processes is very important to well tune the luminescent properties of lanthanide MOFs.

Efficient lanthanide-centered luminescence of MOFs is fulfilled by the use of antenna organic linkers; it is necessary that the lowest triplet state of the organic linkers is located at an energy level nearly equal to or above the resonance level of the lanthanide ions. The energy of the triplet state must be elaborately tuned to maximize the transfer and minimize the back-transfer. Thus, it is of great significance to select or design suitable organic linkers with the appropriate energy level to target the luminescent MOFs. To illustrate the sensitizations effect of organic linkers, we show here two representative examples of such luminescent lanthanide MOFs. The first example is the isostructural lanthanide (Sm^{3+}, Eu^{3+}, Gd^{3+}, Tb^{3+}, Dy^{3+}) MOFs containing 4,4′-disulfo-2,2′-bipyridine-*N*,*N*′-dioxide.[139] The triplet state energy levels of organic linker were determined to be 24 038 cm^{-1}; thus the organic linker is capable of sensitizing the trivalent ions Sm^{3+}, Eu^{3+}, Tb^{3+}, and Dy^{3+} in which strong emissions have been observed in Eu^{3+} and Tb^{3+} MOFs. In the second example, the thiophenyl-derivatized carboxylic acid has been incorporated as the efficient sensitizing chromophore and multicarboxylate linker to construct the lanthanide MOFs.[94] Because of the large radius of the S atom, its lone pair electrons can be easily delocalized within the heterocycle, so this organic linker exhibits very good charge-transfer capacity. The results show that Eu^{3+} and Tb^{3+} MOFs exhibit intense luminescence in the typical visible region, and the Yb^{3+} MOF emits moderate characteristic near-infrared luminescence.

The antenna effect induced by guest molecules has also been observed in the MOF $[Eu_2(adipic\ acid)_3(H_2O)_2]\cdot$4,4′-dipyridyl in which the guest molecule 4,4′-dipyridyl is utilized as a structure-directing agent.[163] When this MOF is excited at the maximum absorption wavelength of the 4,4′-dipyridyl at 236 nm, the emission spectra reveal two characteristic peaks at 595 and 615 nm, respectively, attributed to $^5D_0 \rightarrow {}^7F_1$ and $^5D_0 \rightarrow {}^7F_2$ transitions of Eu^{3+}. It needs to be mentioned that the starting chemical $Eu(NO_3)_3$ does not emit such luminescence when excited at 236 nm, indicating that the template molecule of 4,4′-dipyridyl does sensitize the fluorescence of lanthanide metal centers.

The effect of synergistic energy transfer on the luminescence properties of MOFs through an ancillary second organic ligand picrate has been realized in MOFs $EuL(pic)_3$ and $[EuL(NO_3)_3]_3\cdot 1.5CHCl_3$ (L = 1,1,1-tris-[((2′-benzylaminoformyl)phenoxyl)methyl]ethane, pic = picrate).[138] Both MOFs display five characteristic emissions of Eu^{3+} at 580 nm ($^5D_0 \rightarrow {}^7F_0$), 592 nm ($^5D_0 \rightarrow {}^7F_1$), 616 nm ($^5D_0 \rightarrow {}^7F_2$), 650 nm ($^5D_0 \rightarrow {}^7F_3$), and 693 nm ($^5D_0 \rightarrow {}^7F_4$); however, the emission intensity of the $^5D_0 \rightarrow {}^7F_2$ transition at 616 nm in $EuL(pic)_3$ is approximately 6 times stronger than that in $[EuL(NO_3)_3]_3\cdot 1.5CHCl_3$. This is because the incorporation of this second ancillary ligand picrate results in the synergistic energy transfer from organic linker L to Eu^{3+}. The energy gap between the ligand triplet and Eu^{3+} excited states (7733 cm^{-1}) is too large; the organic linker L in $[EuL(NO_3)_3]_3\cdot 1.5CHCl_3$ cannot efficiently sensitize the Eu^{3+} luminescence. Two possible synergistic energy transfers might lead to such significantly enhanced luminescent intensity in $EuL(pic)_3$: (1) energy transfers from the S_1 excited state of the organic linker L to the S_1 excited state of picrate; from the S_1 excited state to the T_1 excited state of picrate; and from the T_1 excited state of picrate to the emitting level of Eu^{3+}; and (2) energy transfers from the S_1 to the T_1 excited state of the organic linker L; then from the T_1 excited state of the organic linker L to the T_1 excited state of picrate; and from the T_1 excited state of picrate to the emitting level of Eu^{3+}.

Thus, the second ancillary organic ligand picrate offers additional energy transfer routes to improve the energy transfer efficiency from the organic linker to the lanthanide ions.

Energy transfers from one lanthanide to another lanthanide ion have also been observed to enhance the luminescence intensity in heterolanthanide MOFs. For instance, the Eu^{3+} emissions at 595 and 615 nm in the heterolanthanide MOF $[(Eu, Tb)(C_6H_8O_4)_3(H_2O)_2]\cdot(C_{10}H_8N_2)$ ($C_6H_8O_4$ = butane-1,4-dicarboxylate, $C_{10}H_8N_2$ = 4,4′-bipyridine) are much stronger than those in $[Eu(C_6H_8O_4)_3(H_2O)_2]\cdot(C_{10}H_8N_2)$, while the Tb^{3+} emission at 545 nm in the heterolanthanide MOF $[(Eu, Tb)(C_6H_8O_4)_3(H_2O)_2]\cdot(C_{10}H_8N_2)$ is completely quenched.[97] Within heterolanthanide MOF $[(Eu, Tb)(C_6H_8O_4)_3(H_2O)_2]\cdot(C_{10}H_8N_2)$, the Tb^{3+} centers sensitize the Eu^{3+}, leading to effectively enhanced Eu^{3+} emission. Such energy transfer from Tb^{3+} to Eu^{3+} has also been observed in the MOFs $(Eu_{0.2}Tb_{0.8})_2(2,5\text{-pdc})_2(1,4\text{-pda})(H_2O)_2$ and $(Eu_{0.1}Tb_{0.9})_2(2,5\text{-pdc})_2(1,4\text{-pda})(H_2O)_2$ (H_2pdc = 2,5-pyridinedicarboxylic acid, H_2pda = 1,4-phenylenediacetic acid).[164]

The luminescence quantum yield is an important parameter to characterize the lanthanide luminescence, defined as the ratio between the numbers of emitted photons divided by the numbers of absorbed photons. For luminescent lanthanide MOFs, the overall luminescence quantum yield is determined by the efficiency of sensitization and by the intrinsic quantum yield of the lanthanide luminescence. The intrinsic quantum yield is the quantum yield of the lanthanide-centered luminescence upon direct excitation into the 4f levels, which reflects the extent of nonradiative relaxation processes occurring both in the inner- and in the outer-coordination spheres of the lanthanide ion and depends on the energy gap between the emissive state and the highest sublevel of the ground state of lanthanide ion.[159,160] The smaller is this gap, the easier is its closing by nonradiative transition processes through vibrations of bound ligands, particular through those having high energy O−H, N−H, and C−H vibrations.[159] Many efforts for alleviating these nonradiative relaxations have been developed. For example, replacement of the OH oscillators (with typical energy of 3600 cm^{-1}) by low-frequency OD oscillators (energy of 2200 cm^{-1}) will diminish the vibronic de-excitation pathway.[158] If the lanthanide ions can be isolated from these high energy O−H, N−H, and C−H vibrations, the quenching effects can be diminished. For instance, the lanthanide ions Eu^{3+}, Tb^{3+}, or Nd^{3+} are encapsulated with macrocyclic polyamine ligands and then assembled into several rigid lanthanide MOFs.[165] Because these lanthanide ions have their coordination spheres fully occupied by the macrocyclic polyamine ligands, their interactions with small molecules such as water from the environment have been blocked; accordingly, these MOFs exhibit efficient fluorescent emissions both in the visible and in the near-infrared region at room temperature.

Specifically, the luminescence of Ln^{3+} ion from the f−f transitions can be classified as two types of transitions: the parity allowed magnetic dipole transitions and the parity forbidden electric dipole transitions. When the Ln^{3+} ion is inserted into a chemical environment, noncentrosymmetric interactions allow the mixing of electronic states of opposite parity into the 4f wave functions; the terms "forbidden" and "allowed" cannot be applied too rigidly. The electric dipole transitions become partly allowed, and the intensity of some of these transitions is particularly sensitive to the changes in the metal ion environment, so that these transitions are generally called "hypersensitive transitions".[160] The luminescence of lanthanide ions can provide valuable information about their local environments, and thus acts as the structural probe to decipher their symmetry of the chemical environment and the coordination sphere. The lanthanide-centered emission of MOFs is also sensitive to the lowest triplet level of the ligands, which allows us to modulate their luminescence intensity by controlling the interactions among the ligands and the analytes. These interactions may facilitate or disrupt the energy transfer process by modifying the bound ligands' energy transfer ability and/or providing a new path for the energy transfer from the analyte onto the lanthanide ion, enabling luminescent MOFs as useful materials for a variety of analytical probes.

The luminescence of Eu^{3+} ions is an appropriate structural probe to determine the different metal sites, their coordination symmetries, and even hydration numbers. Especially, the emission intensity ratios of the $^5D_0 \rightarrow {}^7F_2$ to $^5D_0 \rightarrow {}^7F_1$ transitions are very sensitive to the coordination symmetries of the Eu^{3+} ions, because the $^5D_0 \rightarrow {}^7F_1$ emission is due to the magnetic dipole and independent of the environment, while the $^5D_0 \rightarrow {}^7F_2$ emission is due to the electric dipole and is sensitive to the crystal field symmetry. Several representative examples of luminescence of Eu^{3+} ions as the structural probe in MOFs are presented below. The emission intensity ratio of the $^5D_0 \rightarrow {}^7F_2$ to $^5D_0 \rightarrow {}^7F_1$ transitions is 5.2 in an as-synthesized Eu-doped MOF $[La_2(H_2O)_4][(C_5H_3N(COO)_2)_2(C_6H_4(COO)_2)]$[166] and is 4.2 in the dehydrated Eu-doped MOF. The as-synthesized Eu-doped MOF contains two water molecules, which are positioned adjacent to each other in one face of the trigonal prism, as part of the nine coordination of the La^{3+} ion. The dehydration gives rise to a seven-coordinated La^{3+} ion that is probably much less strained than the nine-coordinated La^{3+} site, leading to the decreased emission intensity of the $^5D_0 \rightarrow {}^7F_2$ transition.

MOF $Eu_3(2,6\text{-pydc})_3(2,6\text{-Hpydc})(SO_4)(H_2O)_3\cdot 3(H_2O)_3$ (2,6-pydc = pyridine-2,6-dicarboxylate)[167] crystallizes in the triclinic $P\bar{1}$ space group and possesses a 2D metal−organic framework based on hexanuclear $\{Eu_6\}$ SBUs. The asymmetric unit is comprised of three independent Eu^{3+} ions, three $pydc^{2-}$ dianions, one $Hpydc^-$ anion, one sulfate, three coordinated, and three guest water molecules. The emission intensity ratio of the $^5D_0 \rightarrow {}^7F_2$ and $^5D_0 \rightarrow {}^7F_1$ transitions is about 5.2. Furthermore, the symmetry-forbidden emission $^5D_0 \rightarrow {}^7F_0$ is observed at 579 nm. These luminescence features indicate that Eu^{3+} ions have low symmetrical coordination environments.

3.3. Charge-Transfer Luminescence

Charge-transfer luminescence is generated from an allowed transition from the charge-transfer excited state to the ground state. Ligand-to-metal charge transfer (LMCT) and metal-to-ligand charge transfer (MLCT) are typical charge transfers found in MOFs. LMCT involves the electronic transition from an organic linker-localized orbital to a metal-centered orbital, while MLCT corresponds to the electronic transition from a metal-centered orbital to an organic linker-localized orbital. The charge transfer luminescence is frequently observed in d^{10} metal-based MOFs. For example, MOF $Cu_3(C_7H_2NO_5)_2\cdot 3H_2O$ ($C_7H_2NO_5$ = 4-hydroxypyridine-2,6-dicarboxylate) exhibits blue fluorescence at 398 and 478 nm upon excitation at 333 nm, while $CuAg_2(C_7H_3NO_5)_2$ and the free organic linker 4-hydroxypyridine-2,6-dicarboxylic acid display green fluorescence at 515 and 526 nm upon excitation at 358 and 365 nm, respectively.[147] As compared to the free organic linker, MOF $Cu_3(C_7H_2NO_5)_2\cdot 3H_2O$ displays two large blue shifts of 59 and 48 nm, while $CuAg_2(C_7H_3NO_5)_2$ shows one small blue shift of 11 nm, suggesting that the luminescence emission of $Cu_3(C_7H_2NO_5)_2\cdot 3H_2O$ may be

dx.doi.org/10.1021/cr200101d |Chem. Rev. 2012, 112, 1126–1162

originated from MLCT. The calculated energy band structures do indicate that the luminescence of MOF $Cu_3(C_7H_2NO_5)_2 \cdot 3H_2O$ is ascribed to MLCT from the Cu-3d to O-2p and N-2p orbitals, while the luminescence of $CuAg_2(C_7H_3NO_5)_2$ is originated from the $\pi-\pi^*$ transition of the organic linker.

MLCT luminescence has been discovered in a five-coordinated Mn MOF Mn(Hbidc) (H_3bidc = 1*H*-benzimidazole-5,6-dicarboxylic acid).[168] This MOF exhibits a strong red emission in the range of 625−850 nm. The strongest emission in Mn(Hbidc) is located at 726 nm, which is significantly red-shifted from the original emission at 440 nm in the free organic linker H_3bidc. The strong emission of Mn(Hbidc) is attributed to MLCT luminescence in which the relatively large π-conjugated system of benzimidazole ring within $Hbidc^{2-}$ has enforced the charge transfer from Mn^{2+} ion to the organic linker.

Luminescence originated from LMCT has been reported in some MOFs. Because of ligand-to-metal charge transfer, the MOF $[Zn(2,3\text{-pydc})(bpp)] \cdot 2.5H_2O$ and $[Cd(2,3\text{-pydc})(bpp)(H_2O)] \cdot 3H_2O$ (2,3-pydcH_2 = pyridine-2,3-dicarboxylic acid) display intense fluorescent emissions at 436 and 438 nm upon excitation at 372 and 370 nm,[70] respectively, although the organic linker 2,3-pydcH_2 only displays very weak photoluminescent property upon excitation at 370 nm. The homochiral Cd MOF $Cd_3(dtba)_3(bpp)_3$ (H_2dtba = 2,2′-dithiobisbenzoic acid, bpp = 1,3-bis(4-pyridyl)propane) exhibits temperature-dependent luminescence.[143] The room temperature blue emission of $Cd_3(dtba)_3(bpp)_3$ at 434 nm with a shoulder peak at 482 nm when excited at 355 nm is attributed to the metal-perturbed intraligand emissions of dtba or bpp, while the emission at 10 K at about 507 nm is originated from LMCT.

Copper MOFs based on N-heterocyclic organic linker $Cu_5(SCN)_5(3\text{-Abpt})_2$ (3-Abpt = 4-amine-3,5-bis(3-pyridyl)-1,2,4-triazole) and Cu(SCN)(3-Abpt) exhibit strong yellow LMCT luminescence at 559 and 570 nm,[169] respectively. The free 3-Abpt ligand contains pyridyl, and the triazole conjugated group shows a narrow emission at 388 nm and a broad shoulder emission centered at 441 nm. Similarly, $Cu_2(SCN)_2(4\text{-PyHBIm})$ (4-PyHBIm = 2-(4-pyridyl)benzimidazole) and $Cu_2(SCN)_2(3\text{-PyHBIm})$ (3-PyHBIm = 2-(3-pyridyl)benzimidazole) also display LMCT luminescence.

Sometimes, LMCT or MLCT luminescence may compete with ligand-based luminescence, resulting in both LMCT/MLCT and ligand-based emission bands. For example, the zinc MOF $Zn_2(ATA)_3(ATA)_{2/2}$ excited at 320 nm at room temperature produces a weak blue luminescence at 485 nm that may be assigned to the LMCT or MLCT luminescence and a strong emission at 392 nm originated from ligand-based emission.[75]

3.4. Guest-Induced Luminescence

Because of the highly regular channel structures and controllable pore sizes, the MOFs can also serve as rigid/flexible hosts for the encapsulation of the guest luminescent species such as lanthanide ions and fluorescent dyes. An et al. prepared a series of lanthanide ions doped MOFs Ln^{3+}@bio-MOF-1 (Ln^{3+} = Tb^{3+}, Sm^{3+}, Eu^{3+}, or Yb^{3+}) from the as-synthesized bio-MOF-1 via cation exchange process.[170] When excited at 365 nm, the doped MOFs emitted their distinctive colors (Eu^{3+}, red; Tb^{3+}, green; Sm^{3+}, orange-pink), which are readily observed with the naked eye (Figure 5). Tb^{3+}@bio-MOF-1, Sm^{3+}@bio-MOF-1, Eu^{3+}@bio-MOF-1, and Yb^{3+}@bio-MOF-1 exhibit the emission at 545, 640, 614, and 970 nm, respectively. It needs to be mentioned that there exists another main emission at 340 nm

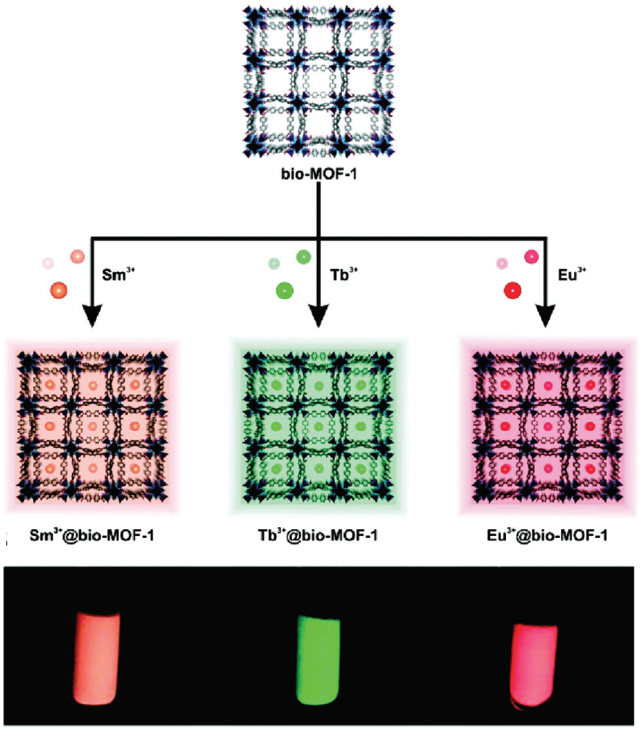

Figure 5. Luminescence of lanthanide ions doped in bio-MOF-1. Reprinted with permission from ref 170. Copyright 2011 American Chemical Society.

in all of these lanthanide ions-doped MOFs, suggesting that energy migrates through the same electronic levels located in the MOF chromophoric structure for doped lanthanide ions. Notably, the characteristic luminescence of lanthanide ions can even be detected in aqueous environments, despite the strong quenching effect of water molecules, indicating that the bio-MOF-1 scaffold can not only effectively sensitize but also sufficiently protect the lanthanide ions. Furthermore, the quantum yields of lanthanide emission are all reasonably high in aqueous environments, demonstrating that the lanthanide ions are well protected within the pores, and the energy transfers from MOFs to lanthanide ions are efficient. Luo et al. prepared the Eu^{3+} and Tb^{3+} doped MOFs, which exhibit tunable luminescence properties and sensing functions for metal ions.[171] The classical fluorescent dye Rh6G has been encapsulated into a large porous MOF, exhibiting the temperature-dependent luminescent properties.[172] In other examples, the fluorescent dye rhodamine B and fluorescent protein have been decorated onto the surface of the MOFs to display their fluorescence properties.[61,173] The guest-induced luminescence makes some luminescent MOF materials suitable for molecular detection and environmental probing, which will be discussed in section 5.

4. SURVEY OF DIFFERENT TYPES OF LUMINESCENT MOFS

From the inorganic chemists' point of view, a variety of luminescent MOFs have been prepared using lanthanide, transition metal, and main group metal ions. Accordingly, it might be straightforward and convenient to make a comprehensive survey based on different metal ions. As such, four categories of luminescent MOFs can be classified: lanthanide-based MOFs, transition-metal-based MOFs, heterometal−organic frameworks, and main

group metal−organic frameworks. The updated survey of luminescent MOFs and their luminescence wavelengths are summarized in Table 1.

4.1. Lanthanide-Based MOFs

Quite a few different organic linkers such as carboxylates, phosphonates, or sulfonates have been utilized to construct lanthanide MOFs.[174−181] Among the lanthanide MOFs, Eu- and Tb-based MOFs have been well studied due to their intense, long-lived, and line-like emission in the visible region, while the near-infrared (NIR) and up-conversion Er-, Nd-, and Yb-based luminescent MOFs are less explored.

Daiguebonne et al. synthesized a series of lanthanide MOFs $Ln_2(1,4\text{-BDC})_3(H_2O)_4$ (Ln = La, Ce, Pr, Nd, Sm, Eu, Gd, Tb, Dy, Ho, Er, Tm, 1,4-BDC = 1,4-benzenedicarboxylate) through the reaction of the corresponding lanthanide ion with the sodium salt of terephthalic acid in water.[182] The three Eu-, Tb-, and Dy-based MOFs emit visible metal-centered red luminescence at 592 and 617 nm (Eu), green luminescence at 491 and 546 nm (Tb), and yellow luminescence at 481 and 575 nm (Dy), respectively. The emission spectrum of $Eu_2(1,4\text{-BDC})_3(H_2O)_4$ is largely dominated by the $^5D_0 \rightarrow {}^7F_2$ transition at 616 nm, which is 6.9 times stronger than the $^5D_0 \rightarrow {}^7F_1$ transition at 295 K. The further splitting of the $^5D_0 \rightarrow {}^7F_1$ transition into three at 589, 593, and 594 nm (corresponding to ligand-field sublevels at 301, 395, and 412 cm^{-1} for $^7F_1$) indicates that the Eu^{3+} ions lie in low-symmetry sites. The luminescence spectrum of $Tb_2(1,4\text{-BDC})_3(H_2O)_4$ is dominated by two multiplets at 491 and 546 nm, which are attributed to the $^5D_4 \rightarrow {}^7F_6$ and $^5D_4 \rightarrow {}^7F_5$ transitions, respectively. The anhydrous $Tb_2(1,4\text{-BDC})_3$ reveals a large quantum yield of 43%.

Han et al. have prepared a series of lanthanide MOFs $Ln_6(1,4\text{-BDC})_9(DMF)_6(H_2O)_3\cdot 3DMF$ (Ln = La, Ce and Nd, 1,4-BDC = 1,4-benzenedicarboxylate), $Ln_2(1,4\text{-BDC})_3(DMF)_2(H_2O)_2$ (Ln = Dy and Eu), and $Ln_2(ADB)_3(DMSO)_4\cdot 6DMSO\cdot 8H_2O$ (Ln = Ce, Sm, Eu, and Gd, H_2ADB = 4,4′-azodibenzoic acid) by a diffusion method.[183] The MOF $Eu_2(1,4\text{-BDC})_3(DMF)_2(H_2O)_2$ displays a characteristic Eu^{3+} luminescence at 616 and 591 nm.

Wang et al. described the syntheses of nine lanthanide MOFs $[La(pta)(H_2O)_4]\cdot 2H_2O$ (H_3pta = 2,4,6-pyridinetricarboxylic acid), $[Ln(pta)(H_2O)_5]\cdot 4H_2O$ (Ln = Sm, Eu, Tb, Ho), and $[Ln(pta)(H_2O)_3]\cdot 4H_2O$ (Ln = Dy, Er, Tm, Yb).[76] The Sm-, Eu-, Tb-, and Dy-based MOFs exhibit their corresponding characteristic luminescence in the visible region at an excitation of 305 nm. The Er-MOF exhibits an emission at 1538 nm attributed to the transition of $^4I_{13/2} \rightarrow {}^4I_{15/2}$ under the excitation of 300 nm, and the Yb-MOF shows a strong emission at 980 nm resulting from the $^2F_{5/2} \rightarrow {}^2F_{7/2}$ transition upon excitation of 302 nm. Gándara et al. synthesized a series of lanthanide MOFs through the hydrothermal reaction of Ln^{3+} (Ln = La, Ce, Pr, Nd, Sm, Eu, Gd, Tb, Dy, Ho, Er, Yb) salt with $H_2hfipbb$ ($H_2hfipbb$ = 4,4′-(hexafluoroisopropylidene)bis(benzoic acid)) in a mixture of solvents.[184] In these framework structures, the lanthanide ions form well-separated chains along the *a* axis with interchain distances around 12.5 Å to prevent the concentration quenching of the luminescence. Among these different Ln-based MOFs, the Eu and Tb MOFs exhibit their characteristic lanthanide luminescence, and the Gd MOF emits broad visible emission, while the rest of the MOFs display emission similar to that of the organic linker, which is slightly dependent on the ions, upon excitation at 364 nm.

Up-conversion luminescent materials can convert lower-energy light to higher-energy light through multiphoton processes and have been extensively investigated for their potential applications in laser, display, bioassay, and bioimaging. In particular, NIR-to-visible up-conversion luminescent materials, which emit visible light upon NIR excitation, have attracted much attention in biomedicine due to the absence of photodamage to live organisms, low autofluorescence background, high signal-to-noise ratio, and high light penetration depth in biological tissues.[4,185] Up to now, a few examples of up-conversion luminescent lanthanide MOFs have also been reported. Yang et al. prepared a MOF $Nd_2(1,4\text{-NDC})_3(DMF)_4\cdot H_2O$ (1,4-NDC = 1,4-naphthalenedicarboxylate),[186] which exhibits a weak UV up-conversion emission at about 391.6 nm and a much stronger blue emission at about 449.5 nm upon pulse laser excitation at 580 nm. Weng et al. reported a Y:Er−Yb codoped MOF $[(Y{:}Er{-}Yb)_3(1,4\text{-BDC})_{3.5}(OH)_2(H_2O)_2]\cdot H_2O$,[187] which exhibits four emission bands of Er^{3+} under 980 nm laser excitation. The red emission attributed to the $^4F_{9/2} \rightarrow {}^4I_{15/2}$ transition is centered at 654 nm, and the green bands ascribed to the transitions of $^4S_{3/2}/{}^2H_{11/2} \rightarrow {}^4I_{15/2}$ are at 545 and 524 nm, respectively. A rarely observed indigo emission at 455 nm can also be observed, corresponding to the transition $^4F_{5/2} \rightarrow {}^4I_{15/2}$. The 545 and 524 nm emissions are described as a two photon up-conversion excitation mechanism, and the up-conversion process is also discussed. First, the Yb^{3+} ions are easily excited to their $^2F_{5/2}$ level by absorbing a 980 nm photon, and then the energy is transferred to the Er^{3+} ions, which can be excited to the $^4I_{11/2}$ level. A second photon transfer from the excited Yb^{3+} ions pumps the Er^{3+} ions from $^4I_{11/2}$ to the $^4F_{7/2}$ level, which can decay nonradiatively to the $^4S_{3/2}$ and $^2H_{11/2}$ levels. Thus, the green emissions observed result from the $^4S_{3/2} \rightarrow {}^4I_{15/2}$ and the $^2H_{11/2} \rightarrow {}^4I_{15/2}$ transitions. Furthermore, the 455 nm emission is explained through the three-photon up-conversion excitation mechanisms.

4.2. Transition-Metal-Based MOFs

Although a variety of transition metal ions have been used to construct MOFs, the Zn and Cd MOFs are the most commonly reported transition-metal-based luminescent MOFs because the d^{10} metal ions not only possess various coordination numbers and geometries, but also exhibit luminescent properties when bound to functional ligands. Recently, four Zn and Cd MOFs with helical nanochannels have been prepared via the solvothermal reactions of Zn or Cd nitrates and V-shaped organic linker of 4,4′-(hexafluoroisopropylidene)bis-(benzoic acid) ($H_2hfipbb$), $Zn(hfipbb)\cdot 0.5H_2O\cdot 0.5DMF$ enantiomers, $Zn(hfipbb)(4,4'\text{-bipy})\cdot DMF$, and $Cd(hfipbb)(DMF)\cdot 0.5DMF$.[188] The free $H_2hfipbb$ ligand shows a weak emission at 595 nm under excitation at 435 nm, and all of the Zn MOFs show the emissions at around 425 nm attributed to the LMCT transitions. Qiu et al. also prepared seven Cd MOFs via hydrothermal methods,[189] which exhibit three-dimensional (3D) frameworks constructed from cadmium octahedrons and tetrazole linkers. These MOFs show broad emission bands at 406, 405, 412, 422, 421, 394, and 395 nm, respectively, indicating that the luminescence can be tuned upon different organic linkers to same metal ions. A 2-fold interpenetrated MOF based on $[Zn_4O(COO)_6]$ clusters has been prepared through the solvothermal reaction of $Zn(Ac)_2$ with fluorene-2,7-dicarboxylic acid (H_2FDC) in DMSO and ethanol.[190] This MOF exhibits a 3D pillared kagomé topology in which $[Zn_4O(COO)_6]$ clusters are interlinked by the fluorene chromophore. The sodium salt of the organic linker (Na_2FDC) exhibits a relatively weak blue emission band at λ_{max} = 450 nm upon excitation at 315 nm, ascribed to the fluorene moiety. The

Table 1. Summary of Luminescent MOFs

metal	MOF	emission wavelength (nm)	ref
	Lanthanide-Based MOFs		
La	$[La(pmtz)(TzC)(H_2O)_3](H_2O)$	530	95
Ce	$[Ce_2(pydc)_2(\mu_4\text{-}SO_4)\cdot 5H_2O]\cdot 2H_2O$	357, 480	177
Nd	$Nd_2(1,4\text{-}NDC)_3(DMF)_4\cdot H_2O$	391.6, 449.5	186
	$[Nd_4(ox)_4(NO_3)_2(OH)_2(H_2O)_2]\cdot 5H_2O$	~1060	67
	$Nd(tta)_3(\mu\text{-bpm})\cdot MeOH$	~440, ~910, ~1070	91
	$Nd(HL_1)(H_2L_2)_{0.5}(H_4L_2)_{0.5}(H_2O)$, H_3L_1 = 5-sulfosaclicylicacid, H_4L_2 = *N*,*N*′-piperazine-(bis-methylenephosphonicacid)	892, 1059, 1349	134
	$[Nd(trans\text{-}DAM)_2(H_2O)_2]ClO_4\cdot 3H_2O$	912, 1059, 1333	136
	$[Nd(trans\text{-}DAM)_2(H_2O)_2]NO_3\cdot 3H_2O$	912, 1059, 1333	136
	$[Nd(trans\text{-}DAM)(cis\text{-}DAM)(H_2O)_2]Cl\cdot 5H_2O$	912, 1059, 1333	136
	$[Nd(trans\text{-}DAM)_2(H_2O)_2]Cl\cdot 5H_2O$	912, 1059, 1333	136
	$[Nd(H_2TETA)]NO_3\cdot 2H_2O$	~910, ~1060, ~1340	165
Sm	$[Sm(pta)(H_2O)_5]\cdot 4H_2O$	558, 592, 639	76
	$[Sm_4(pydc)_2(\mu_4\text{-}C_2O_4)_4\cdot 8H_2O]\cdot 6H_2O$	468, 566, 628	177
	$Sm_2(ATPA)_3(DMF)_2(H_2O)_2$	450, 561, 597, 644	107
Eu	$Eu(1,4\text{-}BDC)_3(H_2O)_4$	592, 617	182
	$Eu_2(1,4\text{-}BDC)_3(DMF)_2(H_2O)_2$	596, 616	183
	$[Eu(pta)(H_2O)_5]\cdot 4H_2O$	589, 613, 695	76
	$[Eu_2(adipic\ acid)_3(H_2O)_2]\cdot 4,4'\text{-dipyridyl}$	595, 615	163
	$Eu_3(2,6\text{-}pydc)_3(2,6\text{-}Hpydc)(SO_4)(H_2O)_3\cdot 3(H_2O)_3$	579, 592, 614, 651, 696	167
	$Na[EuL(H_2O)_4]\cdot 2H_2O$, L = 1,4,8,11-tetraazacyclotetradecane-1,4,8,11-tetrapropionic acid	592, 615, 696	52
	$Eu(PDC)_{1.5}(DMF)\cdot(DMF)_{0.5}(H_2O)_{0.5}$	590, 616, 698	54
	$Eu_2(FMA)_2(OX)(H_2O)_4\cdot 4H_2O$	591, 616, 650, 692	216
	$Eu(BTC)(H_2O)\cdot 1.5H_2O$	590, 616, 698	57
	$[Eu_2(\mu_2\text{-}pzdc)(\mu_4\text{-}pzdc)(\mu_2\text{-}ox)(H_2O)_4]\cdot 8H_2O$	591, 614, 649, 695	225
	$[Eu_4(BPT)_4(DMF)_2(H_2O)_8]\cdot(DMF)_5\cdot(H_2O)_3$	580, 650, 592, 617, 700	98
	$[Eu_2(fumarate)_2(oxalate)(H_2O)_4]\cdot 4H_2O$	591, 617,	227
	$Eu_2(1,4\text{-}BDC)_3(H_2O)_2\cdot(H_2O)_2$	590, 617, 698	60
	ITQMOF-1-Eu	619	56
	ITQMOF-3-Eu	579.0, 580.7, 612.3	235
	$Eu_2(2,5\text{-}pdc)_2(1,4\text{-}pda)(H_2O)_2$	~590, 615, ~698	164
	$Na_4[Eu_2(H_2O)_2(hedp)_2]\cdot H_2O$	~590, 613	135
	$Eu(HL_1)(H_2L_2)_{0.5}(H_4L_2)_{0.5}(H_2O)$, H_3L_1= 5-sulfosaclicylicacid, H_4L_2 = *N*,*N*′-piperazine-(bis-methylenephosphonicacid)	587, 613, 651, 698	134
	$Eu_2(1,4\text{-}BDC)_3(MeOH)_4]\cdot 8MeOH$	~590, ~615	176
	$[Eu_2(L)_3(DMSO)_4]\cdot x$DMSO, L = (*E*)-4,4′-(ethene-1,2-diyl)dibenzoate	447	132
	$Eu_2(L)_3(DMF)_2(H_2O)_2$, L = (*E*)-4,4′-(1,4-bis(methylthio)but-2-ene-2,3-diyl)dibenzoate	579, 591, 615, 696	132
	$[Eu(L)_4](H_2O)_nCl$, L= 4,4′-disulfo-2,2′-bipyridine-*N*,*N*′-dioxide	~590, ~615, ~650	85
	$[Eu(H_2TETA)]NO_3\cdot 2H_2O$	579, 592, 613, 651, 698	165
	$Eu_2(Hbidc)_2(ox)_2\cdot(H_2O)_3$	536, 594, 617, 651, 695	104
	$Eu_2(ATPA)_3(DMF)_2(H_2O)_2$	450, 616	107
	$[Eu_2L_3(DMSO)_2(MeOH)_2]\cdot 2DMSO\cdot 3H_2O$, L = 4,4′-ethyne-1,2-diyldibenzoate	593, 615, 698	109
Gd	$[Gd_2(Hpimda)_2(\mu_4\text{-}C_2O_4)\cdot 4H_2O]\cdot 2H_2O$	319, 476	177
	$[Gd_2(pyda)(\mu_4\text{-}C_2O_4)_2\cdot 4H_2O]\cdot 3H_2O$	299, 546	177
Tb	$Tb(1,4\text{-}BDC)_3(H_2O)_4$	491, 546	182
	$[Tb(pta)(H_2O)_5]\cdot 4H_2O$	491, 546, 584, 623	76
	$K_5[Tb_5(IDC)_4(ox)_4]$	489, 545, 589, 619	213
	$[Tb(Mucicate)_{1.5}\cdot(H_2O)_2]\cdot 5H_2O$	~490, ~545	55
	$Tb(BTC)\cdot methanol$	492, 548, 584, 620	53
	$TbNTA\cdot H_2O$	489, 547, 583, 625	220
	$Na[Tb(OBA)_2]_3\cdot 0.4DMF_3\cdot 1.5H_2O$	545	110
	$[Tb_4(BPT)_4(DMF)_2(H_2O)_8]\cdot(DMF)_5\cdot(H_2O)_3$	490, 544, 587, 621, 650	98

dx.doi.org/10.1021/cr200101d |*Chem. Rev.* 2012, 112, 1126–1162

Table 1. Continued

metal	MOF	emission wavelength (nm)	ref
	$[Tb_2(fumarate)_2(oxalate)(H_2O)_4]\cdot 4H_2O$	494, 545, 587, 621	227
	$Tb_2(2,5\text{-pdc})_2(1,4\text{-pda})(H_2O)_2$	544, ~585, ~620	164
	$Tb(4\text{-hydroxybenzenesulfonate})_3(H_2O)_2\cdot 2H_2O$	~490, ~545	133
	$Tb_3(1,4\text{-BDC})_{4.5}(DMF)_2(H_2O)_3\cdot(DMF)(H_2O)$	370, 430, 490, ~550, ~590	175
	$Tb(1,4\text{-BDC})(MeOH)_4]\cdot Cl\cdot MeOH\cdot 0.25H_2O$	~495, ~550	176
	$[Tb_2(L)_3(DMSO)_4]\cdot x$DMSO, L = (*E*)-4,4′-(ethene-1,2-diyl)dibenzoate)	447	132
	$Tb_2(L)_3(DMF)_2(H_2O)_2$, L = (*E*)-4,4′-(1,4-bis(methylthio)but-2-ene-2,3-diyl)dibenzoate	350−450, 542, 584, 620	132
	$[Tb(L)_4](H_2O)_nCl$, L= 4,4′-disulfo-2,2′-bipyridine-*N*,*N*′-dioxide	~490, ~545, ~585	85
	$[Tb(H_2TETA)]NO_3\cdot 2H_2O$	492, 545, 584, 620	165
	$[Tb_2(Hbidc)_2(ox)(H_2O)_2]\cdot 4H_2O$	490, 548, 590, 620	104
	$Tb_2(ATPA)_3(DMF)_2(H_2O)_2$	450, 489, 545, 587, 619	107
Dy	$Dy(1,4\text{-BDC})_3(H_2O)_4$	481, 575	182
	$[Dy(pta)(H_2O)_3]\cdot 4H_2O$	476, 569	76
	$K_5[Dy_5(IDC)_4(ox)_4]$	479, 573	213
	$[Dy_4(BPT)_4(DMF)_2(H_2O)_8]\cdot(DMF)_5\cdot(H_2O)_3$	480, 573, 662	98
	$Dy_3(1,4\text{-BDC})_{4.5}(DMF)_2(H_2O)_3\cdot(DMF)(C_2H_5OH)_{0.5}(H_2O)_{0.5}$	~370, ~400, ~430	175
	$Dy_2(ATPA)_3(DMF)_2(H_2O)_2$	450	107
Ho	$Ho_3(1,4\text{-BDC})_{4.5}(DMF)_2(H_2O)_3\cdot(DMF)(C_2H_5OH)_{0.5}(H_2O)_{0.5}$	~375, ~430	175
Er	$[Er(pta)(H_2O)_3]\cdot 4H_2O$	1538	76
	$Er_2(1,4\text{-BDC})_3(DMF)_2(H_2O)_2\cdot H_2O$	1550	268
	$Er_2(BDC\text{-}F_4)_3(DMF)(H_2O)\cdot DMF$	1550	268
	$Er_3(1,4\text{-BDC})_{4.5}(DMF)_2(H_2O)_3\cdot(DMF)(C_2H_5OH)_{0.5}(H_2O)_{0.5}$	~380, ~430	175
Yb	$[Yb(pta)(H_2O)_3]\cdot 4H_2O$	980	76
	$Yb(BPT)(H_2O)\cdot(DMF)_{1.5}(H_2O)_{1.25}$	980	224
	$[Yb_2(C_{26}H_{20}O_6)_3(H_2O)_2]\cdot(DMF)_6(H_2O)_{8.5}$	980	267
	$[Yb_2(C_{26}H_{20}O_6)_3(H_2O)_2]\cdot(DMF)_{12}(H_2O)_{10}$	980	267
	$Yb_2(TDC)_3(DMF)(H_2O)\cdot(CH_3CH_2OH)$	980	80
	Transition-Metal-Based MOFs		
Zn	$[Zn_4O(NTB)_2]\cdot 3DEF\cdot EtOH$	433	222
	$Zn_4O(1,4\text{-BDC})_3$	397	131
	$Zn_4(OH)_2(1,2,4\text{-BTC})_2$	428	229
	$Zn_3(TAA)_3(H_2O)_3\cdot(1,4\text{-dioxane})$	438	228
	$[Zn_4O(1,4\text{-BDC})(bpz)_2]\cdot 4DMF\cdot 6H_2O$	470	93
	$Zn_2(bpdc)_2(bpee)$	420	233
	Zn-BCPA	438	234
	$Zn_3(\mu_5\text{-pta})_2(\mu_2\text{-}H_2O)_2$	467	96
	$Zn_3(BTC)_2(DMF)_3(H_2O)\cdot(DMF)(H_2O)$	410	68
	$Zn_3(4,4'\text{-stilbene dicarboxylic acid})_3(DMF)_2$	396, 420, 441	66
	$Zn_4O(4,4'\text{-stilbene dicarboxylic acid})_3(DMF)(CHCl_3)$	371, 390, 409	66
	$[Zn(2,3\text{-pydc})(bpp)]\cdot 2.5H_2O$	436	70
	$Zn_2(ATA)_3(ATA)_{2/2}$	485	75
	$Zn(hfipbb)\cdot 0.5H_2O\cdot 0.5DMF$	425	188
	$Zn(hfipbb)(4,4'\text{-bipy})\cdot DMF$	425	188
	$Zn_5(\mu_3\text{-OH})_2(BTA)_2(tp)_3$	348	72
	$Zn(BTA)(chdc)_{0.5}$	380	72
	$Zn(BTA)(ap)_{0.5}$	360	72
	$Zn(BTA)(gt)_{0.5}$	358	72
	Zn(DFDA)	405, 422	82
	$[Zn_2(DFDA)_2(bis(imidazol\text{-}1\text{-}ylmethyl)benzene)_2]_23H_2O$	405, 426	82
	Zn(DFDA)(1,1′-(1,4-butanediyl)bis(imidazole))	405, 427	82
	Zn(DFDA)(2,2′-bipyridine)	411, 427	82
	$[ZnL_2(NCS)_2]CH_3CN$, L = *N*′,*N*′-bis[1-(pyridin-4-yl)methylidene]benzil dihydrazone	342	200
	$ZnL_2(NCS)_2$, L = *N*′,*N*′-bis[1-(pyridin-3-yl)methylidene]benzil dihydrazone	342	200
	$Zn_2(3\text{-tzba})(N_3)(OH)(2,2'\text{-bipy})$	420	116

dx.doi.org/10.1021/cr200101d |*Chem. Rev.* 2012, 112, 1126–1162

Table 1. Continued

metal	MOF	emission wavelength (nm)	ref
	$[Zn(3\text{-tzba})(2,2'\text{-bipy})(H_2O)]\cdot 3H_2O$	437, 465	116
	$[Zn_2(3\text{-tzba})_2(phen)_2]\cdot H_2O$	427	116
	$[Zn_2L_2(DMSO)_2]\cdot 1.6H_2O$, L = 4,4′-ethyne-1,2-diyldibenzoate	411, 487	109
	$Zn(cin)_2(L)]\cdot H_2O$, L = 1,1′-(1,4-butanediyl)bis(2-methylbenzimidazole)	423	114
	$Zn(cin)_2$(1,1′-(1,4-butanediyl)bis(2-ethylbenzimidazole))	465	114
	$[Zn(adi)(L)]\cdot H_2O$, L = 1,1′-(1,4-butanediyl)bis(2-methylbenzimidazole)	412, 441	114
	$[Zn(adi)(L)_{0.5}]$, L = 1,1′-(1,4-butanediyl)bis(2-ethylbenzimidazole)	390	114
	$Zn(sfdb)(bpy)(H_2O)]\cdot 0.5CH_3OH$	359	115
	$Zn_3(CTC)_2(bipy)\cdot(DMF)(H_2O)_2$	447, 552	73
	$Zn_3(CTC)_2(Bpe)\cdot(DMF)(H_2O)_2$	456, 560	73
Cd	$Cd(BDC\text{-}NH_2)(bpy)\cdot 4H_2O\cdot 2.5DMF$	435	58
	$Cd_4(BTC)_3(DMF)_2(H_2O)_2\cdot 6H_2O$	405	68
	$[Cd(2,3\text{-pydc})(bpp)(H_2O)]\cdot 3H_2O$	438	70
	$[Cd(dtba)(bpp)]_{3n}$	434, 482	143
	Cd(hfipbb)(DMF)·0.5DMF	425	188
	$Cd(5MT)_2$	406	189
	$Cd_5(N_3)(5MT)_9\cdot 0.12H_2O$	405	189
	$Cd_3(OH)Cl_{1.39}(N_3)_{0.61}(5MT)_3$	412	189
	$Cd_3(OH)Cl(N_3)(ATA)_3$	422	189
	$Cd_2(OH)Br(ATA)_2$	421	189
	$Cd_7Cl_2(5BT)_{12}(H_2O)_2$	394	189
	$Cd_7Br_2(5BT)_{12}(H_2O)_2$	395	189
	$Cd_2(BPVIC)_2(SCN)_4$	562	79
	$Cd(DFDA)(C_2H_5OH)$	418	82
	$Cd_2(DFDA)_2$(bis(imidazol-1-ylmethyl)benzene)$_2$	407, 428	82
	Cd(DFDA)(1,1′-(1,4-butanediyl)bis(imidazole))(DMF)	407, 428	82
	$[Cd_4(3\text{-tzba})_2(N_3)_4(2,2'\text{-bipy})_3]\cdot H_2O$	495	116
	$Cd_2L(H_2O)_2$, H_4L = tetrakis[3-(carboxyphenyl)oxamethyl] methane acid	398	103
	$Cd(cin)_2(L)]\cdot H_2O$, L = 1,1′-(1,4-butanediyl)bis(2-methylbenzimidazole)	438	114
	$Cd(cin)_2$(1,1′-(1,4-butanediyl)bis(2-ethylbenzimidazole))	408	114
	$[Cd(adi)(L)]\cdot 2H_2O$, L = 1,1′-(1,4-butanediyl)bis(2-methylbenzimidazole)	365, 441	114
	Cd(adi)(1,1′-(1,4-butanediyl)bis(2-ethylbenzimidazole))	360	114
	$[Cd(adi)(L)]\cdot 2H_2O$, L = 1,1′-(1,4-butanediyl)bis(2-benzylbenzimidazole)	445	114
	$[Cd(sfdb)(phen)_2]\cdot 2H_2O$	380	115
	$[Cd(sfdb)(bpy)_2]\cdot H_2O$	396	115
	Cd(sfdb)(quin)	385	115
	$Cd_3(sfdb)_2(Hsfdb)_2(phen)_2$	394	115
	Cd(sfdb)(bpy)	365	115
	$Cd_2(ABTC)(DMF)_3\cdot(DMF)_2$	402	126
	$Cd_3(CTC)_2(TED)(H_2O)_2\cdot(H_3O)_2Cl_2$	522	73
	$Cd_3(CTC)_2(bipy)(DMF)_2\cdot(DMF)(H_2O)_2$	449, 550	73
	$Cd_3(CTC)_2(Bpe)(DMF)_2\cdot(DMF)(H_2O)_2$	453, 556	73
Ag	$[Ag(4\text{-cyanobenzoate})L]\cdot H_2O$	427, 513, 566, 617	245
	$[Ag_8(L)_4](NO_3)_8\cdot 4H_2O$, L = bis(3,5-bis((1*H*-imidazol-1-yl)-methyl)-2,4,6-trimethylphenyl)methane	495	199
	$[\{Ag_2(L)_2\}(ClO_4)_2(CH_3CN)]$, L = *N*,*N*′-bis(pyridin-2-ylmethylene)benzene-1,4-diamine	451, 521	198
	$[\{Ag_2(L)_2\}(ClO_4)_2]$, L = 3,3′-dimethyl-*N*,*N*′-bis(pyridin-2-ylmethylene)biphenyl-4,4′-diamine	409, 432, 505, 526	198
	$[AgL]ClO_4$, L = *N*′,*N*′-bis[1-(pyridin-4-yl)methylidene]benzil dihydrazone	340	200
	$[AgL_2]BF_4$, L = *N*′,*N*′-bis[1-(pyridin-4-yl)methylidene]benzil dihydrazone	342	200
	$[AgL(NO_3)](CH_3CH_2OH)$, L = *N*′,*N*′-bis[1-(pyridin-4-yl)methylidene]benzil dihydrazone	339	200
	$[AgL(NO_3)]$, L = *N*′,*N*′-bis[1-(pyridin-3-yl)methylidene]benzil dihydrazone)	344	200
	$[Ag_2(PhPPy_2)_2Cl](ClO_4)$	∼510	197
	Ag(MES)$(L)_{0.5}$, L = 1,1′-(1,4-butanediyl)bis(2-methylbenzimidazole)	479	114
	$[Ag(MES)(L)_{0.5}]\cdot H_2O$, L = 1,1′-(1,4-butanediyl)bis(2-ethylbenzimidazole)	363	114
Cu	Cu_6(5,6-diphenyl-1,2,4-triazine-3-thiol)$_6\cdot(H_2O)$(DMSO)	660	223

dx.doi.org/10.1021/cr200101d |*Chem. Rev.* 2012, 112, 1126–1162

Table 1. Continued

metal	MOF	emission wavelength (nm)	ref
	$Cu_3(L)_2 \cdot 3H_2O$, L = 2,6-dicarboxy-4-hydroxypyridine	398, 478	147
	$Cu_5(SCN)_5$(3-Abpt)$_2$	559	169
	Cu(SCN)(3-Abpt)	570	169
	$Cu_2(SCN)_2$(4-PyHBIm)	569	169
	$Cu_2(SCN)_2$(3-PyHBIm)	530	169
	Cu(SCN)(4-Ptz)	435	169
	$Cu_2(SCN)_2$(2-PyBIm)(2-PyHBIm)	440	169
	$[Cu_{12}Br_2(CN)_{6/2}(SCH_3)_6][Cu(SCH_3)_2]$	575	196
	Cu_2I_2(DABCO)$_2$	551	35
	Cu_2I_2(piperazine)$_2$	560	35
	$Cu_2(CN)_2$(bpzm)	473	194
	$Cu_2(CN)_2$(bpze)	529	194
	$Cu_2(CN)_2$(bpzp)	515	194
	$[Cu(Pz)]_3$	542	144
	$[Cu_2(Bpz)]_n$	598	144
	$Cu_2(ABTC)(H_2O)_2 \cdot (DMF)_2(H_2O)$	392	126
Co	Co(L)(2,2′-bipy), L = dibenzothiophene-5,5′-dioxide-3,7-dicarboxylate	409	120
Mn	Mn(Hbidc)	726	168
	$[MnL_2(NCS)_2] \cdot (CH_3CH_2OH)$, L = *N*′,*N*′-bis[1-(pyridin-3-yl)methylidene]benzil dihydrazone)	356	200
Fe	$[FeL_2Cl_2] \cdot CH_3CN$, L = *N*′,*N*′-bis[1-(pyridin-3-yl) methylidene]benzil dihydrazone)	353	200
	Heterometal−Organic Frameworks		
Pr−Cu	$Pr(pydc)_3Cu_3(bipy)_3 \cdot m(H_2O)$	488, 532	207
Nd−Cd	$[NdCd(imdc)(SO_4)(H_2O)_3] \cdot 0.5H_2O$	430	201
Nd−Cu	$Nd(pydc)_3Cu_3(bipy)_3 \cdot 5(H_2O)$	895, 1062, 1345	207
Sm−Ag	$[SmAg(PDA)_2(H_2O)_3] \cdot 3H_2O$	563, 601, 644	205
Sm−Cu	$Sm(pydc)_3Cu_3(bipy)_3 \cdot 4(H_2O)$	563, 603, 645	207
	SmCu(nds)(isonicotinic acid)$_2 \cdot H_2O$	561, 599, 645	122
Sm−Ba	$Ba_2(H_2O)_4[SmL_3(H_2O)_2](H_2O)_nCl$, L = 4,4′-disulfo-2,2′-bipyridine-*N*,*N*′-dioxide	∼605, ∼640	139
Eu−Mn	$[Eu(PDA)_3Mn_{1.5}(H_2O)_3] \cdot 3.25H_2O$	∼590, 618	51
Eu−Fe	$[Eu(PDA)_3Fe_{1.5}(H_2O)_3] \cdot 1.5H_2O$	613	203
Eu−Ag	$[EuAg(PDA)_2(H_2O)_3] \cdot 3H_2O$	581, 593, 617, 651, 695	205
	$EuAg(pydc)_2(Hnic)_{0.5}$	∼580, ∼615	202
	EuAg(inic)$_2$(nicO)$\cdot 0.5H_2O$	∼580, ∼620	202
Eu−Ba	$Ba_2(H_2O)_4[EuL_3(H_2O)_2](H_2O)_nCl$, L = 4,4′-disulfo-2,2′-bipyridine-*N*,*N*′-dioxide	∼615	139
Eu−Cd	$[EuCd(imdc)(SO_4)(H_2O)_3] \cdot 0.5H_2O$	∼590, ∼618	201
Eu−Cu	$Eu(pydc)_3Cu_3(bipy)_3 \cdot 4(H_2O)$	579, 593, 615, 651	207
	$[EuCu(nic)_2(ox)] \cdot 2H_2O$	579, 591, 594, 616, 618	105
	EuCu(nds)(isonicotinic acid)$_2 \cdot H_2O$	579, 592, 619, 654, 704	122
Gd−Cd	$[GdCd(imdc)(SO_4)(H_2O)_3] \cdot 0.5H_2O$	355, 400−465, 544	201
Gd−Cu	$Gd(pydc)_3Cu_3(bipy)_3 \cdot 4(H_2O)$	488, 532	207
Gd−Mn	$[(Gd_2L)Mn(H_2O)_6] \cdot 0.5(H_2O)$, L = 3,3′-(4-Amino-4*H*-1,2,4-triazole-3,5-diyl)dibenzoic acid	428	242
Gd−Ba	$Ba_2(H_2O)_4[GdL_3(H_2O)_2](H_2O)_nCl$, L = 4,4′-disulfo-2,2′-bipyridine-*N*,*N*′-dioxide	416, 435, 448	139
Tb−Mn	$[Tb(PDA)_3Mn_{1.5}(H_2O)_3] \cdot 3.25H_2O$	∼490, ∼550	51
Tb−Ag	$[TbAg(PDA)_2(H_2O)_3] \cdot 3H_2O$	490, 545, 584, 622	205
Tb−Cd	$[TbCd(imdc)(SO_4)(H_2O)_3] \cdot 0.5H_2O$	490, 544, 584, 620	201
Tb−Cu	$Tb(pydc)_3Cu_3(bipy)_3 \cdot 4(H_2O)$	492, 544, 583, 622	207
	TbCu(nds)(isonicotinic acid)$_2 \cdot H_2O$	489, 544, 590, 619	122
Tb−Ba	$Ba_2(H_2O)_4[TbL_3(H_2O)_2](H_2O)_nCl$, L = 4,4′-disulfo-2,2′-bipyridine-*N*,*N*′-dioxide	∼490, ∼545	139
Dy−Ag	$[DyAg(PDA)_2(H_2O)_3] \cdot 3H_2O$	483, 573	205
Dy−Cd	$[DyCd(imdc)(SO_4)(H_2O)_3] \cdot 0.5H_2O$	478, 573, 657	201
Dy−Ba	$Ba_2(H_2O)_4[DyL_3(H_2O)_2](H_2O)_nCl$, L = 4,4′-disulfo-2,2′-bipyridine-*N*,*N*′-dioxide	∼640	139
Ho−Ag	$HoAg_5$(1,2-BDC)$_4$	995, 1400−1600	208
Er−Ag	$ErAg_5$(1,2-BDC)$_4$	1450−1650	208
	$ErAg_3(L)_3(H_2O)$, L = pyridine-2,6-dicarboxylic acid	1548	204

dx.doi.org/10.1021/cr200101d |*Chem. Rev.* 2012, 112, 1126–1162

Table 1. Continued

metal	MOF	emission wavelength (nm)	ref
	$ErAg_3(L)_2(H_2O)$, L = 4-hydroxylpyridine-2,6-dicarboxylic acid)	1540	204
Er−Cu	$Er(pydc)_3Cu_3(bipy)_3\cdot 4(H_2O)$	488, 532	207
Yb−Cd	$[YbCd(imdc)(SO_4)(H_2O)_3]\cdot 0.5H_2O$	433	201
Yb−Ag	$YbAg_5(1,2\text{-}BDC)_4$	950−1050	208
Yb−Cu	$Yb(pydc)_3Cu_3(bipy)_3\cdot 4(H_2O)$	980	207
Eu−Ce	$[Eu(dipicH)(H_2O)_6][Ce(dipic)_3]_3\cdot 7H_2O$	∼590, ∼615	99
Eu−Tb	$Eu_{1-x}Tb_x(BTC)(H_2O)$	540, 589, 615	239
	$Tb(1,3,5\text{-}BTC)(H_2O)\cdot 3H_2O{:}Eu^{3+}$	487, 543, 580, 620	240
	$[(Eu, Tb)(C_6H_8O_4)_3(H_2O)_2]\cdot(C_{10}H_8N_2)$	545, 595, 615	97
	$(Eu_{0.2}Tb_{0.8})_2(2,5\text{-}pdc)_2(1,4\text{-}pda)(H_2O)_2$	∼545, ∼595, ∼620	164
Dy−Ce	$[Dy(dipicH)(H_2O)_6][Ce(dipic)_3]_3\cdot 7H_2O$	∼480, ∼575	99
Er−Yb	Er_xYb_{1-x}-PVDC-1	980, 1530	269
Gd−Eu	$Gd_{0.95}(1,4\text{-}BDC)_{1.5}(H_2O)_2{:}Eu_{0.05}$	red luminescence	63
Gd−Tb	$Gd_{0.95}(1,4\text{-}BDC)_{1.5}(H_2O)_2{:}Tb_{0.05}$	green luminescence	63
Zn−Ir	$[Zn_4(\mu_4\text{-}O)(Ir(2\text{-pyridyl-benzoic acid})_3)_2]\cdot 6DMF\cdot H_2O$	538	232
Cu−Ag	$CuAg_2(L)_2$, L = 2,6-dicarboxy-4-hydroxypyridine	515	147
	Main Group Metal−Organic Frameworks		
In	$In_2(OH)_2(TBAPy)$	471	210
Bi	$Bi_3(\mu_3\text{-}O)_2(pydc)_2(Hpydc)(H_2O)_2$	430, 460, 480, 556	209
Pb	$Pb(pydc)(H_2O)$	441, 470, 520, 563	209
	$Pb_4(1,3\text{-}BDC)_3(\mu_4\text{-}O)(H_2O)$	424	211
	Pb(bpdc)	480	212
Mg	$Mg(DHT)(DMF)_2$	508 (in DMSO)	156

emission at 450 nm is quenched, while a new intense emission at 553 nm appeared in the formed MOF.

Liu et al. prepared a Cd MOF $Cd_2(BPVIC)_2(SCN)_4$ by using a large π-conjugated bidentate organic linker 2,8-bis[2-(2-pyridyl)vinyl]-5,11-di(2-ethylhexyl)-indolo[3,2-b]carbazole (BPVIC).[79] Upon excitation at 452 nm, the free organic linker shows a maximum emission at 477 nm, while the emission peak of the Cd MOF is significantly red-shifted to 562 nm under excitation at 480 nm with significantly enhanced intensity. The luminescence lifetime of the resulting MOF is 3 times longer than that of the free organic linker. The luminescence and lifetime differences between the MOF and free organic linker are explained by the intramolecular and intermolecular electronic and steric factors. In this Cd MOF, a new π-electron system with an optimized delocalization environment and a narrow $\pi-\pi^*$ energy gap can be formed due to the Cd^{2+} ions coordination, which results in the relatively easy transition between S_0 and S_1 states. Furthermore, the $\pi-\pi$ and C−H$\cdots$ π interactions between the organic linkers are eliminated due to the infinite $Cd(NCS)_2$ zigzag chain in the Cd MOF, decreasing the probability of nonradiative decay.

The mixed-ligands approach by the judicious choice of organic linkers has been widely utilized to construct novel transition-metal-based MOFs.[72,73,82,86,191−193] Yang et al. synthesized four Zn MOFs, $Zn_5(\mu_3\text{-}OH)_2(BTA)_2(tp)_3$, $Zn(BTA)(chdc)_{0.5}$, $Zn(BTA)(ap)_{0.5}$, and $Zn(BTA)(gt)_{0.5}$ (BTAH = benzotriazole, H_2tp = terephthalic acid, H_2chdc = 1,4-cyclohexanedicarboxylic acid, H_2ap = adipic acid, and H_2gt = glutaric acid), by the reaction of zinc chloride and BTAH with four different aromatic/aliphatic binary acids under similar hydrothermal conditions.[72] The structures of MOFs are highly related to the spacers of the secondary dicarboxylate organic linkers: the MOF $Zn_5(\mu_3\text{-}OH)_2(BTA)_2(tp)_3$ is an eight-connected self-penetrating framework based on pentanuclear Zn^{2+} clusters; $Zn(BTA)(chdc)_{0.5}$ is a 3D infinite network with empty 34-membered hexanuclear Zn^{2+} metallamacrocycle channels; and $Zn(BTA)(ap)_{0.5}$ and $Zn(BTA)(gt)_{0.5}$ are frameworks with 1D Zn-BTA helical chains motifs. These MOFs all exhibit enhanced ligand-based luminescence due to the increasing rigidity of organic linkers within the coordination polymers. Guo et al. also synthesized a series of Zn and Cd MOFs using the 9,9-dipropylfluorene-2,7-dicarboxylate anion (H_2DFDA) and three N-donor 1,4-bis-(imidazol-1-ylmethyl)benzene, 1,1′-(1,4-butanediyl)-bis(imidazole), and 2,2′-bipyridine auxiliary ligands.[82] The MOFs all show the ligand-based fluorescence in which the N-donor ligands do not contribute to the fluorescent emission.

A series of luminescent Cu and Ag MOFs have been reported.[35,144,169,194−198] A 12-connected pseudo-pcu topological Cu MOF $[Cu_{12}Br_2(CN)_{6/2}(SCH_3)_6][Cu(SCH_3)_2]$ has been synthesized through the solvothermal reaction of copper thiocyanate (CuSCN) with tetrabutylammonium bromide in acetonitrile and methanol.[196] This MOF displays a strong broad yellow-luminescent emission band in the solid state at 575 nm upon excitation at 386 nm. Density functional theory calculation indicates that the luminescence may be mainly attributed to the coupling of MLCT and metal-centered transitions. The unusual solid-state reactions of copper iodide with 1,4-diazabicyclo-[2.2.2]octane (DABCO) and piperazine resulted in the formation of Cu MOFs $Cu_2I_2(DABCO)_2$ and $Cu_2I_2(piperazine)_2$,[35] which exhibit bright emissions in the solid state at room temperature. Their emissions were significantly red-shifted at 77 K. Furthermore, these two isostructural 2D MOFs exhibit unusually long luminescence lifetime of 125 and 53 ms, respectively, at room temperature. At 77 K, they have ever longer luminescence lifetimes of 609 and 420 ms, respectively. The Ag MOF $[Ag_8(L)_4](NO_3)_8\cdot 4H_2O$ with 3-fold interpenetrating dia-g net has been solvothermally synthesized by the reaction of a

tetradentate imidazolate organic linker bis(3,5-bis((1*H*-imidazol-1-yl)methyl)-2,4,6-trimethylphenyl)methane (L) with $AgNO_3$.[199] This MOF displays a fluorescence emission at 495 nm attributed to the ligand-centered emission under the excitation at 364 nm.

Two examples of Fe and Mn luminescent MOFs $[FeL_2Cl_2]\cdot CH_3CN$ and $[MnL_2(NCS)_2]\cdot(CH_3CH_2OH)$ (L = *N*′,*N*′-bis-[1-(pyridin-3-yl)methylidene]benzil dihydrazone) have been reported.[200] Both MOFs show one-dimensional chain structures containing bimetallic 34-membered quadrangular rings. The free organic linker exhibits emission at 336 nm upon excitation at 237 nm, and the two formed MOFs display similar broad-band fluorescent emission at 353 and 356 nm ascribed to the ligand-centered emission upon excitation at 242 and 238 nm, respectively.

4.3. Heterometal−Organic Frameworks

Luminescent heterometal−organic frameworks (HMOFs) are currently attracting a great deal of interest because the coexistence of heterometallic ions in MOFs not only contributes to the construction of fascinating structures but also tunes the energy levels of the MOFs.[201−208] So far, most of the reports are focused on transition-lanthanide (d−f) HMOFs, which can be prepared through the reaction of a mixture of d−f heterometallic ions with the multidentate bridging ligand containing both N- and O-donor atoms. Because there exists the competitive reaction between lanthanide and transition metal ions with the organic ligands by this approach, sometimes homometallic MOFs instead of heterometallic MOFs were constructed.

Sun et al. prepared a series of Ln−Cd HMOFs $[LnCd(imdc)(SO_4)(H_2O)_3]\cdot 0.5H_2O$ (Ln = Tb, Eu, Dy, Gd, Er, Yb, Nd, and Pr) using the H_3imdc organic linker.[201] The frameworks display both 1D helical channels occupied by water molecules and SO_4^{2-} anions and helical tubes constructed from three distinct helical chains. The Eu−Cd, Tb−Cd, and Dy−Cd HMOFs display the characteristic emission of lanthanide ions, while the Gd−Cd HMOF exhibits three broad bands, which may be attributed to the LMCT transition, ligand-centered fluorescence, and ligand phosphorescence, respectively. The Nd−Cd and Pr−Cd NMOFs do not exhibit near-infrared (NIR) luminescence, indicating that the organic linker cannot efficiently sensitize Pr^{3+} and Nd^{3+} ions to generate the NIR luminescence.

Eu−Ag HMOFs $EuAg(pydc)_2(Hnic)_{0.5}$ (Hnic = nicotinic acid) and $EuAg(inic)_2(nicO)\cdot 0.5H_2O$ (H_2nicO = 2-hydroxynicotinic acid) were presented by Gu et al.[202] The structures of these two Eu−Ag HMOFs consist of 1D inorganic heterometallic chains, which are bridged by linear organic linkers. Because of the inefficient ligand-to-silver energy transfer, these HMOFs only exhibit the characteristic transition of $^5D_0 \rightarrow {}^7F_J$ ($J = 0-4$) of Eu^{3+} ions upon excitation at 320 nm, and the appearance of the symmetry-forbidden $^5D_0 \rightarrow {}^7F_0$ emission at 580 nm indicates that Eu^{3+} ions possess the noncentrosymmetric coordination environment. Eight Ln-Ag HMOFs $[PrAg(PDA)_2(H_2O)_3]\cdot 2.5H_2O$ (H_2PDA = pyridine-2,6-dicarboxylic acid), $[LnAg(PDA)_2(H_2O)_3]\cdot 3H_2O$ (Ln = Ce^{3+}, Nd^{3+}, Sm^{3+}, Eu^{3+}, Tb^{3+}, Dy^{3+}), and $[CeAg_2(PDA)_3(Py)_4]\cdot H_2O$ (Py = pyridine) have been synthesized under hydrothermal conditions.[205] The Sm−Ag, Eu−Ag, Tb−Ag, and Dy−Ag HMOFs exhibit the characteristic bands of the corresponding lanthanide ions both in the solid state and in DMF at room temperature. Interestingly, the emission intensity of Dy−Ag and Tb−Ag HMOF increases significantly and slightly, respectively, while the emission intensity of Eu−Ag HMOF decreases slightly, upon addition of Mg^{2+} in DMF.

A series of NIR luminescent Ln−Ag HMOFs, $LnAg_5(1,2\text{-}BDC)_4$ (Ln = Yb, Er, Ho, 1,2-BDC = 1,2-benzenedicarbolylate), have been reported by Jin et al.[208] The HMOF $YbAg_5(1,2\text{-}BDC)_4$ shows a broad emission band ranging from 950 to 1050 nm assigned to the $^2F_{5/2} \rightarrow {}^2F_{7/2}$ transition of the Yb^{3+} ion, and the $ErAg_5(1,2\text{-}BDC)_4$ exhibits a broad emission band extending from 1450 to 1650 nm attributed to the $^4I_{13/2} \rightarrow {}^4I_{15/2}$ transition of an Er^{3+} ion. The $HoAg_5(1,2\text{-}BDC)_4$ displays an emission at 995 nm assigned to the $^5F_5 \rightarrow {}^5I_7$ transition of Ho^{3+} ion and a band from 1400 to 1600 nm corresponding to the splitting of $^5F_5 \rightarrow {}^5I_6$ transition. Especially, the NIR emission for these HMOFs shows shift, splitting, or broadening emission spectra as compared to the isolated lanthanide ions, which might be attributed to the interaction and influence of 4d and 4f orbitals. Jin et al. speculated that the Ag−Ln distance becomes much shorter (ranging from 3.71 to 3.75 Å) upon formation of the Ag−Ln HMOFs, so the 4d orbital of the Ag^+ ion and 4f orbital of the Ln^{3+} ions may interact and influence each other, resulting in the tuned inner levels of the Ag−Ln system and shifting and/or split of the lower energy states of Ln^{3+} ions. Other NIR luminescent HMOFs include a infinite triple-stranded helical framework $ErAg_3(L)_3(H_2O)$ (L = pyridine-2,6-dicarboxylic acid) and a sandwich-type 3D framework $ErAg_3(HO-L)_2(H_2O)$ (HO−L = 4-hydroxylpyridine-2,6-dicarboxylic acid).[204] The HMOF $ErAg_3(L)_3(H_2O)$ shows a broad emission band at 1548 nm ascribed to the $^4I_{13/2} \rightarrow {}^4I_{15/2}$ transition of Er^{3+} ion. Similarly, $ErAg_3(HO-L)_2(H_2O)$ exhibits an emission band with the strongest peak at 1540 nm.

Several examples of Ln−Cu HMOFs with mixed bridging ligands $Ln(pydc)_3Cu_3(bipy)_3\cdot m(H_2O)$ (Ln = Pr, Nd, $m = 5$; Ln = Sm, Eu, Gd, Tb, Er, Yb, $m = 4$; pydc = 2,6-pyridinedicarboxylate anion; bipy = 4,4′-bipyridine) have reported by Bo et al.[207] During the self-assembly process, the heterometallic ions are interconnected by mixed ligands to produce spindle-shaped heterometallic rings $[Ln_6(pydc)_6Cu_{12}(bipy)_6]$ as the SBUs, which are pillared by bridging bipy molecules to yield the porous 3D pillared-layer Ln−Cu HMOFs. The Nd−Cu HMOFs display the strongest emission band at 1062 nm ascribed to the $^4F_{3/2} \rightarrow {}^4I_{11/2}$ transition of Nd^{3+} ion, a broad emission band centered at 895 nm attributed to the $^4F_{3/2} \rightarrow {}^4I_{9/2}$ transition, and a sharp weak emission at 1345 nm corresponding to the $^4F_{3/2} \rightarrow {}^4I_{13/2}$ emission. The Yb−Cu HMOF also displays a strong emission at 980 nm attributed to the $^2F_{5/2} \rightarrow {}^2F_{7/2}$ transition of the Yb^{3+} ion in the near-infrared region upon the excitation at 275 nm. All Sm−Cu, Eu−Cu, and Tb−Cu HMOFs exhibit the characteristic emission of the corresponding lanthanide ions, while the Pr−Cu, Gd−Cu, and Er−Cu HMOFs display two intense emission peaks at 488 and 532 nm, similar to those found in Cu(I) complexes, which are assigned to the emission from MLCT transition.

4.4. Main Group Metal−Organic Frameworks

Up to date, only a few luminescent main group metal−organic frameworks such as bismuth-, lead-, indium-, and magnesium-based MOFs have been reported.[156,209−212] An example of luminescent In-pyrenetetrabenzoate MOF was reported by Stylianou et al.[210] They incorporated a highly fluorescent pyrene-derived organic linker with an indium ion to form a permanently microporous fluorescent metal−organic framework $In_2(OH)_2(TBAPy)$ (H_4TBAPy = 1,3,6,8-tetrakis(*p*-benzoic acid)pyrene). Upon excitation at 390 nm, the free ligand TBAPy displays an emission band at 529 nm, while the MOF

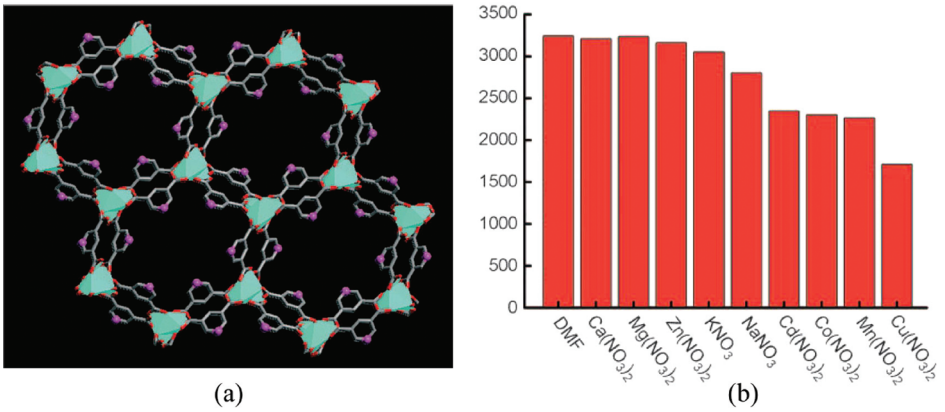

Figure 6. (a) Crystal structure of $Eu(PDC)_{1.5}(DMF)\cdot(DMF)_{0.5}(H_2O)_{0.5}$, viewed along the *a* axis, indicating immobilized Lewis basic pyridyl sites oriented toward pore centers. C gray, N purple, O red, Eu green polyhedra. Hydrogen atoms, terminal DMF molecules, and solvent molecules are omitted for clarity. (b) Comparison of the luminescence intensity of dehydrated MOF $Eu(PDC)_{1.5}$ incorporating different metal ions in 10 mM DMF solutions of $M(NO_3)_x$. Reprinted with permission from ref 54. Copyright 2009 Wiley-VCH.

shows a strong linker-centered fluorescence band at 471 nm. Its lifetime of about 0.11 ms is longer than that of the uncoordinated TBAPy ligand. When the desolvated MOF was immersed in different solvents, solvent-dependent luminescent spectra were observed. The combination of linker-based fluorescence with large robust pores and a high BET surface area (>1000 m^2/g) allows the emission wavelength, lifetime, and luminescent intensity to be tuned by varying the amount and chemical nature of the guest species in the pores.

A novel 3D lead MOF $Pb_4(1,3\text{-BDC})_3(\mu_4\text{-O})(H_2O)$ (1,3-BDC = 1,3-benzenedicarboxylate) exhibiting an eight connected bcu-type topological motif has been synthesized by Yang et al.[211] Upon excitation at 374 nm, the lead MOF shows a slightly stronger emission at 424 nm, while the organic linker exhibits a emission at 385 nm upon excitation at 327 nm, corresponding to the $\pi^* \rightarrow$ n transitions. The strong emission of this MOF is assigned to LMCT from delocalized π bonds of carboxylate groups to p orbitals of Pb^{2+} ions. Another lead MOF Pb(bpdc) (bpdc = 4,4′-biphenyldicarboxylate) has been reported by Hu et al.[212] In this MOF, the oxygen atoms of the carboxylate groups link the Pb^{2+} to form metal−carboxylate layers, and the bpdc ligands display a μ_6 coordination mode and act as pillars to connect adjacent layers into a 3D pillared framework. The free ligand bpdc shows an emission peak at approximately 440 nm upon excitation at 340 nm, while the MOF displays an enhanced luminescent peak at 480 nm attributed to the LMCT transitions under excitation at 376 nm. Wibowo et al. also reported a bismuth MOF $Bi_3(\mu_3\text{-O})_2(pydc)_2(Hpydc)(H_2O)_2$ and a lead MOF Pb-(pydc)(H_2O),[209] which exhibit white photoluminescence.

5. APPLICATIONS

Luminescent MOFs have been widely examined for their potential applications in fluorescent sensors, nonlinear optics, photocatalysis, displays, electroluminescent devices, and biomedical imaging. Of particular interest are their chemical sensors for their potentially practical applications in environmental and biological system. As we mentioned before, the collaborative functionalities of permanent porosity and luminescent property have enabled luminescent MOFs to be a very promising new type of sensing materials. Luminescent MOFs might also be utilized as light-emitting devices for white light and near-infrared light emitting. Nanoscale luminescent MOFs have started to be explored for their applications on tissue and cell imaging, as well as drug delivery monitoring and treatment.

5.1. Chemical Sensors

As mentioned before, the luminescent properties of MOFs are very sensitive to and dependent on their structural characteristics, coordination environment of metal ions, nature of the pore surfaces, and their interactions with guest species through coordination bonds, and $\pi-\pi$ interactions and hydrogen bonding etc., which have provided the solid rationale to develop luminescent sensing MOFs. The permanent porosity within some porous luminescent MOFs has enabled the reversible uptake and release of some sensing substrates; thus the exploration of reversible luminescent sensing MOFs will be feasible, so sensing MOFs can be regenerated and repeatedly utilized. The tunable pore sizes for their selective recognition of small molecules/ions and functional sites such as Lewis basic/acidic sites and open metal sites for their differential interactions with guest molecules within porous luminescent MOFs will certainly enhance their sensing sensitivity, while the mesoporous nature of some mesoporous luminescent MOFs will make sensing of some large molecules such as biologically active species possible. Over the past few years, a wide range of luminescent MOFs, particularly lanthanide-based MOFs, for sensing cations, anions, small molecules, vapors, and explosives have been realized and reported.

5.1.1. Sensing of Cations and Anions. In 2004, the first lanthanide MOF $Na[EuL(H_2O)_4]\cdot 2H_2O$ (L is 1,4,8,11-tetraazacyclotetradecane-1,4,8,11-tetrapropionic acid) for sensing cations was reported by Liu et al.[52] The effects of the different cations Cu^{2+}, Ag^+, Zn^{2+}, Cd^{2+}, and Hg^{2+} on the fluorescence spectrum of the MOF, in which the cation enters the empty coordination site in the azacycle of the ligand, indicate that the cations Cu^{2+}, Zn^{2+}, Cd^{2+}, and Hg^{2+} can reduce the fluorescence intensity of the MOF. Significantly, when Ag^+ enters into the empty coordination site, the emission spectrum of Eu^{3+} changed from multiple peaks to a single peak in which the emission intensity of the hypersensitive $^5D_0 \rightarrow {}^7F_2$ transition increased by 4.9 times, while the other $^5D_0 \rightarrow {}^7F_J$ transition (J = 1, 4) transitions largely diminished. Such luminescent change could be attributed to enhanced rigidity and modified paramagnetic spin state of the MOF through the coordination of Ag^+.

dx.doi.org/10.1021/cr200101d |*Chem. Rev.* 2012, 112, 1126–1162

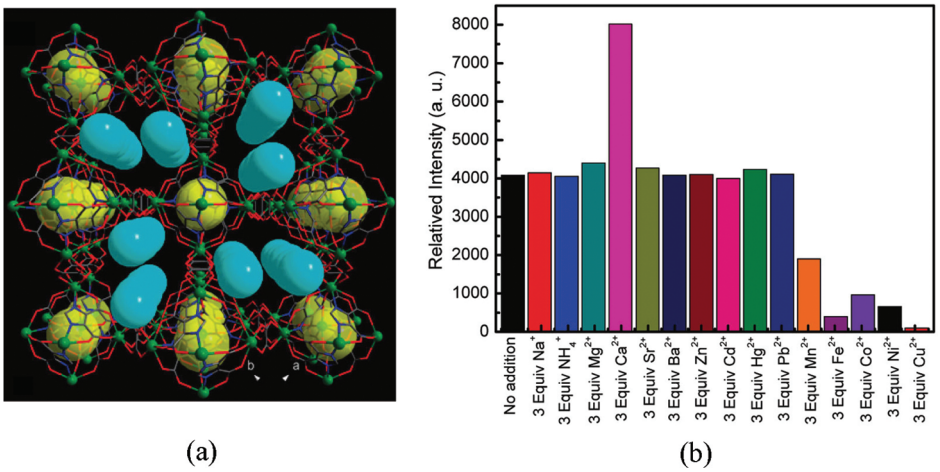

Figure 7. (a) View of MOF $K_5[Tb_5(IDC)_4(ox)_4]$ along the *c* axis, in which K^+ ions are located within the 1D channels (yellow spheres, octahedronaccessible cages; turquoise spheres, K^+ ions; the water molecules are omitted for clarity). (b) Luminescent intensities of a $^5D_4 \rightarrow {}^7F_5$ transition of $K_5[Tb_5(IDC)_4(ox)_4]$ in DMF (10^{-3} M) upon the addition of various cations. Reprinted with permission from ref 213. Copyright 2009 American Chemical Society.

To immobilize Lewis basic sites within porous MOFs as sensing sites, Chen et al. synthesized a luminescent MOF $Eu(PDC)_{1.5}(DMF)\cdot(DMF)_{0.5}(H_2O)_{0.5}$ (PDC = pyridine-3,5-dicarboxylate) by making use of the preferential binding of lanthanide ions to carboxylate oxygen atoms over pyridyl nitrogen atoms in Ln^{3+}-pyridinecarboxylate MOF (Figure 6a).[54] Because of the different binding of these free Lewis basic pyridyl sites with metal ions, the activated MOF $Eu(PDC)_{1.5}$ exhibits a sensing function for metal ions: alkali metal ions and alkaline-earth metal ions have a negligible effect on the luminescence intensity, whereas Co^{2+}, especially Cu^{2+}, can reduce the luminescence intensity significantly (Figure 6b). It is speculated that the binding of the pyridyl nitrogen atoms to Cu^{2+} or Co^{2+} reduces the antenna efficiency of the PDC organic linkers to magnify the f−f transitions of Eu^{3+}, resulting in quenching of the luminescence.

The unusual examples of heterometal−organic frameworks for recognition and sensing of metal ions were explored by Zhao and Cheng et al.,[51,203,205] who synthesized a series of Ln−Mn, Ln−Fe, and Ln−Ag heterometal−organic frameworks. The Ln−Mn-based frameworks $[Eu(PDA)_3Mn_{1.5}(H_2O)_3]\cdot 3.25H_2O$ and $[Tb(PDA)_3Mn_{1.5}(H_2O)_3]\cdot 3.25H_2O$ (PDA = pyridine-2,6-dicarboxylic acid) display a significant increase of fluorescence intensity after the addition of Zn^{2+}, while the introduction of other metal ions such as Mn^{2+}, Ca^{2+}, Mg^{2+}, Fe^{2+}, Co^{2+}, and Ni^{2+} would not change or even reduce the luminescence intensity. The authors suggested that the Zn^{2+}-sensitive sensor operates through a photoinduced electron-transfer process and the enhanced luminescence may result from more effective intramolecular energy transfer from the ligand to the Eu^{3+}or Tb^{3+}. Zhao et al. also reported a Ln−Fe-based MOF $[Eu(PDA)_3Fe_{1.5}(H_2O)_3]\cdot 1.5H_2O$ (PDA = pyridine-2,6- dicarboxylic acid) for metal ions sensing.[203] In contrast to the previous examples, introduction of Zn^{2+} would weaken the Eu^{3+} luminescence of the $^5D_0 \rightarrow {}^7F_2$ transition, but the emission intensity of $[Eu(PDA)_3Fe_{1.5}(H_2O)_3]\cdot 1.5H_2O$ increased gradually with the increase of the Mg^{2+} concentration. The similar work for sensing of Mg^{2+} based on Dy−Ag heterometal−organic frameworks was also reported.[205]

The luminescent properties of a MOF could be tuned through the exchange of metal ions or organic cations within anionic MOFs, which provide another possible route to probe cations. Lu et al. presented a lanthanide anionic MOF $K_5[Tb_5(IDC)_4(ox)_4]$ (IDC = imidazole-4,5-dicarboxylate, ox = oxalate),[213] in which the guest K^+ ions can be exchanged with various cations (Figure 7a). The intensity of the $^5D_4 \rightarrow {}^7F_5$ emission of Tb^{3+} is significantly enhanced upon the addition of Ca^{2+} ions. Furthermore, the fluorescence lifetime increased from 158.90 to 287.48 μs upon the addition of 3 equiv of Ca^{2+}. Other cations such as Na^+, NH_4^+, Mg^{2+}, Sr^{2+}, Ba^{2+}, Zn^{2+}, Cd^{2+}, Hg^{2+}, and Pb^{2+} do not affect the luminescent intensity, and the transition-metal ions such as Mn^{2+}, Fe^{2+}, Co^{2+}, Ni^{2+}, and Cu^{2+} can weaken dramatically the luminescent intensities (Figure 7b). The sensing mechanism could be attributed to the stronger interactions between Ca^{2+} and ox^{2-}, which make ox^{2-} more rigid, thus reducing the vibration-induced deactivation of ox^{2-} and increasing the energy transfer efficiency from the ligand to Tb^{3+}.

In living biological systems, particularly in the brain, Cu^{2+} is one of the most essential and important ions.[214,215] The efficient, straightforward, and real time detection of trace amounts of Cu^{2+} in the brain is helpful to diagnose and treat the diseases induce by copper metabolism disorders. Recently, the first example of lanthanide MOFs for highly sensitive and selective sensing of Cu^{2+} in aqueous solution and simulated physiological aqueous solution was demonstrated by Xiao et al.[216] These authors prepared a luminescent MOF $Eu_2(FMA)_2(OX)(H_2O)_4\cdot 4H_2O$ (FMA = fumarate; OX = oxalate), whose luminescent intensity is heavily metal ion dependent: alkaline metal ion and alkaline-earth metal ions have basically no effect on the luminescence intensity, while Cu^{2+} has the largest quenching effect, and the fluorescence lifetime of 394.60 ms in $Eu_2(FMA)_2(OX)(H_2O)_4\cdot 4H_2O$ is very significantly reduced to 30.45 ms in the presence of 10^{-2} M Cu^{2+}. The sensing of Cu^{2+} in the simulated physiological aqueous solution is also explored, and the comparable result is observed, indicating this MOF is suitable to probe Cu^{2+} ion in a biological system. A similar example for sensing of Cu^{2+} and Co^{2+} in aqueous solution is reported by Luo et al.[171] Instead of lanthanide MOFs, they utilized a lanthanide-doped approach to obtain luminescent MOF. The Eu^{3+}- and Tb^{3+}-doped MOFs were prepared by immersing the the $[NH_4]_2[ZnL]\cdot 6H_2O$ (L = 1,2,4,5-benzenetetracarboxylate) in $EuCl_3$ or $Tb(ClO_4)_3$

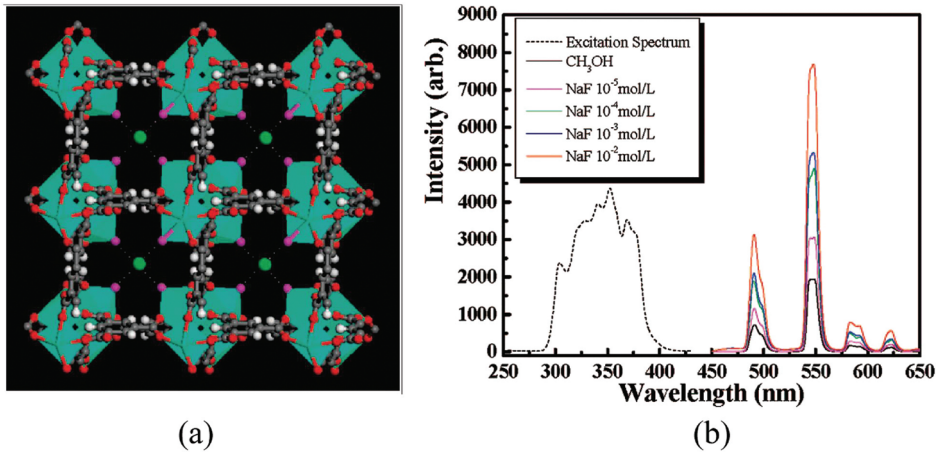

Figure 8. (a) Single crystal X-ray structure of MOF-76b activated in methanol containing NaF with the model of fluoride (green) at the center of the channel involving its hydrogen-bonding interaction with terminal methanol molecules (methanol oxygen, purple; the methyl group from methanol is omitted for clarity). (b) Excitation (dotted) and PL spectra (solid) of MOF-76b solid activated in different concentrations of NaF methanol solution (excited and monitored at 353 and 548 nm, respectively). Reprinted with permission from ref 53. Copyright 2008 American Chemical Society.

solutions through ion exchange of NH_4^+. Subsequently, the obtained lanthanide-doped MOFs were immersed in the MCl_x (M = Na^+, K^+, Zn^{2+}, Ni^{2+}, Mn^{2+}, Co^{2+}, Cu^{2+}) solutions to monitor the luminescent intensity. These doped MOFs show a negligible effect on the luminescence intensity for the Na^+, K^+, Zn^{2+}, while they are highly sensitive to the Co^{2+} (in Tb@MOF) and Cu^{2+} (in Eu@-MOF), respectively. The highly sensitive and selective sensing of metal ions in aqueous solution will certainly extend the application of luminescent MOFs in biology and biomedicine.

In environmental and biological systems, many inorganic anions such as F^-, Cl^-, Br^-, SO_4^{2-}, PO_4^{3-}, and CN^- play fundamental roles;[217,218] therefore, the sensing of anions by MOFs is also an interesting theme. Wong et al. prepared a lanthanide-mucicate framework $[Tb(Mucicate)_{1.5}\cdot(H_2O)_2]\cdot 5H_2O$,[55] which can act as a luminescent receptor for reversible selective anion monitoring. This MOF features a 2D coordination network with a 1D channel that runs across the coordination layers. The luminescent intensity of the Tb^{3+} was enhanced upon addition of an aqueous solution of sodium salts of I^-, Br^-, Cl^-, F^-, CN^-, and CO_3^{2-} to a solid sample of $[Tb(Mucicate)_{1.5}\cdot(H_2O)_2]\cdot 5H_2O$: CO_3^{2-}, CN^-, and I^- anions increased the luminescence, while SO_4^{2-} and PO_4^{3-} showed no significant enhancement. Hydrogen-bonding interactions between the guest ions in the channels and the OH groups of the organic skeleton are thought to reduce the vibrational movements of the channels and diminish the quenching effect of O−H bond stretching. Chow et al. discussed an interesting example for CN^- detection by use of the heterometallic Ru^{2+}−Cu^{2+} donor−acceptor complex.[219]

Chen et al. reported a luminescent MOF $Tb(BTC)\cdot G$ (MOF-76b, BTC = 1,3,5-benzenetricarboxylate, G = methanol) with OH groups in the terminal solvents (Figure 8a).[53] MOF-76b exhibits increased luminescence upon the addition of Br^-, Cl^-, F^-, SO_4^{2-}, and CO_3^{2-} in methanol. Because F^- has much stronger interactions with the terminal methanol molecules to confine the O−H bond stretching and thus reduce its quenching effect, the addition of F^- significantly enhances the luminescence intensity (Figure 8b). This selective sensing function with respect to F^- is also observed in the solvent of DMF, featuring the bright promise for these kinds of porous luminescent MOFs for the sensing of fluoride anion. Recently, Xu et al. investigated the selective detection of PO_4^{3-} anion through a Tb-based MOF $TbNTA\cdot H_2O$ (NTA = nitrilotriacetate).[220] The luminescent intensity of $TbNTA\cdot H_2O$ shows a negligible change upon exposure to solutions of a range of anions (such as F^-, Cl^-, Br^-, I^-, NO_3^-, NO_2^-, HCO_3^-, CO_3^{2-}, and SO_4^{2-}). In contrast, the PO_4^{3-} demonstrates a tremendous luminescence quench effect on its incorporated MOF. Xu et al. also discussed and explained the possible sensing mechanism by the matching degree of $TbNTA\cdot H_2O$ with different anions. In short, after the incorporation of PO_4^{3-} anions into $TbNTA\cdot H_2O$, the Tb−O bonds may dilute the energy that transferred to Tb^{3+} via non radioactive relaxation. By controlling the interactions between the MOFs and anions through the alteration of pore structures, linkers, solvents, and so on, more luminescent MOFs are expected to be realized for anion sensing.

A luminescent MOF based on ligand-centered fluorescence for sensing of anions is provided by Qiu et al.[221] In their report, a highly symmetric tetragonal cadmium-based MOF with 5-methyl-1*H*-tetrazole as ligand was synthesized. In DMF suspension, this MOF exhibits an emission at around 370 nm attributed to the intraligand transitions. The emission intensity decreased continuously upon the addition of NO_2^-, and was basically unchanged after the addition of ClO_4^-, NO_3^-, Cl^-, and I^-. The anion sensing function was also observed in a water suspension.

5.1.2. Sensing of Small Molecules. Lee et al.[222] and Chen et al.[57] have demonstrated the luminescent MOFs for recognition and sensing of small molecules. Lee et al. explored the guest-dependent luminescence properties of MOF $[Zn_4O(NTB)_2]\cdot 3DEF\cdot EtOH$ (1) (H_3NTB = 4,4′,4″-nitrilotrisbenzoic acid, DEF = *N*,*N*′-diethylformamide) in different solvents. The luminescence seems to be originating from the ligands, but the possibility of zinc clusters-based LMCT luminescence cannot be excluded. Bai et al. reported a two-dimensional porous framework $Cu_6L_6\cdot(H_2O)(DMSO)$ (HL = 5,6-diphenyl-1,2,4-triazine-3-thiol), which exhibited highly selective absorption for aromatic molecules in water and different fluorescent quenching effect for toluene, nitrobenzene, aniline, and *o*-, *p*-, and *m*-dimethylbenzene.[223]

Chen et al. pointed out that the open luminescent lanthanide sites such as Eu^{3+} and Tb^{3+} will play a crucial role in molecular recognition processes for binding of substrates[57] and described a MOF $Eu(BTC)(H_2O)\cdot 1.5H_2O$ (BTC = benzenetricarboxylate) with 1D channels of about 6.6 × 6.6 Å (Figure 9a). The

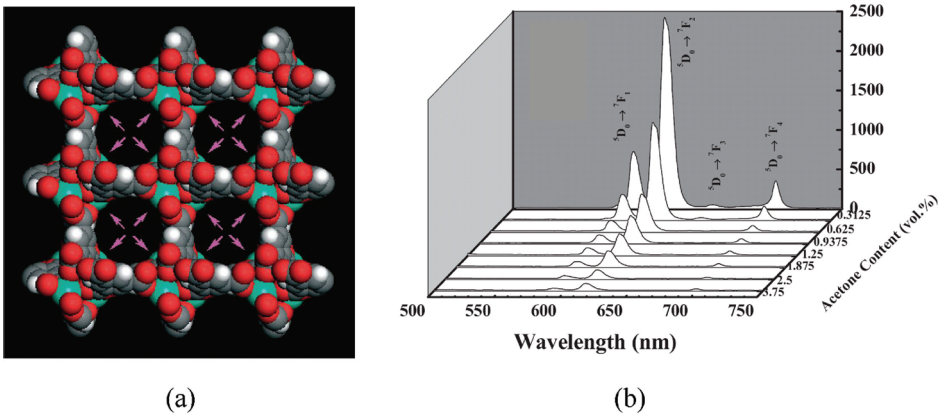

Figure 9. (a) X-ray crystal structure of $Eu(BTC)(H_2O)\cdot 1.5H_2O$ viewed along the *c* axis, exhibiting 1D channels of about 6.6 × 6.6 Å, and uniformly immobilized accessible Eu^{3+} sites within the framework, shown by the pink arrows. The free and terminal water molecules are omitted for clarity; Eu, light green; O, red; C, gray; H, white. (b) The PL spectra of 1-propanol emulsion of EuBTC in the presence of various content of acetone solvent. Reprinted with permission from ref 57. Copyright 2007 Wiley-VCH.

luminescence intensity of activated EuBTC is largely dependent on the solvent molecules, particularly in the case of DMF and acetone, which exhibit the most significant enhancing and quenching effects, respectively. Furthermore, a gradual decrease of the fluorescence intensity was observed upon the addition of acetone to the 1-propanol emulsion of EuBTC, and the $^5D_0 \rightarrow {}^7F_2$ emission intensity of Eu^{3+} versus the volume ratio of acetone could be well fitted with a first-order exponential decay (Figure 9b). It is suggested that the binding interaction of the open metal sites with guest solvent molecules definitely plays an important role, and the weakly coordinated 1-propanol molecules on the Eu^{3+} sites can be gradually replaced by DMF and acetone molecules, leading to the luminescence enhancement and diminishment, respectively. Guo et al. reported an example of NIR luminescent ytterbium MOF $Yb(BPT)(H_2O)\cdot(DMF)_{1.5}\cdot(H_2O)_{1.25}$ (BPT = biphenyl-3,4′,5-tricarboxylate) for sensing of small molecules.[224] This MOF crystallizes in a tetragonal space group $P4_3$. Each ytterbium atom is coordinated by six oxygen atoms from the carboxylate groups of BPT and one terminal water molecule. Yb atoms are bridged by BPT organic linkers to form a 3D rod-packing structure. The activated MOF Yb(BPT) exhibits typical NIR emission from the $^2F_{5/2} \rightarrow {}^2F_{7/2}$ transition of the Yb^{3+} ion at 980 nm, when excited at 326 nm. Similar to the EuBTC, the luminescent intensity exhibits the most significant enhancing and quenching effects in the case of DMF and acetone, respectively. The decreasing trend of the fluorescence intensity of the $^2F_{5/2} \rightarrow {}^2F_{7/2}$ transition of Yb^{3+} at 980 nm versus the volume ratio of acetone could be well fitted with a first-order exponential decay, indicating that fluorescence quenching of Yb(BPT) by acetone is diffusion-controlled. This work extends the sensing function of luminescent MOFs into the NIR region, providing their potentials for the sensing of substrates in biological systems.

Another example of MOF $[Eu_2(\mu_2\text{-pzdc})(\mu_4\text{-pzdc})(\mu_2\text{-ox})\cdot(H_2O)_4]\cdot 8H_2O$ (H_2pzdc = 2,5-pyrazinedicarboxylic acid, H_2ox = oxalic acid) for recognition and sensing of acetone was also reported by Ma et al.[225] Xiao et al. reported the similar recognition functionality in MOF-76, $Tb(BTC)\cdot(DMF)\cdot(H_2O)$.[226] The mechanism of luminescence enhancing and quenching effects was proposed by the energy transfer between solvent molecules and ligands. Another example of recognition of small solvents molecules was reported by Lin et al.,[110] who synthesized a new family of MOFs

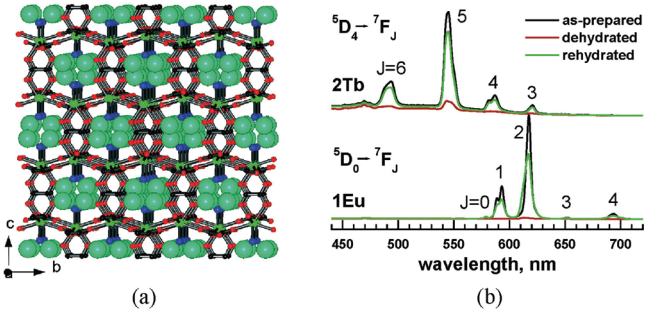

Figure 10. (a) The views of MOFs $[Ln_2(fumarate)_2(oxalate)(H_2O)_4]\cdot 4H_2O$ (Ln = Eu, Tb) along the *a* axis. Color scheme: Ln, green; C, black; O of fum and ox, red; the coordination water, blue; and the lattice water, cyan. H atoms are omitted for clarity. (b) The emission spectra of $Eu_2(fumarate)_2(oxalate)(H_2O)_4]\cdot 4H_2O$ and $Tb_2(fumarate)_2(oxalate)(H_2O)_4]\cdot 4H_2O$ upon the dehydration and rehydration processes. Reprinted with permission from ref 227. Copyright 2007 American Chemical Society.

with 4,4′-oxybis(benzoate) (OBA) ligands and suitable cationic species. The MOF $Na[Tb(OBA)_2]_3\cdot 0.4DMF_3\cdot 1.5H_2O$ exhibits the strongest emission in BuOH and EtOH suspensions, but much weaker emission in MeOH and H_2O suspensions.

Generally, the O−H oscillators in the water molecules act as efficient quenchers for the lanthanide luminescence. However, Zhu et al. reported a rare example of luminescent MOF for sensing water in which hydration of a MOF induces luminescence.[227] The two MOFs $[Ln_2(fumarate)_2(oxalate)(H_2O)_4]\cdot 4H_2O$ (Ln = Eu, Tb) have 3D framework structures consisting of oxalate pillared lanthanide−fumarate layers with intersected channels occupied by water molecules (Figure 10a) and exhibit strongly sensitized luminescence of Eu^{3+} and Tb^{3+}. Interestingly, the luminescence intensity decreases upon the dehydration while it increases back upon rehydration (Figure 10b), indicating that water molecules effectively enhance the luminescence in these two special MOFs. Based on powder XRD analysis, the dehydrated MOFs are very low crystalline and amorphous phases resulting from the loss of coordinated water and probable collapse the open frameworks, and can change back to their original crystalline structures upon exposure to water vapor. The involvement of water molecules in stabilizing the lanthanide

coordination environments of the as-synthesized MOF might play an important role for such a reversible luminescent change.

The porosity of MOFs also plays a crucial role in luminescence sensing of molecules. Jiang et al. proposed a new route to obtain non-, micro-, and mesoporous frameworks materials with tunable pore sizes based on the same ligands and metal ions.[58] The microporous MOF $Cd(L)(bpy)\cdot 4H_2O\cdot 2.5DMF$ (L = 2-amino-1,4-benzenedicarboxylic acid) exhibits a strong emission around 435 nm assigned to LMCT, which was almost quenched upon desolvation possibly due to the collapse of framework. The desolvated MOF in different solvent emulsions exhibits strong guest-dependent luminescence properties, indicating that it could be a promising luminescent probe for detecting small molecules.

Other recent examples of luminescent MOFs for sensing small aromatic compounds were reported by Zhang et al.[228,229] and by Hou et al.[93] The d^{10} metal−organic framework $Zn_4(OH)_2(1,2,4\text{-BTC})_2$ (1,2,4-BTC = benzene-1,2,4-tricarboxylate) exhibits a significant quenching effect with respect to nitrobenzene. Hou et al. synthesized a mixed-ligand MOF, $[Zn_4O(1,4\text{-BDC})(bpz)_2]\cdot 4DMF\cdot 6H_2O$ (1,4-BDC = 1,4-benzenedicarboxylate, bpz = 3,3′,5,5′-tetramethyl-4,4′-bipyrazolate), which shows an excellent luminescent detection behavior for benzene molecules.

The luminescent MOF sensors mentioned above generally detect a single target molecule among several molecules, but cannot differentiate multiple molecules simultaneously. Recently, a clever molecular decoding strategy using MOFs as hosts has been developed by Takashima et al.[59] Amazingly, the MOFs can accommodate a class of molecules and further distinguish among them with characteristic different visible light emission for each different guest molecule (Figure 11). They synthesized a 1,4,5,8-naphthalenediimide (NDI)-based interpenetrating MOF, $Zn_2(1,4\text{-BDC})_2(dpNDI)\cdot 4DMF$ (1,4-BDC = 1,4-benzenedicarboxylate; dpNDI, *N*,*N*′-di(4-pyridyl)-1,4,5,8-naphthalenediimide), which will undergo a dynamic structural transformation to confine a class of aromatic volatile organic compounds, or tropospheric air pollutants. In the structure of the interpenetrating MOF $Zn_2(1,4\text{-BDC})_2(dpNDI)\cdot 4DMF$, one of the frameworks is intergrown at the central position of the void that is created by the other framework. The void spaces can be classified as two different environments: the characteristic slit between dpNDI and 1,4-BDC (site A) and the remaining void space (site B) (Figure 12). The aromatic volatile organic compounds (VOCs) such as benzene, toluene, xylene, anisole, and iodobenzene can be introduced by immersion of a dry MOF into the liquid of each aromatic VOC. The guest-exchanged MOF shows a significant framework displacement, in which one framework slid along the main axis of one 1,4-BDC molecule. The MOF $Zn_2(1,4\text{-BDC})_2(dpNDI)$ shows a very weak fluorescence with a very low quantum yield and a short average lifetime. In contrast, all VOC incorporated $Zn_2(1,4\text{-BDC})_2(dpNDI)$ exhibit intense fluorescence in the visible light region, and the emission color is dependent on the chemical substituent of the aromatic guest. Furthermore, the normalized emission spectra exhibit a gradual red shift as the electron-donating capability of VOCs increased upon excitation at 370 nm (Figure 13). The multicolor luminescence is attributed to the enhanced naphthalenediimide−aromatic guest interaction through the induced-fit structural transformation of the interpenetrating framework.

It needs to be mentioned that the excellent dispersible nature of the nanoscale MOFs enables them to directly interact with chemical species even without activation. Xu et al. reported a rare luminescent nanoscale MOF $Eu_2(1,4\text{-BDC})_3(H_2O)_2\cdot(H_2O)_2$ (1,4-BDC = 1,4-benzenedicarboxylate) for the straightforward and highly sensitive

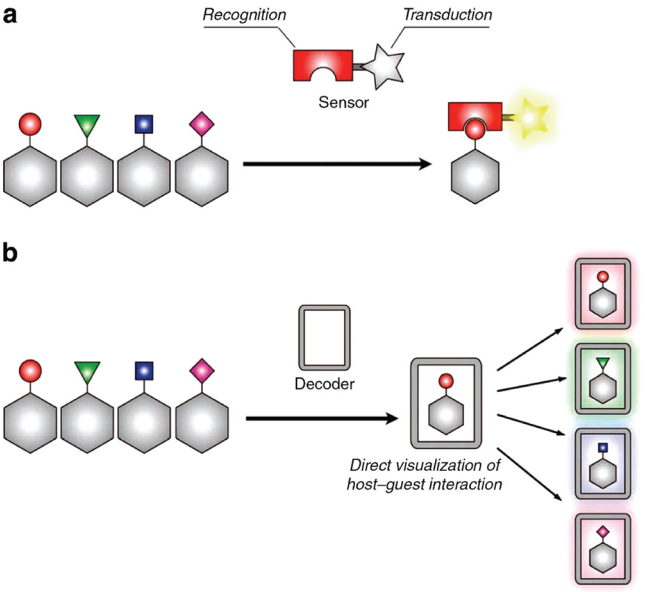

Figure 11. Schematic representation of conventional molecular sensing (a) and molecular decoding (b). Reprinted with permission from ref 59. Copyright 2011 Macmillan Publishers Limited.

sensing of nitroaromatic explosives in ethanol solution.[60] Interestingly, the analytes such as benzene, toluene, chlorobenzene, phenol, *o*-cresol, and 4-bromophenol basically do not affect the luminescence intensity, while the nitroaromatic compounds such as nitrobenzene, 2,4-DNT (2,4-dinitrotoluene), and TNT (2,4,6-trinitrotoluene) significantly weaken the luminescence of $Eu_2(1,4\text{-BDC})_3(H_2O)_2\cdot(H_2O)_2$ in ethanol, which might be attributed to a competition of absorption of the light source energy and the electronic interaction between the nitroaromatic compounds and ligands. Because a variety of different organic ligands can be assembled into the nanoscale MOFs for their matching competitive absorption with the different analytes, this strategy provides another very promising approach for the sensing of small molecules.

5.1.3. Sensing of Gases and Vapors. Gas sensors have a wide range of application in the fields of aerodynamics, environmental analysis, analytical chemistry, and biochemistry.[230,231] As the luminescent properties of MOFs can also be perturbed by gases and vapors, some luminescent MOFs for sensing of gases and vapors have been also explored.

Xie et al. recently synthesized a Zn−Ir(2-phenylpyridine) M′MOF using $Ir(ppy)_3$ derivatives (Figure 14a).[232] The structure possesses open channels of 7.9 Å × 4.3 Å that are perpendicular to the (1,−1,6) plane and contain guest solvent molecules (Figure 14b). To demonstrate its applicability for O_2 sensing, the M′MOF was gradually loaded with O_2 from 0.05 to 1.0 atm, leading to the gradually decreased luminescence intensity at 538 nm. Furthermore, the luminescence measurements after alternating cycles of O_2 loading at 0.1 atm (30 s) and O_2 removal under vacuum (120 s) indicate that the luminescence is reversibly quenched by O_2, with <5% of the original luminescence lost after eight cycles (Figure 14c). The luminescence of this M′MOF is from the $Ir(ppy)_3$ (ppy = 2-phenylpyridine) moieties whose MLCT phosphorescence can be readily quenched by molecules with a triplet ground state through the incorporation of O_2 into the framework. Another example of luminescent MOFs for sensing oxygen was performed by a Yb^{3+} encapsulated MOF

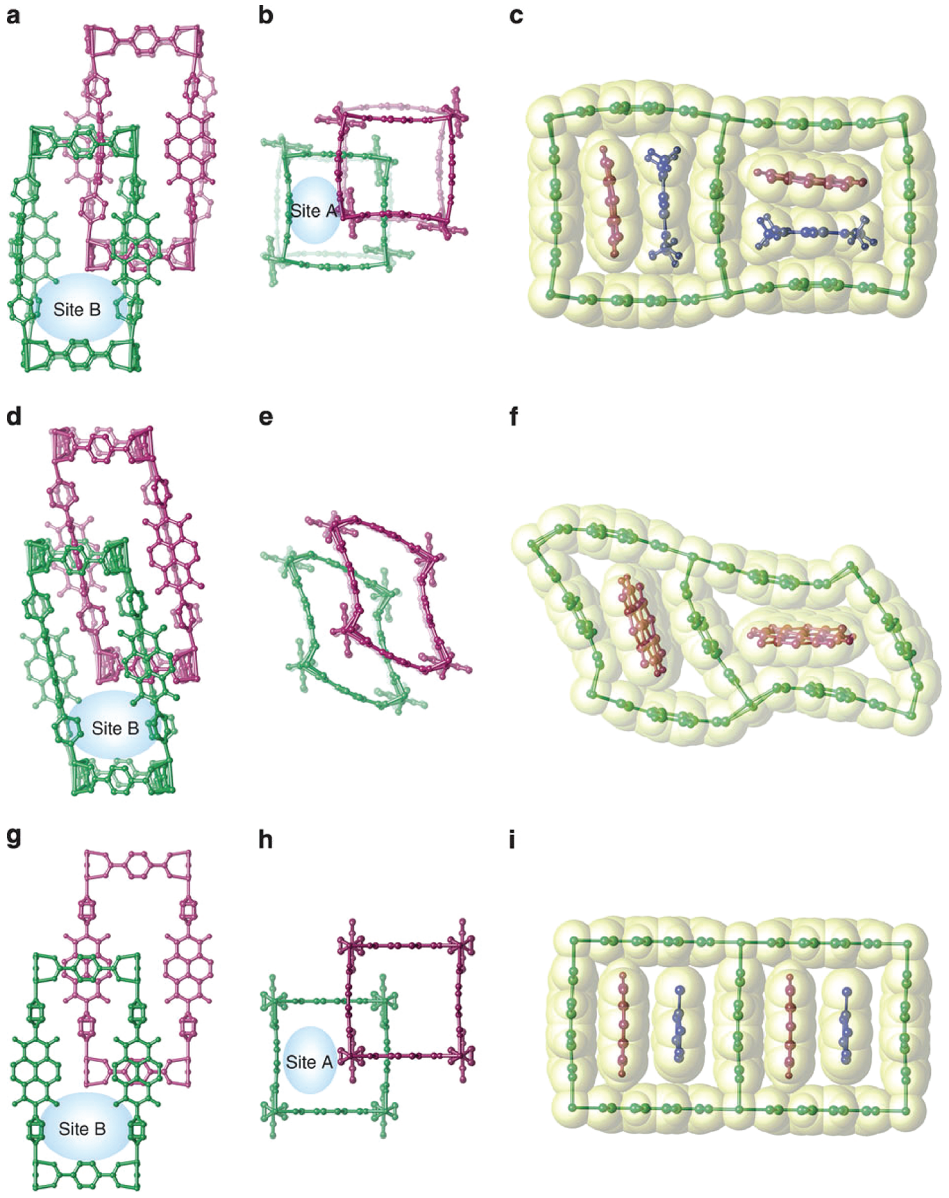

Figure 12. Structural dynamics of $Zn_2(1,4\text{-bdc})_2(dpNDI)\cdot 4DMF$ on the removal and incorporation of guest molecules. Reprinted with permission from ref 59. Copyright 2011 Macmillan Publishers Limited.

Yb^{3+}@bio-MOF-1, reported by An et al.[170] In their report, the porous anionic bio-MOF-1 was chosen to sensitize and protect the lanthanide ions. Yb^{3+}@bio-MOF-1 exhibits a clear Yb^{3+}-centered emission at 980 nm. An approximate 40% signal decrease was observed within the first 5 min of introducing O_2 gas to a purged chamber under ambient pressure. Furthermore, this sensing behavior is reversible, and the Yb^{3+} signal can maintain its original luminescence intensity after several cycles of exposure to O_2 and N_2.

Harbuzaru et al. reported a new MOF named ITQMOF-1-Eu with 4,4′-(hexafluoroisopropylidene)bis(benzoicacid) as ligand,[56] which crystallizes in long needles that can be handled individually. Interestingly, by placing one of the MOF crystals parallel or perpendicular to the detector, it has been determined that these MOFs exhibit a strong anisotropic luminescence. This fluorescence anisotropy is a consequence of the alignment of all of the chromophores in a preferred direction and proves that the crystallization as long needles is a manifestation of the ordering at the molecular level.[18,56] Under an air stream alternatively saturated and unsaturated with ethanol, the luminescence intensity of ITQMOF-1-Eu shows a rapid decrease in the presence of ethanol and a rapid recovery, almost to the initial value, when the sample is exposed to air. This is a very rare example of luminescent MOFs with fast response time and rapid reversible behavior for sensing ethanol vapor molecules. The sensing mechanism was rationalized by considering that ethanol may coordinate to the Ln^{3+} ions, thus quenching the emission through coupling with the vibrational states of the O−H oscillators.

Chemical sensors for rapid detection of explosives in the gas phase are attracting increasing attention due to homeland security, environment monitoring, and humanitarian implications. Lan et al. reported a MOF $Zn_2(bpdc)_2(bpee)$ (bpdc = 4,4′-biphenyldicarboxylate; bpee = 1,2-bipyridylethene) for detection of both DNT and DMNB (2,3-dimethyl-2,3-dinitrobutane) with rapid response and high sensitivity.[233] Within 10 s, the fluorescence quench

dx.doi.org/10.1021/cr200101d |*Chem. Rev.* 2012, 112, 1126–1162

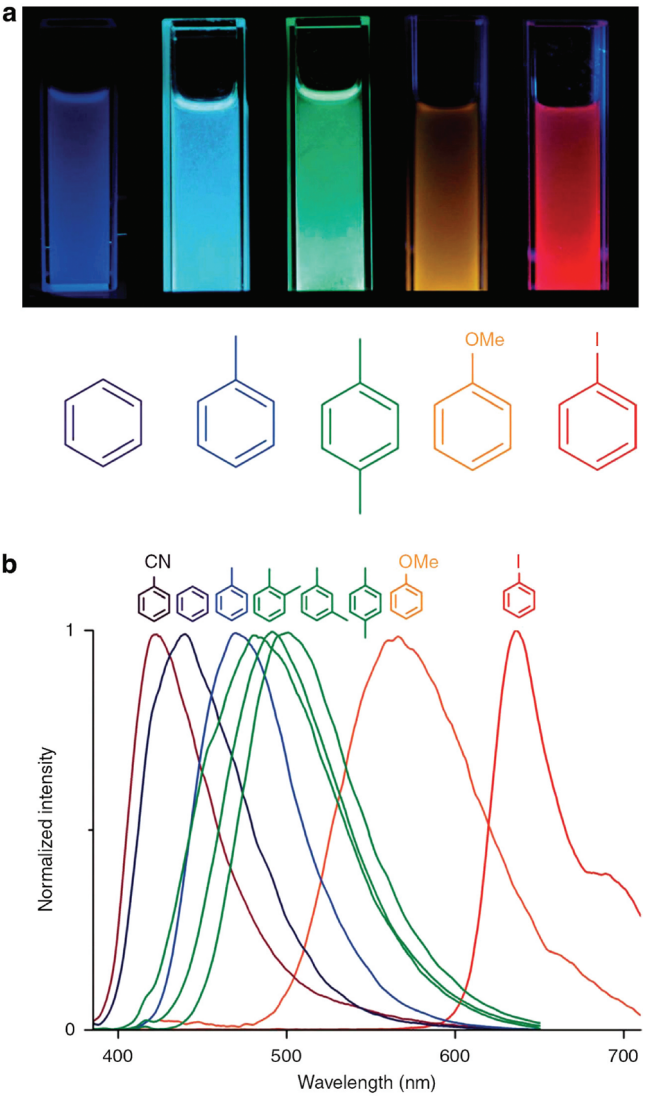

Figure 13. Multicolour luminescence of VOC incorporated $Zn_2(1,4\text{-bdc})_2(dpNDI)$. (a) The resulting luminescence of crystal powders of $Zn_2(1,4\text{-bdc})_2(dpNDI)$ suspended in each VOC liquid after excitation at 365 nm using a commercial ultraviolet lamp. (b) Height-normalized luminescent spectra of VOC incorporated $Zn_2(1,4\text{-bdc})_2(dpNDI)$ after excitation at 370 nm. Reprinted with permission from ref 59. Copyright 2011 Macmillan Publishers Limited.

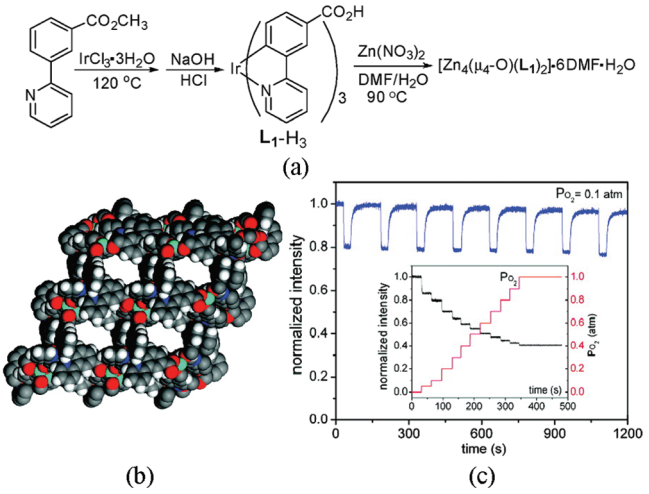

Figure 14. (a) Synthesis route of the Zn−Ir(2-phenylpyridine) MOF. (b) Space-filling model of the Zn−Ir(2-phenylpyridine) MOF viewed perpendicular to the (1,−1,6) plane. (c) Reversible quenching of phosphorescence of the Zn−Ir(2-phenylpyridine) MOF upon alternating exposure to 0.1 atm O_2 and application of vacuum. Inset shows rapid equilibration of phosphorescence of MOF after each dose of O_2. Reprinted with permission from ref 232. Copyright 2010 American Chemical Society.

percentages of the MOF thin film reach almost the maxima upon the exposure of both DNT and DMNB (ca. 85% and 84%, respectively). The sensitivity of the MOF thin films for DMNB exceeds previously reported conjugated polymer thin films. The infinite 3D framework structure, the large surface area, and the pore confinement of the analyte inside the molecular-sized cavities facilitate stronger interactions between the DMNB and the luminescent framework. Because of its very fast responses and high sensitivity, this work will certainly promote the extensive exploration of luminescent MOFs for the sensing of explosives in the future.

To realize the detection for nitroaliphatic explosives, Zhang et al. synthesized a nanoscale MOF by making use of 9,10-bis(*p*-carboxyphenyl) anthracene (BCPA) as the ligand. Self-assembly of Zn^{2+} with BCPA led to the construction of cubic nanoscale MOFs particles with strong fluorescence.[234] Upon exposure to the nitromethane vapor, the luminescence intensity of nanoscale MOF Zn-BCPA decreased significantly. Even when the vapor pressure of nitromethane was diluted down to 1% of the saturated vapor, the emission was still quenched, and the detection limit of nitromethane can reach the range of a few ppm. Zhang et al. also speculated the quenching mechanism and attributed it to the photoinduced electron transfer from the excited MOFs to the surface adsorbed explosive molecules. The enhanced exciton migration caused by the strong resonance coupling between the neighboring anthryl groups can facilitate the interfacial charge transfer, resulting in amplified emission quenching. The significant luminescence quenching for both nitroaromatic and nitroaliphatic explosives enables the luminescent MOFs to have wider usage for infield explosives monitoring.

5.1.4. Other Sensing. MOFs can also be used to detect pH value, temperature, and ionizing radiation. Harbuzaru et al. synthesized a new MOF ITQMOF-3-Eu with 1,10-phenanthroline-2,9-dicarboxylic acid (H_2PhenDCA) as ligand, in which both carboxylate and phenanthroline moieties may coordinate to the metal center.[235] The MOF ITQMOF-3-Eu can be described as a layered MOF with two well-defined sheets, and each sheet contains one type of Eu^{3+} ions (Eu1 or Eu2) in a different crystallographic position. Because of the two different Eu^{3+} environments, ITQMOF-3-Eu exhibits two nondegenerate $^5D_0 \rightarrow {}^7F_0$ emission lines at 579.0 (Eu2) and 580.7 (Eu1) nm, respectively (Figure 15). The luminescence features of each Eu^{3+} site may be rationalized in terms of the relationship between the covalency of the Eu−(O,N) bonds and the nephelauxetic effect that influences the energy of the $^5D_0 \rightarrow {}^7F_0$ transition: a site with more covalent Eu-(O,N) bonds has a $^5D_0 \rightarrow {}^7F_0$ transition at lower energy and a longer emission lifetime. Intriguingly, only one of the two Eu^{3+} emitting sites is affected by the pH variation in the range 5−7.5, and thus the sensor does not require external calibration. By following the intensity ratio of the $^5D_0 \rightarrow {}^7F_0$ emissions of the two Eu^{3+} types, it is possible to determine the pH of the solution. The high emission quantum efficiency and pH-sensing capability enable ITQMOF-3-Eu to be used in a new

dx.doi.org/10.1021/cr200101d |*Chem. Rev.* 2012, 112, 1126–1162

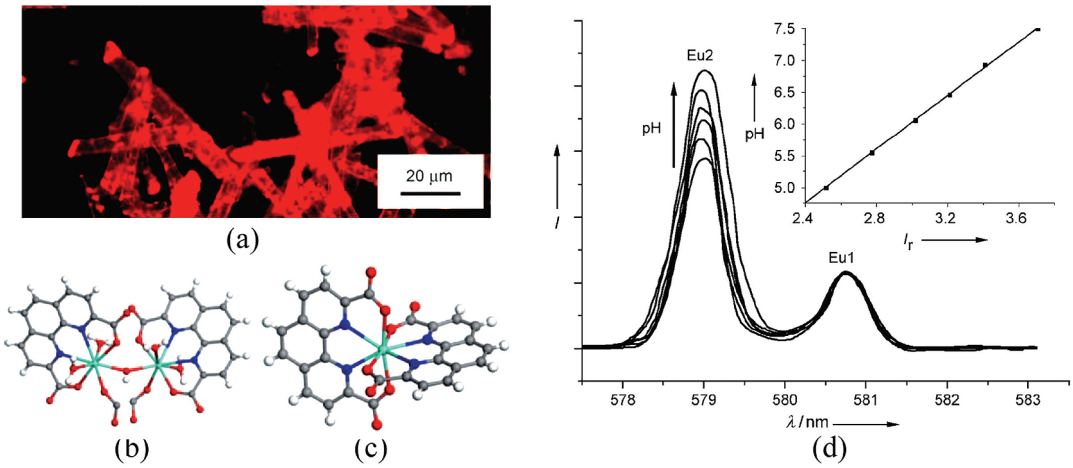

Figure 15. (a) Optical microscopy image of ITQMOF-3-Eu under UV light. (b) Eu2 coordination environment. (c) Eu1 coordination environment. C, gray; H, white−gray; N, blue; Eu, green; O, red. (d) Intensity variation of the Eu2 $^5D_0 \rightarrow {}^7F_0$ transition from pH value of 7.5 to 5; the inset shows the linear variation of intensity ration of the $^5D_0 \rightarrow {}^7F_0$ emissions with the pH value. Reprinted with permission from ref 235. Copyright 2009 Wiley-VCH.

miniaturized pH sensor prototype by combining the material with a commercial fiber optic 1.5 mm in diameter.

The MOF $Cd_3(bpdc)_3(DMF)]\cdot 5DMF\cdot 18H_2O$ (H_2bpdc = 4,4′-biphenyldicarboxylic acid) reported by Fang et al. can be assembled with nanosized rhodamine 6G (Rh6G) dye molecules and displays favorable temperature-dependent luminescent properties.[172] Rh6G is a well-known xanthene derivative used as lasers dye, and it exhibits strong absorption in the visible region and a very high fluorescence quantum yield. Recently, a large amount of Rh6G doped hybrid organic−inorganic materials has been investigated due to its potential applications in solid-state lasing, optical filters, and optoelectronics. In this report, the MOF $Cd_3(bpdc)_3(DMF)]\cdot 5DMF\cdot 18H_2O$ possesses a 1D hexagonal nanotube-like channels of 24.5 × 27.9 Å, allowing the entry of the Rh6G dye molecules (Figure 16a,b). The Rh6G-filled MOF exhibits a strongest emission peak at 563 nm originating from the dye Rh6G, which is similar to the previous results obtained on Rh6G-doped materials. When the temperature varies from 298 to 77 K, the emission peak remains unchanged, while the luminescence intensity is gradually enhanced (Figure 16c), indicating it is a potential candidate for applications in temperature-sensing devices.

Doty et al. reported two new Zn-stilbenedicarboxylate MOF-S1 (3D) and MOF-S2 (2D), which exhibit luminescence when exposed to high energy protons and alpha particles.[236] The ion-beam-induced luminescence (IBIL) spectra of the MOFs lie in approximately the same wavelength region as ligand molecules, and the emission band of free ligand has a maximum at 468 nm and is considerably narrower than the IBIL spectra of either MOF. The 3D MOF-S1 exhibits a large red shift in its IBIL spectra when compared to its fluorescence emission spectrum, indicating its structural change on ionization. The minimal overlap between the optical absorption and the IBIL emission favors their usage in radiation detection, because the self-absorption should be minimal, allowing light to escape from the MOFs. Doty et al. speculated the possible structural distortion based on previous experiments and theory. They suggested that the partial rotation about the linker C═C bond may be occurring and the dihedral angle between neighboring stilbene dicarboxylic acid linkers is decreasing such that they closely resemble a cofacial dimer pair. The luminosity of these materials is comparable to commercially available organic scintillators, and they show good resistance to radiation damage, making these new MOFs attractive in fast-neutron detection.

A mesoporous MOF, $[Tb_{16}(TATB)_{16}(DMA)_{24}]\cdot(DMA)_{91}(H_2O)_{108}$ (H_3TATB = 1,3,5-tribenzoic acid), containing cages of 3.9 and 4.7 nm in diameter,[237] emits strong green light originated from Tb^{3+} at 488, 541, 584, and 620 nm. Upon ferrocene being introduced into the framework by a sublimation procedure at 100 °C, no strong green emission is observed; instead, a weak and broad emission from the included ferrocene molecules appears. This may be attributed to the efficient energy transfer from the host framework to the ferrocene molecules. Removal of the ferrocene under vacuum and high temperature leads to recovery of the green emission from the MOF; moreover, the spectrum exactly matched that of the evacuated host crystals, and the ferrocene emission disappeared. This reversible change of luminescence enables the MOF useful in the sensing of ferrocene.

5.2. Light-Emitting Devices

MOFs are excellent candidates for light-emitting devices due to their structural diversity and tunable luminescence. So far, a variety of luminescent MOFs with tunable emission for light-emitting devices have been designed and investigated.

5.2.1. Luminescence Tuning and White Light Emitting.

The interest in white light-emitting devices stems from their broad applications in lighting and displays, and this topic is undoubtedly the most addressed in the literature. High-quality white light illumination requires a source with the Commission International ed'Eclairage (CIE) coordinates (0.333; 0.333), with correlated color temperature (CCT) between 2500 and 6500 K, and color rendering index (CRI) above 80.[159,238] Emission from organic or inorganic luminescent materials can only cover part of the visible spectrum. To overcome this limitation, various architectures of devices combining monochromatic emission from different compounds have been suggested. In principle, white light-emitting devices may be obtained by tuning the emission color and controlling the relative amount of these monochromatic emissions. In luminescent MOFs, besides the characteristic f−f emission of lanthanide ions, the broad emission band ascribed to organic linkers can be observed. The relative luminescence intensity between the lanthanide ions and linkers strongly depends on the nature of the

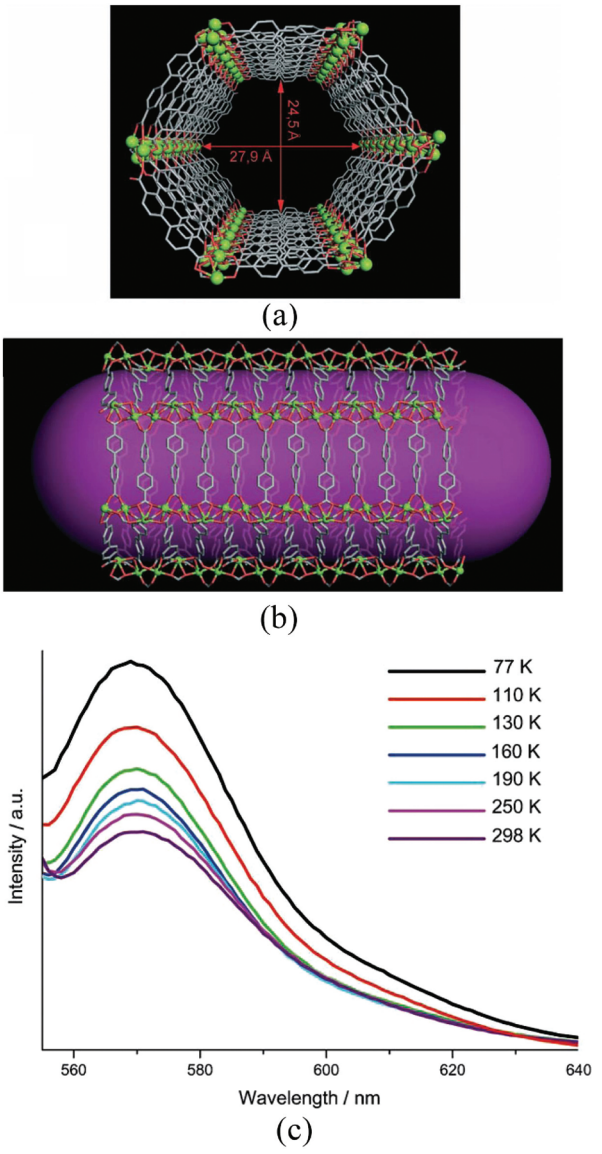

Figure 16. Representation of a hexagonal nanotube-like channel of $Cd_3(bpdc)_3(dmf)] \cdot 5dmf \cdot 18H_2O$ of dimensions of 24.5 Å × 27.9 Å viewed along the [001] (a) and [100] (b) directions. Cd, green (ball); O, red; C, gray. (c) Fluorescence spectra of Rh6G-filled MOF at different temperatures. Reprinted with permission from ref 172. Copyright 2007 Wiley-VCH.

energy transfer, thus allowing the fine-tuning of the MOFs emission color across the CIE diagram. In addition, the emission color can also be readily modulated both by chemical factors (Ln^{3+} types and concentration, ligand structure, coordination status, guest species) and by physical parameters (excitation wavelength and temperature).

Guo et al. discussed a method to tune the luminescence by modifying the lanthanide ions concentration.[239] In the $Eu_{1-x}Tb_x$-MOF nanocrystals, the luminescence peak located at 540 nm corresponds to the $^5D_4 \rightarrow {}^7F_5$ transition of the Tb^{3+} ions, and the two main peaks at around 589 and 615 nm are assigned to the $^5D_0 \rightarrow {}^7F_1$ and $^5D_0 \rightarrow {}^7F_2$ transitions of the Eu^{3+} ions, respectively. The fluorescence intensity at 540 nm changes with the Tb^{3+}/Eu^{3+} ratio, due to the existence of Tb^{3+} to Eu^{3+} energy transfer. Liu et al. reported a terbium 1,3,5-benzenetricarboxylate MOF doped with Eu^{3+} ion, $Tb(1,3,5\text{-BTC})(H_2O) \cdot 3H_2O{:}Eu^{3+}$, whose

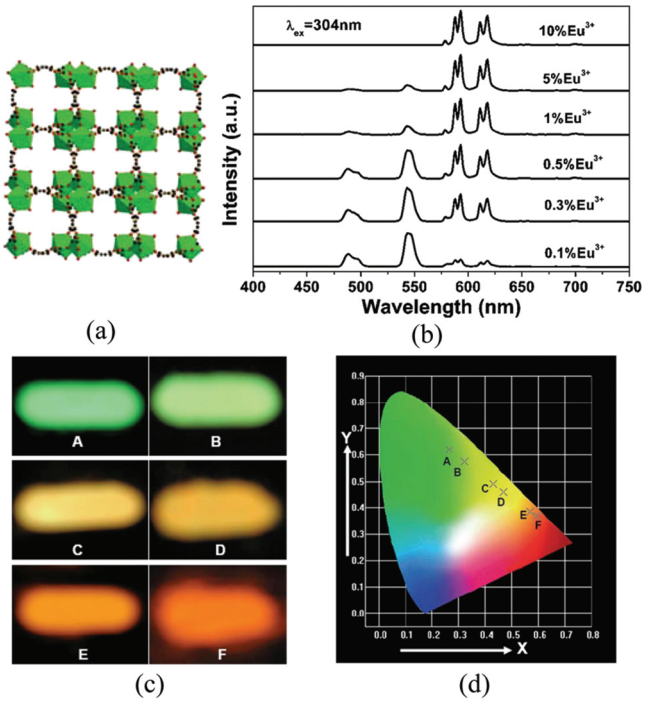

Figure 17. (a) Perspective view of the packing along the *c* axis of the $Tb(1,3,5\text{-BTC})(H_2O) \cdot 3H_2O$. (b) Emission spectra of the $Tb(1,3,5\text{-BTC})(H_2O) \cdot 3H_2O{:}Eu$ ($x = 0.1-10$ mol %) under 304 nm excitation. (c) The photographs for the luminescent MOF $Tb(1,3,5\text{-BTC})(H_2O) \cdot 3H_2O{:}Eu$ ($x = 0$ for A, 0.1% for B, 0.3% for C, 0.5% for D, 5% for E, and 10% for F) under excitation of a 254 nm ultraviolet lamp. (d) CIE chromaticity diagram for the $Tb(1,3,5\text{-BTC})(H_2O) \cdot 3H_2O{:}Eu$. Reprinted with permission from ref 240. Copyright 2010 The Royal Society of Chemistry.

luminescence color can be easily tuned from green to green-yellow, yellow, orange, and red-orange.[240] The emission spectrum of the nanoscale MOF $Tb(1,3,5\text{-BTC})(H_2O) \cdot 3H_2O$ consists of four bands located at about 487, 543, 580, and 620 nm, which correspond to the $^5D_4 \rightarrow {}^7F_J$ ($J = 6, 5, 4$, and 3, respectively) transitions of the Tb^{3+} ions. The strongest one is located at 543 nm, in the green region. In addition, the emission from the $^5D_3$ level has been quenched due to the cross relaxation process, which results in the strong emission from $^5D_4$ to the ^7F_J levels. However, in the Eu^{3+}-doped MOF $Tb(1,3,5\text{-BTC})(H_2O) \cdot 3H_2O{:}Eu$ (x = 0.1−10 mol %), which has phase and morphology similar to the host MOF, the green emission changes greatly. Besides the main emission of the Tb^{3+}, the characteristic emission of the Eu^{3+} is also observed. With the increase of Eu^{3+} concentration, the luminescence intensity of the Tb^{3+} decreases, while that of the Eu^{3+} increases. When the Eu^{3+} concentration is 1%, the luminescence of the Eu^{3+} reaches the maximum, and then begins to decrease due to the concentration quenching effect (Figure 17). Finally, the characteristic emissions of the Tb^{3+} almost disappear when the Eu^{3+} concentration increases to 10%. This may be attributed to the enhanced probability of energy transfer from the Tb^{3+} to Eu^{3+} ions. Therefore, the photoluminescence color of the Eu^{3+} doped MOF can be tuned from green to green-yellow, yellow, orange, and red-orange, and the corresponding CIE chromaticity coordinates change from (0.264, 0.62) to (0.596, 0.37) by changing the doping concentration of the Eu^{3+} ions (Figure 17). This efficient strategy may open a new and convenient pathway for tuning luminescence properties of MOFs by selecting the appropriate MOFs host and lanthanide ions.

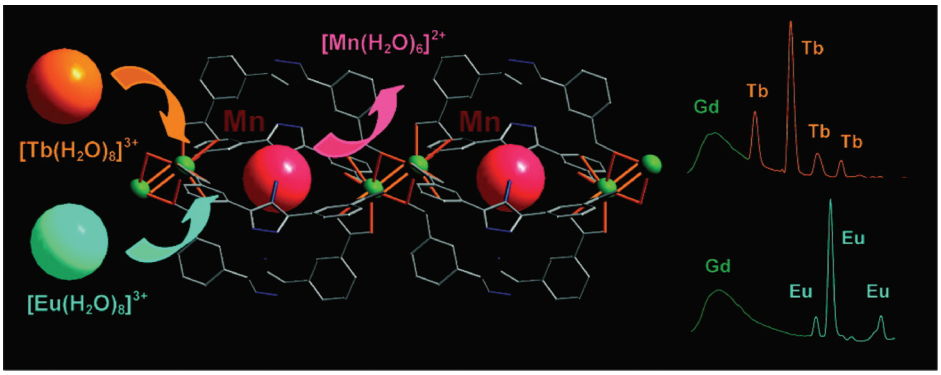

Figure 18. Tunable luminescence based on reversible ion-exchange in MOF $[(Gd_2L)Mn(H_2O)_6]\cdot 0.5(H_2O)$ (L = 3,3′-(4-amino-4*H*-1,2,4-triazole-3,5-diyl)dibenzoic acid). Reprinted with permission from ref 242. Copyright 2007 American Chemical Society.

Replacement and modification of the guest species can also produce substantial changes in the luminescence spectrum of MOFs. Jiang et al. prepared a crown-ether-like, hollow Pb^{2+}-framework $[Pb_2L_2]$ (L = 1,5-bis(*m*-carboxyphenoxy)-3-oxapentane) by a leaching approach, and then the Eu^{3+}, Tb^{3+}, and Nd^{3+} hydrates can be intercalated into the cavity.[241] Interestingly, the incorporated MOFs can be reversibly displaced, which enable the dual- and bimodal emissions, and the emission peaks and intensities can be tuned by controlling the lanthanide ions displacement. For example, when MOF $[Pb_2L_2]$ was immersed in an aqueous solution of $Tb(ClO_4)_3$ for 3 h, the solid-state luminescence spectrum indicates that the maximal emission intensity of Tb^{3+} was obtained. After the MOF containing $[Tb(H_2O)_8]^{3+}$ species was treated with excess $Eu(ClO_4)_3$ solution, the emission spectrum indicated that the original incorporated $[Tb(H_2O)_8]^{3+}$ was partially replaced by $[Eu(H_2O)_8]^{3+}$, generating a heterometallic host−guest system. Thus, the emission intensities originate from the different lanthanide species and can be tuned by controlling the Eu/Tb displacement. Besides UV/vis emitter, the incorporated $[Tb(H_2O)_8]^{3+}$ can also be displaced by the NIR-lanthanide emitter such as Nd^{3+}, and a similar modulation of emission can also be observed.

Another similar example was reported by Wang et al.,[242] who synthesized a new family of lanthanide-based MOFs consisting of the nanosized Ln_2L (L = 3,3′-(4-amino-4*H*-1,2,4-triazole-3,5-diyl)dibenzoic acid) cagelike units, which encapsulate the $[Mn(H_2O)_6]^{2+}$ cations by utilizing the bent five-membered heteroatom-ring-bridged ligands as the building blocks. The MOF $[(Gd_2L)Mn(H_2O)_6]\cdot 0.5(H_2O)$ exhibits an emission maximum at 428 nm, which is blue-shifted as compared to the ligand emission due to the ligand-to-metal charge transfer. The porous frameworks are able to undergo a reversible and controllable cation exchange; thus the encapsulated $[Mn(H_2O)_6]^{2+}$ species are readily replaced reversibly by the $[Tb(H_2O)_8]^{3+}$ or $[Eu(H_2O)_8]^{3+}$ cations with preservation of the original crystal structure. After ions exchange, the typical emission intensities of Tb^{3+} or Eu^{3+} increased, while the fluorescence intensity of the $[(Gd_2L)Mn(H_2O)_6]\cdot 0.5(H_2O)$ decreased (Figure 18). In short, these MOFs show the tunable luminescent properties based on reversible ion-dependent exchange. Importantly, it may provide a promising and convenient approach to access the tunable luminescent materials by controlling the different type of guest species.

Other possible routes to tune luminescence include controlling the number of guest molecules, varying the excitation wavelength, and changing the heat-treatment temperature. The former approach was realized by Huang et al.[243] They synthesized a MOF $[Cd_3L_6]\text{-}(BF_4)_2(SiF_6)(OH)_2\cdot 13.5H_2O$ (abbreviated as $A\cdot 13.5H_2O$, L = 2,6-di(4-triazolyl)pyridine), where the guest species in the open channels can be removed and reintroduced reversibly without destroying the porous framework. When the MOF was heated at different temperatures (180, 200, 225, 250 °C) for 1 day, a series of dehydrated products $A\cdot xH_2O$ (x = 11.5, 10.5, 6.5, 4.5) were obtained in air. The original MOF and the series of dehydrated MOFs display intense luminescence with emission maxima λ_{max} ranging from UV (380 nm) to visible light (438 nm). This behavior may be rationalized by the energy transfer between ligand and metal center. In the original crystal, abundant lattice water molecules and anions fill the network, preventing the effective energy transfer from ligand to the metal center. Accordingly, the intense UV luminescence assigned to intraligand emission was observed. When some guest molecules are removed from the MOF, energy can be effectively transferred from the ligand to the metal center, and then the luminescence assigned to LMCT bands was observed. Fu et al. reported a zinc phosphate by using the purple luminescent 2-methylpiperazine as structure-directing agent, which was encapsulated into the frameworks through electrostatic interactions and hydrogen bonding.[244] Interestingly, this zinc phosphate displays purple, bright white, yellow, and orange-red emission after heat treatment at different temperatures. Furthermore, the luminescent color of the zinc phosphate heated at 250 °C can be reversibly tuned among yellow-green, purple-blue, bright white, and blue-green by easily changing the excitation wavelength.

Recently, a direct white-light-emitting MOF, $[AgL]_n\cdot nH_2O$ (L = 4-cyanobenzoate), with tunable yellow to white luminescence by variation of excitation light was reported by Wang et al.[245] The MOF displays a maximum emission at around 427 and 566 nm when excited at 355 and 330 nm, respectively. When irradiated at 330 nm, the emission intensity at 427 nm is decreased, but the emission intensity at approximately 513, 566, and 617 nm is enhanced, generating yellow luminescence. When adjusting the excitation light to 350 nm, the emission peaks at 427 and 566 nm are very strong, which results in direct white light to the naked eye (Figure 19). The CIE chromaticity coordinates of the white-light emissions excited at 350 and 349 nm are approximately (0.31, 0.33) and (0.33, 0.34), respectively, comparable to that of pure white light. Therefore, the MOF can be tuned from yellow to white by direct variation of excitation wavelength, indicating it can be potentially used as a single white phosphor for a white light-emitting device equipped with a deep UV GaN LED, which has light output at 325−350 nm. Wibowo et al. also presented two

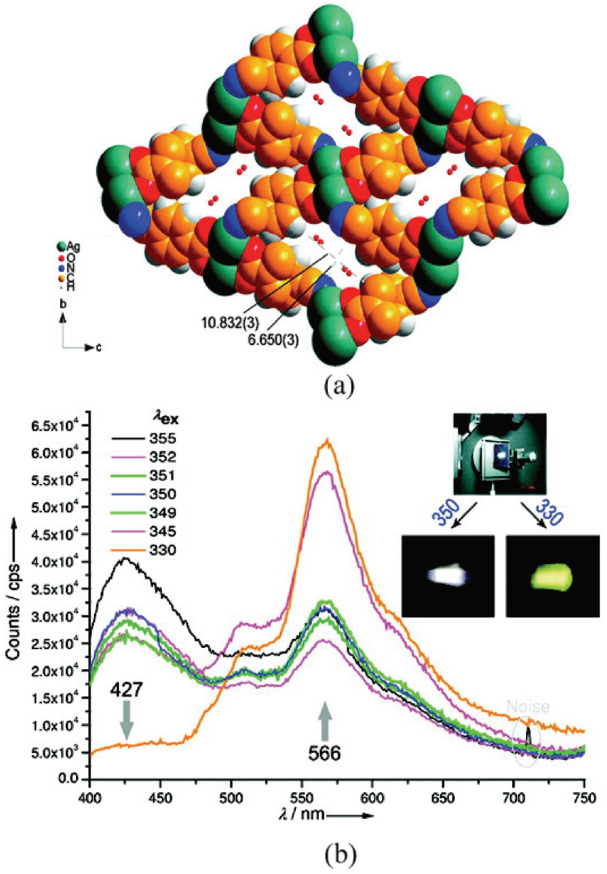

Figure 19. (a) 3-D packing diagram of $[Ag(4\text{-cyanobenzoate})]_n \cdot nH_2O$ viewed along the *a* direction. (b) Solid-state PL spectra of $[Ag(4\text{-cyanobenzoate})]_n \cdot nH_2O$ by variation of excitation light under the same metrical condition. Inset shows the PL images of a sample excited by 350 and 330 nm light, respectively. Reprinted with permission from ref 245. Copyright 2009 American Chemical Society.

single component white-light-emitting phosphors based on the bismuth and lead MOFs.[209] When excited at 380 nm, the bismuth MOF $Bi_3(\mu_3\text{-}O)_2(pydc)_2(Hpydc)(H_2O)_2$ emits white composite light with a broad emission spectrum from about 400 to 600 nm, and three distinct maxima at 430, 460, and 480 nm with a shoulder around 556 nm can be identified, which is significantly blue-shifted as compared to the emission of ligand. This blue shift is attributed to LMCT transition and a change in the intraligand $\pi \rightarrow \pi^*$ and/or $n \rightarrow \pi^*$ transitions. Similarly, the lead MOF $Pb(pydc)(H_2O)$ exhibits slightly "whiter" composite photoluminescence, with a distinct emission maximum at 441 nm and three broad shoulders around 470, 520, and 563 nm. These studies have paved the way for the utilization of luminescent MOFs in white lighting devices.

5.2.2. Near-Infrared (NIR) Emitting. Near-infrared (NIR) light-emitting devices have a wide range of potential applications in the fields of identification in military action, night-vision illumination sources, consumer electronics, and spectroscopic analysis, especially in optical telecommunication systems.[246−248] Lanthanide ions such as Er^{3+} (1530 nm), Nd^{3+} (1060 nm), and Yb^{3+} (980 nm), as well as the less studied Pr^{3+} (1300 nm) and Tm^{3+} (1500 nm), have attracted their special usage as NIR luminescent materials.[248−265] So far, a series of NIR light-emitting MOFs based on Er^{3+}, Yb^{3+}, Nd^{3+}, and Ho^{3+} have been prepared.[76,207,208,266] However, examples of NIR light-emitting lanthanide frameworks are scarce in comparison to visible emitting MOFs, due to the presence of high-energy C−H, N−H, and O−H oscillators in the ligands and solvents, which significantly quench the metal excited states nonradiatively, leading to decreased luminescence intensities. This effect is particularly dramatic for NIR emitting Ln^{3+} because of relatively small energy gaps between ground and excited electronic states.[159,160,247,267] To alleviate nonradiative decays, a variety of strategies have been adopted to shield the ion excited levels to high nonradiative transition probability by O−H, C−H, and N−H oscillators.

Chen et al. demonstrated that the NIR luminescence intensity of MOFs can be significantly enhanced by incorporation of fluorinated organic linkers.[268] In their report, two erbium−organic frameworks $Er_2(1,4\text{-BDC})_3(DMF)_2(H_2O)_2 \cdot H_2O$ (1,4-BDC = 1,4-benzenedicarboxylate) and $Er_2(BDC\text{-}F_4)_3(DMF)(H_2O) \cdot DMF$ (BDC-F_4 = 2,3,5,6-tetrafluoro-1,4-benzenedicarboxylate) have been synthesized. After heat treatment under vacuum at 140 °C overnight, the desolvated Er-BDC framework displays an NIR emission band around 1.55 μm assigned to the $^4I_{13/2} \rightarrow {}^4I_{15/2}$ transition of Er^{3+} ion at the excitation wavelength of 808 nm. Interestingly, the emission intensity of Er-BDC-F_4 framework is significantly enhanced by 3 times that of Er-BDC framework because the fluorescence quenching effect of the C−F vibration on the Er^{3+} NIR emission is much lower than that of the C−H vibration. Chen et al. speculated that the luminescent intensity of the fluorinated framework can be further enhanced by eliminating the quenching effect of the remaining DMF solvents.

Another example of enhanced NIR emission by tailoring the MOF architecture was presented by White et al.,[267] who chose the 4,4′-[(2,5-dimethoxy-1,4-phenylene)di-2,1-ethenediyl]bisbenzoic acid (H_2-PVDC) for the sensitization of Yb^{3+} ions and prepared two MOFs, named $[Yb_2(C_{26}H_{20}O_6)_3(H_2O)_2] \cdot (DMF)_6(H_2O)_{8.5}$ (Yb-PVDC-1) and $[Yb_2(C_{26}H_{20}O_6)_3(H_2O)_2] \cdot (DMF)_{12}(H_2O)_{10}$ (Yb-PVDC-2). These MOFs display the typical Yb^{3+} emission band in the NIR range with an apparent maximum at 980 nm, but the lowest energy excitation band of Yb-PVDC-2 is red-shifted to 500 nm from 470 nm in Yb-PVDC-1, and it was proposed that the close $\pi-\pi$ interactions between the PVDC linkers decrease the energy of the $\pi \rightarrow \pi^*$ transition, resulting in a lowered excitation energy. Additionally, the quantum yield of Yb-PVDC-2 is 5 times higher than that of Yb-PVDC-1 when excited through the lower energy band (490 nm). This may be attributed to the octa-coordinate Yb^{3+} of Yb-PVDC-1 coordinating two water molecules, which quench ytterbium emission and lower the quantum yield.

Recently, White et al. created a new barcode system based on MOFs that simultaneously emit several independent NIR signals arising from different lanthanide compositions.[269] They designed Er_xYb_{1-x}-PVDC-1 (x = 0.32, 0.58, 0.70, and 0.81) MOFs with different amounts of Yb^{3+} and Er^{3+} ions that were sensitized by the same ligand PVDC. These MOFs displayed sharp signals from both Er^{3+} (1530 nm) and Yb^{3+} (980 nm), and the excitation spectrum of either the Er^{3+} or Yb^{3+} emission band contains two similar bands with apparent maxima at 370 and 470 nm. The NIR emission intensity of Er^{3+} and Yb^{3+} varies linearly with their concentration in the MOF when either excitation band is used (Figure 20), indicating that the respective signal intensity of the lanthanide ions can be quantitatively tuned by controlling the lanthanide composition. This features their potential usage as NIR barcodes. Furthermore, the number and diversity of barcodes may be increased by using a large number of Ln/Ln ratios or by incorporating additional lanthanide ions into the material. The latter concept was demonstrated in MOF $Nd_{0.09}Er_{0.55}Yb_{0.36}$-PVDC-1, which displays a more sophisticated barcode signal

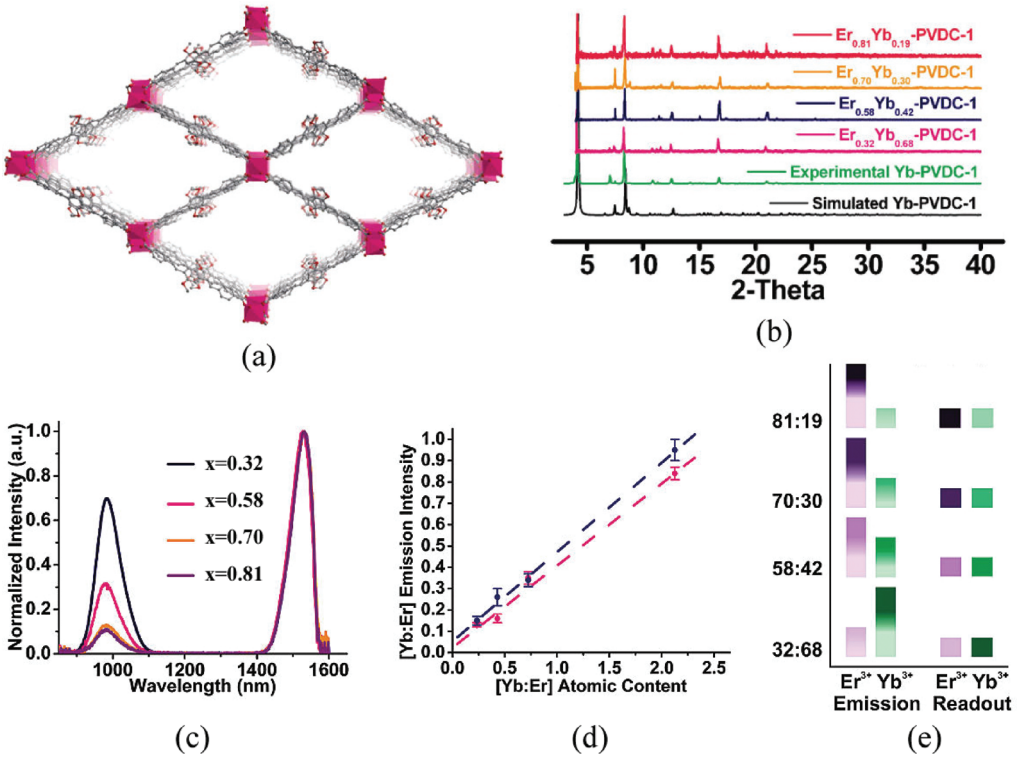

Figure 20. (a) Crystal structure of Yb-PVDC-1 viewed along the crystallographic *c* axis. (b) PXRD patterns for Yb-PVDC-1 and analogues Er_xYb_{1-x}-PVDC-1 (x = 0.32, 0.58, 0.70, and 0.81). (c) Yb^{3+} (980 nm) and Er^{3+} (1530 nm) emission spectra of Er_xYb_{1-x}-PVDC-1 (x = 0.32, 0.58, 0.70, and 0.81) normalized to the Er^{3+} signal upon 490 nm excitation. (d) Plot of the ratio of integrated emission intensities versus their atomic ratio. (e) Color-coded schematic of the barcode readout. Reprinted with permission from ref 269. Copyright 2009 American Chemical Society.

consisting of NIR emissions from three lanthanide ions. These MOFs retain their NIR luminescence when coated in superglue, demonstrating the possibility for practical application.

A quite rare application of MOFs for electroluminescent (EL) devices was reported by Xamena et al.[270] They prepared an EL device by spreading uniformly a thin film of as-synthesized MOF-5 wet paste on a transparent conductive ITO electrode. Under an alternating current of 60 V and 180 Hz, the EL spectrum of MOF-5 consists of a broad (fwhm = ~135 nm) and almost symmetric band, with a small shoulder on the high-energy side. From this spectrum, a value of about 565 nm was derived for $\lambda_{EL(max)}$, which is very close to the value of 540 nm obtained for the corresponding photoluminescence emission maximum. The light intensity is measured to be 0.4 cd m^{-2}, which approximately corresponds to an electricity-to-light efficiency conversion of about 2 lm $watt^{-1}$.

5.3. Biomedicine

In the past decades, there has been an explosion in the development of nanobiotechnology. Nanoscale theranostic systems that incorporate molecular targeting, therapeutic agents, and diagnostic imaging capabilities are emerging as the next generation of personalized medicines and have the potential to dramatically improve the therapeutic outcome of drug therapy.[271] MOFs on the nanometer scale can offer an interesting approach to designing novel theranostic nanomedical devices, because their compositions can be systematically tuned by judicious choice of building blocks. The inherent high porosity and mesoporous nature within some porous luminescent MOFs might secure their very large loadings of biological molecules such as anticancer drugs or biogases into their pores. In addition, the highly available functionality in MOFs, in the form of either open metal sites or functional Lewis basic and acidic sites on the linkers, leads to opportunities to effectively control the interaction with biological system and the release into the environment.[50,173,272−274]

Recently, the use of nanoscale lanthanide MOFs for biological and biomedical applications has garnered increasing attention. The interest of these functional materials relies on the combination of the chemical or biofunctional behavior of MOFs and the unique luminescence properties of lanthanide ions, such as high photostability, long decay rates, large Stokes shifts, and narrow emission bands. Besides their luminescent characteristics, lanthanide MOFs can possess paramagnetic properties, which help to increase the relaxation rate of water protons in the tissues being imaged, making them useful as contrast agents in magnetic resonance imaging (MRI) spectroscopy.

5.3.1. Multimodal Imaging. Multimodal imaging is a new imaging technique, which combines more than one imaging modality, such as X-ray, nuclear, ultrasound, computed tomography (CT), MRI, and fluorescence imaging. Multimodal imaging is becoming more popular because of its improved sensitivity, high resolution, and morphological visualization. In particular, the combination of fluorescence imaging and MRI can ally the sensitivity of the fluorescence component with the high degree of spatial resolution of MRI. Recently, some initial works on the usage of MOFs as multimodal imaging agents have been reported by the Lin group.[49,62−64] For example, Reiter et al. synthesized nanorods of MOF $Gd(1,4\text{-}BDC)_{1.5}(H_2O)_2$ through a reverse microemulsion method, which has allowed the control of the morphologies and sizes by alteration of the water−surfactant ratio of the microemulsion system.[63] These nanomaterials display large longitudinal relaxivities ($R1$) of 35.8 mM^{-1} s^{-1}

dx.doi.org/10.1021/cr200101d |*Chem. Rev.* 2012, 112, 1126–1162

and transverse relaxivities ($R2$) of 55.6 mM^{-1} s^{-1} on a per Gd^{3+} basis and extraordinarily large $R1$ of 1.6 × 10^7 mM^{-1} s^{-1} and $R2$ of 2.5 × 10^7 mM^{-1} s^{-1} on a per nanoparticle basis. The level of $R1$ is unprecedented and at least an order of magnitude higher than those of Gd^{3+}-containing liposomes, which have been shown to be effective target-specific MRI contrast agents for cancer and cardiovascular disease. In addition, the analogues $Gd_{0.95}(1,4\text{-BDC})_{1.5}(H_2O)_2$:$Eu_{0.05}$ and $Gd_{0.95}(1,4\text{-BDC})_{1.5}(H_2O)_2$:$Tb_{0.05}$ were also synthesized. Ethanol suspensions of these materials are highly luminescent upon UV excitation with characteristic red and green luminescence from Eu^{3+} and Tb^{3+}, respectively, suggesting that they can be used as potential contrast agents for multimodal imaging. Taylor et al. also synthesized a nano-MOF $Gd_2(bhc)(H_2O)_6$ (bhc = benzenehexacarboxylate) for multimodal imaging application, but instead they use a surfactant-assisted synthesis method.[64] These MOF particles were found to have a modest $R1$ of 1.5 mM^{-1} s^{-1} and an impressive $R2$ of 122.6 mM^{-1} s^{-1} on a per-Gd basis. Similarly, the Eu- and Tb-doped nanoparticles of $Gd_2(bhc)(H_2O)_6$ are highly luminescent and exhibit characteristic Eu and Tb luminescence under ultraviolet excitation.

For biological and biomedical applications, the surface modification and functionalization of the NMOFs are of key importance because they must be chemically compatible with biomolecules such as enzymes, proteins, antibodies, DNA, etc. Furthermore, surface modification and functionalization could stabilize the NMOFs suspensions, introduce specific functionality, and ensure that the nano-MOFs reach the active sites and bioadhesion. Jung et al. have incorporated the green fluorescent protein (EGFP) onto the surface of the 1D-MOF $(Et_2NH_2)(In(pda)_2)$ (H_2pda = 1,4-phenylenediacetic acid), 2D-MOF $Zn(bpydc)(H_2O)(H_2O)$ (bpydc = 2,2′-bipyridine-5,5′-dicarboxylate), and 3D-MOF IRMOF-3, respectively.[173] Under the confocal laser scanning microscope, the EGFP-decorated MOFs emit uniform green fluorescence, and most green emissions are observed from the surface of crystals, indicating that the anchored EGFP is still functional (Figure 21). The amounts of EGFP coated on the MOFs are determined as 0.048, 0.052, 0.064 mg g^{-1} of the 1D-, 2D-, and 3D-MOFs, respectively. Jung et al. also conjugated an enzyme CAL-B, which is one of the most widely used enzymes because of its high activity and selectivity, with the three MOFs. The CAL-B-coated MOFs display several hundred-fold higher activities and the same enantioselectivity of the product as compared to the native CAL-B. Especially, the CAL-B on IRMOF-3 shows activity about 103-fold higher than that of free CAL-B. This approach is an important step toward the bioactive modification of MOFs for biological and biomedical application.

Reiter et al.[62] developed a general surface modification method to coat NMOFs with silica shells of variable thickness. In their report, the NMOF $Gd(1,4\text{-BDC})_{1.5}(H_2O)_2$ mentioned above was surface modified with polyvinylpyrrolidone (PVP), and then coated with a silica shell through a sol−gel process with tetraethyl orthosilicate to afford core−shell nanostructures. The silica shell thickness can be simply controlled by the alteration of reaction time. Interestingly, the NMOF core could be completely removed when placed in an acidic solution to afford hollow silica shells with varied thickness and aspect ratios. The release of cargo from such core−shell nanostructures could be controlled by taking advantage of slow diffusion of metal and organic constituents through the silica shell. In addition, a silica-coated Eu-doped NMOF was prepared by the same method and further functionalized with a silylated Tb-EDTA monoamide derivative (Tb-EDTM) to yield a dual lanthanide biosensor for probe dipicolinic acid (DPA), which is a major constituent of many pathogenic spore-forming bacteria. When excited at 278 nm, this material only gave Eu^{3+} luminescence because the Tb-EDTM moiety is essentially nonemissive. Upon exposure to DPA, the Tb^{3+} luminescence became clearly visible due to the formation of the Tb-EDTM−DPA complex, while the Eu^{3+} emission from the NMOF core acts as noninterfering internal calibration. The DPA detection limit for this system was estimated to be about 48 nM, suggesting its feasibility of the selective detection of DPA in the presence of physiological prevalent interferences such as amino acids.

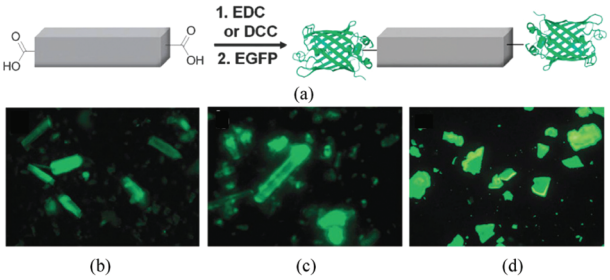

Figure 21. (a) Schematic representation of the bioconjugation of the MOF $(Et_2NH_2)(In(pda)_2)$ with EGFP. (b−d) Fluorescence microscopic images of EGFP-coated $(Et_2NH_2)(In(pda)_2)$, $Zn(bpydc)(H_2O)(H_2O)$, and IRMOF-3, respectively. Reprinted with permission from ref 173. Copyright 2011 The Royal Society of Chemistry.

An interesting surface functionalization approach allowing for target-specific imaging was reported by Taylor et al.[61] They synthesized two Mn NMOFs, $Mn(1,4\text{-BDC})(H_2O)_2$ and $Mn_3(BTC)_2(H_2O)_6$, and coated them with a thin silica shell using the method mentioned above, and subsequently functionalized with a cyclic peptide c(RGDfK) and a fluorescence dye Rhodamine B (Figure 22a), in which c(RGDfK) can target angiogenic cancers (such as HT-29) by binding to the upregulated $\alpha_v\beta_3$ integrin, whereas Rhodamine B provides characteristic fluorescence for optical imaging. In MR imaging, the HT-29 cells incubated with the targeted particles show much higher signals than those that were not incubated with nanoparticles as well as those that were incubated with the nontargeted particles. Confocal microscopic imaging studies also confirmed the selected uptake of the particles with the targeting peptide (Figure 22b−d). The successful functionalization of NMOFs to engender stability, biocompatibility, luminescence, and other specific properties makes them promising for targeted delivery, multimodal imaging, and therapeutic agents.

5.3.2. Targeted Drug Delivery and Treatment. The combination of molecular imaging and drug delivery in MOFs will lead to the exciting possibility of MOF-based theranostics, in which imaging will be used to guide, follow, and quantify the drug delivery process. Up to now, core−shell architectures combining diverse functionalities and surface modifications into a single NMOF have been designed as biosensing platforms for imaging, targeting, diagnostics, and therapy. Taylor-Pashow et al. demonstrated a novel strategy of delivering an fluorescence imaging contrast agent and an anticancer drug by postsynthetic modifications of a highly porous MOF.[274] They synthesized an amino-functionalized iron-carboxylate MOF by incorporating 2-aminoterephthalic acid (NH_2-BDC). To load a optical imaging contrast agent, the MOF was treated with 1,3,5,7-tetramethyl-4,4-difluoro-8-bromomethyl-4-bora-3*a*,4*a*-diaza-*s*-indacene (Br-BODIPY) to yield a BODIPY-loaded particles with a loading capacity of 5.6−11.6 wt %. In addition, the ethoxysuccinato-cisplatin (ESCP), which is a prodrug of cisplatin, was also loaded into the MOF (Figure 23). To improve the biological stability, the BODIPY- and ESCP-loaded MOF particles were also coated with silica shells using Na_2SiO_3 as the

silica source to afford novel core−shell nanostructures. Laser scanning confocal microscopy images show that the BODIPY-loaded particles could cross the cell membrane and release the BODIPY dye inside of the cell; thus the fluorescence was present in cells incubated with BODIPY-loaded particles but absent in cells incubated without nanoparticles, suggesting that the MOF is an efficient platform for delivering an optical contrast agent (Figure 24). In addition, the modified BODIPY ligand was incubated with the cells, but no fluorescence was observed at all within the cells, indicating that the core−shell nanostructure was required for cell uptake. Treatment of HT-29 cells with ESCP-loaded MOF particles shows appreciable cytotoxicity (IC_{50} = 29 μM), which is slightly less cytotoxic than cisplatin under the same conditions (IC_{50} = 20 μM). Further functionalization of silica-coated particles with silyl derived c(RGDfK), which is a cyclic peptide known to target the $\alpha_v\beta_3$ integrin, shows that these particles have cytotoxicity (IC_{50} = 21 μM) comparable to that of cisplatin. The generality of this approach could be utilized for the design of a wide range of nanomedical devices for theranostic applications.

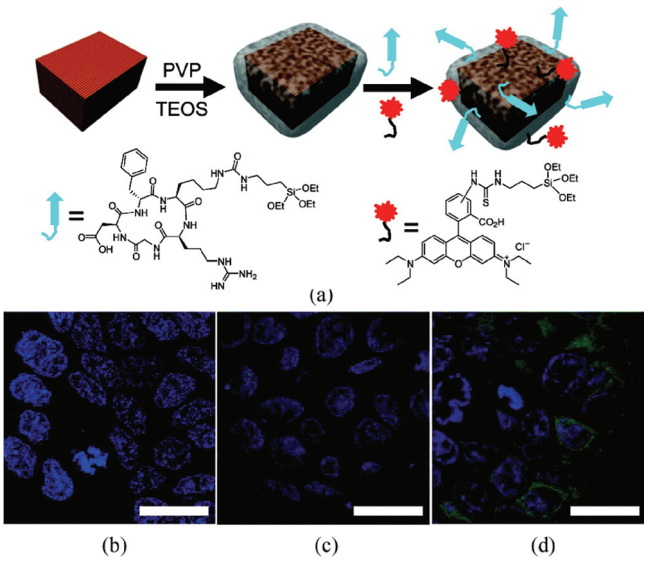

Figure 22. (a) Schematic representation of the surface modification with silica sell and functionalization with a fluorophore and a cell-targeting peptide for the Mn nano-MOFs. (b−d) Confocal microscopic images of HT-29 cells that were incubated with no silica-coated MOF (b), non-targeted silica-coated MOF (c), and c(RGDfK)-targeted silica-coated MOF (d). The blue color was from DRAQ5 used to stain the cell nuclei while the green color was from rhodamine B. The bars represent 20 μm. Reprinted with permission from ref 61. Copyright 2008 American Chemical Society.

A novel nanoscale theranostic device with tumor targeting, diagnostic imaging, and treatment capability was demonstrated by Rowe et al.[271] The theranostic device was prepared through attachment of well-defined functional polymer chains, such as cellular level imaging agent *O*-methacrylate, targeting moiety *H*-glycinearginine-glycine-aspartate-serine-NH_2 (GRGDS-NH_2), and antineoplastic drug methotrexate (MTX) to gadolinium metal−organic framework (Gd MOF) nanoparticles, with preservation of all of the functions of the individual components (Figure 25). The average thickness of the polymer shell coated on the Gd MOF nanoparticles is approximately 9 nm. Using fluorescence imaging, it is demonstrated that the polymer-modified Gd MOF nanoparticles show active targeting toward FITZ-HSA, which is an $\alpha_v\beta_3$-expressing canine endothelial sarcoma cell line. In the cell growth inhibition studies, the polymer-modified Gd MOF nanoparticles show a dose-dependent inhibition of growth of the FITZ-HSA tumor cells that was comparable to that of the free MTX drug on an equal concentration of MTX basis. The development of nanoscale theragnostic

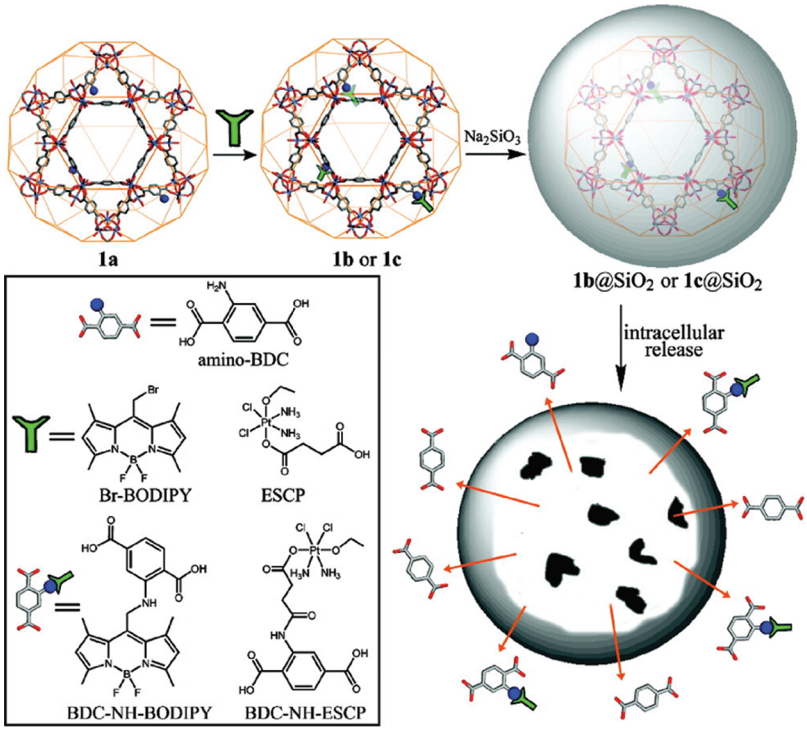

Figure 23. (a) Functionalization of iron-carboxylate MOF with an optical imaging contrast agent (BODIPY) and a prodrug of cisplatin (ESCP) through postsynthetic modifications. Reprinted with permission from ref 274. Copyright 2009 American Chemical Society.

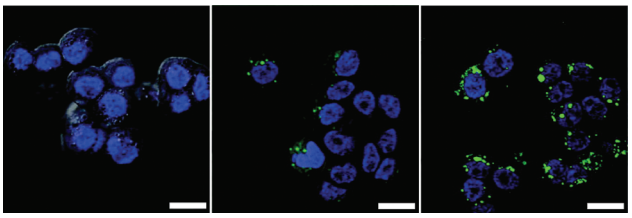

Figure 24. Overlayed DIC and confocal fluorescence images of the DRAQ5 channel (blue, nuclear stain) and the BDC-NH-BODIPY channel (green) of HT-29 cells incubated with no particles (left), 0.19 mg/mL of BODIPY-loaded MOF particles (equivalent to 17 μM BODIPY) (middle), and 0.38 mg/mL of BODIPY-loaded MOF particles (equivalent to 34 μM BODIPY) (right). The bars represent 25 μm. Reprinted with permission from ref 274. Copyright 2009 American Chemical Society.

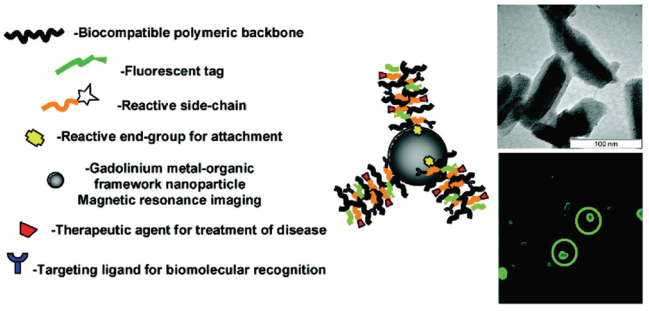

Figure 25. Polymer-modified Gd MOF nanoparticles as a nanomedicine construct for targeted imaging and treatment of cancer. Reprinted with permission from ref 271. Copyright 2009 American Chemical Society.

devices for the diagnosis and treatment represents one of the primary targets of the general field of nanomedicine. Despite that research on biomedical applications of MOFs in drug delivery and as theranostic device is gaining more interest, their clinical application is yet to be realized. The systematic investigation concerning the stability of MOFs under biological environment, toxicology, and biocompatibility of both the metal and the bridging ligand may accelerate the implementation of MOFs in medicine.

Photodynamic therapy is an emerging treatment that uses a photosensitizing drug and red laser light to kill cells, usually cancer cells. The mechanism is based on the interaction between the excited photosensitizer and surrounding molecules, generating reactive oxygen species, such as singlet oxygen, which will cause oxidative damage to diseased cells and tissues. Zhang et al. proposed a new design of versatile photosensitizers for photodynamic therapy.[275,276] They utilized the up-conversion luminescent nanoparticles as core and coated with a porous, thin layer of silica. During the coating process, the photosensitizing drug molecules with high absorbance in the spectral window matching the emission of the nanoparticles are doped in the silica shell, and an antibody as targeting moiety is covalently attached to the silica shell surface. When irradiated by infrared light, emission from the up-conversion luminescent nanoparticles will be absorbed by the photosensitizing molecules. Subsequently, excited photosensitizing molecules will produce reactive oxygen species, leading to oxidative damage of the neighboring target cells. The utilization of up-conversion luminescent materials excited in the NIR spectral range minimizes background autofluorescence, photobleaching, and photodamage to biological specimens.

Up to now, MOFs acting as efficient up-conversion luminescent materials are still scarce. Although some up-conversion luminescent MOFs have been prepared,[100,166,186,187] only the photoluminescence properties are reported. To the best of our knowledge, no examples of luminescent MOFs for photodynamic therapy application are reported. Clearly, it would be interesting to utilize up-conversion luminescent MOFs in photodynamic therapy because the high loading capacity and controllable drug release of MOFs can facilitate the delivery and release of the photodynamic therapy drug. Moreover, the attractive multifunctionality of MOFs makes it possible to combine the up-conversion luminescence and drug delivery in a single component.

6. CONCLUSIONS AND OUTLOOK

Luminescent MOFs are certainly very promising multifunctional materials for chemical sensors, light-emitting devices, and biomedicine. As compared to the research on functional MOFs for gas storage, separation, and heterogeneous catalysis, the research on luminescent MOFs is still at the early stage. In fact, some practically useful MOFs for gas storage, separation, and heterogeneous catalysis have been realized at lab scale. With the input of the industrial partners, some of these promising MOFs for these very important applications will be implemented in our daily life in the near future.

The basic principles and the promises of luminescent MOFs as multifunctional materials have been established, as outlined in this Review. On the one hand, comprehensive experimental studies and screening the luminescence properties of those reported and future synthesized MOFs are still necessary to establish the database of luminescent MOFs. These basic studies should not only focus on temperature- and excitation wavelength-dependence luminescence, but also should cover other important luminescent properties, particularly quantum yield and lifetime. On the other hand, some in-depth studies on the mechanism of the luminescence behavior including the origin of the luminescence and structure-luminescent property relationship need to be carried out through the collaboration with theoretical scientists.

The deliberate selection of organic linkers is very important to ensure the construction of MOF materials with luminescence. In this regard, those organic linkers with high-conjugated π electrons such as pyrene- and naphthalene-based organic linkers will be extensively explored for functional luminescent MOFs. Heterometal−organic frameworks (HMOFs; sometimes also termed as mixed-metal−organic frameworks (M′MOFs)) have revealed some unique luminescent properties and will be paid more attention in the future.

Rational control on structure, pore size, and functional sites within luminescent MOFs will be enforced to target highly sensitive and selective luminescent sensing MOFs. Further efforts should be focused on the construction of porous luminescent MOFs with multifunctional sites to collaboratively induce their preferential and highly sensitive and selective binding with different ions, leading to highly selective and sensitive luminescent MOF probes for different ions. If the luminescent sensing could be combined with the sieving function of the micropores to allow small molecules to go through, while excluding larger species, it would be possible to obtain some highly sensitive sensors for small molecules.

The simple yet sophisticated decoding approach developed by Kitagawa et al. is one of the breakthroughs on the exploration of functional luminescent MOFs. This approach will certainly initiate extensive research endeavors not only on luminescent light emitting MOFs, but also on MOF sensor devices due to the combination of turn-on emission and multicolor luminescence.

Some technically important devices will be explored based on luminescent MOFs. Although luminescent MOF-based OLED devices have not been realized, it is theoretically feasible to incorporate

nanoscale electroluminescence MOF between two conductors for such useful electronic devices. To realize such an important functionality, electroluminescence MOFs need to be realized first. Nanoscale luminescent MOFs will be expected to be fabricated into thin films for their straightforward and instant sensing devices in the future.

Nanoscale luminescent MOFs have a bright future for their applications in tissue and cell imaging, as well as drug delivery monitoring and treatment, and will be extensively pursued for theranostic nanomedicine in the near future. In this regard, close multidisciplinary collaboration among chemists, materials scientists, biomedical scientists, and bioengineers will certainly facilitate the implementation of some promising luminescent MOFs materials and technologies for practical applications in theranostic nanomedicine.

AUTHOR INFORMATION

Corresponding Author

*E-mail: gdqian@zju.edu.cn (G.Q.), banglin.chen@utsa.edu (B.C.).

BIOGRAPHIES

Yuanjing Cui was born in Jiangsu, China. He received his Ph. D. in Materials Science from Zhejiang University in 2006 under the supervision of Prof. Minquan Wang and Prof. Guodong Qian. Currently, he is an associate professor in the Department of Materials Science and Engineering at Zhejiang University, and he is also a visiting scholar in Chemistry, University of Texas at San Antonio. His research interest focuses on organic−inorganic hybrid photonic materials.

Yanfeng Yue was born in 1977, Shandong, China. In 2008, he obtained his Ph.D. in chemistry from Peking University under the supervision of Professor Chunhua Yan. At Peking University, his thesis focused on molecular magnetism. In 2008, he started his postdoctoral research at the University of Liverpool, United Kingdom, and began exploring the porous properties of metal−organic frameworks under the guidance of Professor Matthew J. Rosseinsky. He currently holds a postdoctoral fellowship at the University of Texas at San Antonio, where he continues to work on functional porous metal−organic frameworks under the guidance of Professor Banglin Chen.

Guodong Qian was born in Zhejiang, China. He received his bachelor's (1988) and master's (1992) degrees in Materials Science from Zhejiang University in China. He joined the Materials Department of Zhejiang University after obtaining his Ph.D. degree from Zhejiang University in 1997. He was promoted to associate professor and full professor in 1999 and 2002, respectively.

Banglin Chen was born in Zhejiang, China. He received B.S. (1985) and M.S. (1988) degrees in Chemistry from Zhejiang University in China, and his Ph.D. from National University of Singapore in 2000. He has been working with Professors Omar M. Yaghi at University of Michigan, Stephen Lee at Cornell University, and Andrew W. Maverick at Louisiana State University as the postdoctoral fellow during 2000−2003 before joining the University of Texas-Pan American in 2003. He moved to the University of Texas at San Antonio in August 2009, and now he is a Professor of Chemistry.

ACKNOWLEDGMENT

This work was supported by the Award CHE 0718281 from the NSF and AX-1730 from the Welch Foundation (B.C.). We gratefully acknowledge financial support of this work from the

National Natural Science Foundation of China (nos. 50802084, 50928201, 50972127, and 51010002) and the Fundamental Research Funds for the Central Universities.

LIST OF ABBREVIATIONS

3-Abpt	4-amine-3,5-bis(3-pyridyl)-1,2,4-triazole
ABTC	3,3′,5,5′-azobenzenetetracarboxylate
adi	adipate
ATA	5-amino-tetrazole
ATPA	2-aminoterephthalate
BCPA	9,10-bis(*p*-carboxyphenyl) anthracene
1,2-BDC	1,2-benzenedicarboxylate
1,3-BDC	1,3-benzenedicarboxylate
1,4-BDC	1,4-benzenedicarboxylate
BDC-F_4	2,3,5,6-tetrafluoro-1,4-benzenedicarboxylate
bhc	benzenehexacarboxylate
bipy	4,4′-bipyridine
bpdc	4,4′-biphenyldicarboxylate
Bpe	*trans*-bis(4-pyridyl)ethylene
bpee	1,2-bipyridylethene
bpp	1,3-bis(4-pyridyl)propane
BPT	biphenyl-3,4′,5-tricarboxylate
bpydc	2,2′-bipyridine-5,5′-dicarboxylate
BPVIC	2,8-bis[2-(2-pyridyl)vinyl]-5,11-di(2-ethylhexyl)-indolo[3,2-*b*]carbazole
bpz	3,3′,5,5′-tetramethyl-4,4′-bipyrazolate
bpzb	bis(pyrazole-1-yl)butane
bpze	bis(pyrazole-1-yl)ethane
bpzm	bis(pyrazole-1-yl)methane
bpzp	bis(pyrazole-1-yl)prothane
Br-BODIPY	1,3,5,7-tetramethyl-4,4-difluoro-8-bromomethyl-4-bora-3*a*,4*a*-diaza-*s*-indacene
BTAH	benzotriazole
BTB	4,4′,4″-benzenetribenzoate
BTC	1,3,5-benzenetricarboxylate
CCT	correlated color temperature
chdc	1,4-cyclohexanedicarboxylate
CIE	Commission International ed'Eclairage
cin	cinnamate
CRI	color rendering index
CT	computed tomography
CTAB	cetyltrimethylammonium bromide
CTC	*cis*,*cis*-1,3,5-cyclohexanetricarboxylate
DABCO	1,4-diazabicyclo[2.2.2]octane
dbm	dibenzoylmethane
DFDA	9,9-dipropylfluorene-2,7-dicarboxylate
DHT	2,5-dihydroxyterephthalate
dipicH_2	dipicolinic acid
DMA	dimethylammonium
DMNB	2,3-dimethyl-2,3-dinitrobutane
2,4-DNT	2,4-dinitrotoluene
dpNDI	*N*,*N*′-di(4-pyridyl)-1,4,5,8-naphthalenediimide
EL	electroluminescent
ESCP	ethoxysuccinato-cisplatin
ESET	excited-state electron transfer
ESIPT	excited-state intramolecular proton transfer
ESPT	excited-state proton transfer
FMA	fumarate
H_2ADB	4,4′-azodibenzoic acid
H_2ap	adipic acid
H_3bidc	1*H*-benzimidazole-5,6-dicarboxylic acid
H_2chdc	1,4-cyclohexanedicarboxylic acid
HDAM	*N*,*N*′-diacetic acid imidazolium
H_2DFDA	9,9-dipropylfluorene-2,7-dicarboxylate anion
H_2dtba	2,2′-dithiobisbenzoic acid
H_2FDC	fluorene-2,7-dicarboxylic acid
H_2gt	glutaric acid
H_2hfipbb	4,4′-(hexafluoroisopropylidene)bis(benzoic acid)
Hinic	isonicotinic acid
HMOFs	heterometal−organic frameworks
Hnic	nicotinic acid
H_2nicO	2-hydroxynicotinic acid
H_3NTB	4,4′,4″-nitrilotrisbenzoic acid
H_2ox	oxalic acid
H_2pda	1,4-phenylenediacetic acid
H_2PhenDCA	1,10-phenanthroline-2,9-dicarboxylic acid
H_4TETA	1,4,8,11-tetraazacyclotetradecane-1,4,8,11-tetra-acetic acid
3-H_2tzba	3-(5*H*-tetrazolyl)benzoic acid
H_2-PVDC	4,4′-[(2,5-dimethoxy-1,4-phenylene)di-2,1-ethenediyl]bis-benzoic acid
H_4TETA	1,4,8,11-tetraazacyclotetradecane-1,4,8,11-tetra-acetic acid
H_2tp	terephthalic acid
IBIL	ion-beam-induced luminescence
IDC	imidazole-4,5-dicarboxylate
ILAG	ion- and liquid-assisted grinding
imdc	4,5-imidazoledicarboxylate
LAG	liquid-assisted grinding
LMCT	ligand-to-metal charge transfer
Ln^{3+}	lanthanide ions
MES	2-(*N*-morpholino)ethanesulfonate
MLCT	metal-to-ligand charge transfer
MOFs	metal−organic frameworks
MRI	magnetic resonance imaging
5MT	5-methyl-tetrazole
1,4-NDC	1,4-naphthalenedicarboxylate
nds	2,6-naphthanlenedisulfonate
nic	nicotinate
NIR	near-infrared
NMOFs	nano-MOFs
NMP	1-methyl-2-pyrrolidone
NTA	nitrilotriacetate
OBA	4,4′-oxybis(benzoate)
ox	oxalate
PDA	pyridine-2,6-dicarboxylic acid
pdc	2,5-pyridinedicarboxylate
Phen	1,10-phenanthroline
$PhPPy_2$	bis(2-pyridyl)phenylphosphine
pimda	2-propyl-4,5-imidazole-dicarboxylate
Pmtz	5-(pyrimidyl)-tetrazolato
ppy	2-phenylpyridine
pta	2,4,6-pyridinetricarboxylate
4-Ptz	5-(4-pyridyl)tetrazole
pydc	pyridine-dicarboxylate
2,6-pydc	pyridine-2,6-dicarboxylate
2,3-pydcH_2	pyridine-2,3-dicarboxylic acid
3-PyHBIm	2-(3-pyridyl)benzimidazole
4-PyHBIm	2-(4-pyridyl)benzimidazole
Pz	3,5-dimethylpyrazole
pzdc	2,5-pyrazinedicarboxylate
quin	2,2′-biquinoline
Rh6G	rhodamine 6G

dx.doi.org/10.1021/cr200101d |*Chem. Rev.* 2012, 112, 1126–1162

SBUs	secondary building units
sfdb	4,4′-sulfonyldibenzoic acid
TAA	1*H*-tetrazole-5-acetate
TBAPy	1,3,6,8-tetrakis(*p*-benzoic acid)pyrene
TDC	thiophene-2,5-dicarboxylate
TEAF	triethylammonium fluoride
TED	triethylenediamine
TFA	trifluoroacetic acid
TNT	2,4,6-trinitrotoluene
tta	2-thenoyltrifluoroacetone
TzC	5-carboxylato-tetrazolato
UV	ultraviolet
VOCs	volatile organic compounds

REFERENCES

(1) Eliseeva, S. V.; Bunzli, J. C. G. *Chem. Soc. Rev.* **2010**, *39*, 189.
(2) Binnemans, K. *Chem. Rev.* **2009**, *109*, 4283.
(3) Hwang, S. H.; Moorefield, C. N.; Newkome, G. R. *Chem. Soc. Rev.* **2008**, *37*, 2543.
(4) Carlos, L. D.; Ferreira, R. A. S.; de Zea Bermudez, V.; Julián-López, B.; Escribano, P. *Chem. Soc. Rev.* **2011**, *40*, 536.
(5) Lo, S.-C.; Burn, P. L. *Chem. Rev.* **2007**, *107*, 1097.
(6) Grimsdale, A. C.; Leok Chan, K.; Martin, R. E.; Jokisz, P. G.; Holmes, A. B. *Chem. Rev.* **2009**, *109*, 897.
(7) Veinot, J. G. C.; Marks, T. J. *Acc. Chem. Res.* **2005**, *38*, 632.
(8) Janiak, C. *Dalton Trans.* **2003**, 2781.
(9) Cahill, C. L.; de Lill, D. T.; Frisch, M. *CrystEngComm* **2007**, *9*, 15.
(10) Suh, M.; Cheon, Y.; Lee, E. *Coord. Chem. Rev.* **2008**, *252*, 1007.
(11) Maspoch, D.; Ruiz-Molina, D.; Veciana, J. *Chem. Soc. Rev.* **2007**, *36*, 770.
(12) Rocha, J.; Carlos, L. D.; Paz, F. A. A.; Ananias, D. *Chem. Soc. Rev.* **2011**, *40*, 926.
(13) Allendorf, M. D.; Bauer, C. A.; Bhakta, R. K.; Houk, R. J. T. *Chem. Soc. Rev.* **2009**, *38*, 1330.
(14) Chen, B.; Xiang, S.; Qian, G. *Acc. Chem. Res.* **2010**, *43*, 1115.
(15) Meek, S. T.; Greathouse, J. A.; Allendorf, M. D. *Adv. Mater.* **2011**, *23*, 249.
(16) Shekhah, O.; Liu, J.; Fischer, R. A.; Wöll, C. *Chem. Soc. Rev.* **2011**, *40*, 1081.
(17) Férey, G. *Chem. Soc. Rev.* **2008**, *37*, 191.
(18) Silva, C. G.; Corma, A.; García, H. *J. Mater. Chem.* **2010**, *20*, 3141.
(19) Kuppler, R. J.; Timmons, D. J.; Fang, Q.-R.; Li, J.-R.; Makal, T. A.; Young, M. D.; Yuan, D.; Zhao, D.; Zhuang, W.; Zhou, H.-C. *Coord. Chem. Rev.* **2009**, *253*, 3042.
(20) Janiak, C.; Vieth, J. K. *New J. Chem.* **2010**, *34*, 2366.
(21) Li, H.; Eddaoudi, M.; O'Keeffe, M.; Yaghi, O. M. *Nature* **1999**, *402*, 276.
(22) Chen, B. L.; Eddaoudi, M.; Hyde, S. T.; O'Keeffe, M.; Yaghi, O. M. *Science* **2001**, *291*, 1021.
(23) Ma, L. Q.; Abney, C.; Lin, W. B. *Chem. Soc. Rev.* **2009**, *38*, 1248.
(24) Li, J. R.; Kuppler, R. J.; Zhou, H. C. *Chem. Soc. Rev.* **2009**, *38*, 1477.
(25) Murray, L. J.; Dinca, M.; Long, J. R. *Chem. Soc. Rev.* **2009**, *38*, 1294.
(26) Jiang, H.-L.; Xu, Q. *Chem. Commun.* **2011**, *47*, 3351.
(27) Long, J. R.; Yaghi, O. M. *Chem. Soc. Rev.* **2009**, *38*, 1213.
(28) Tian, Y.-Q.; Chen, Z.-X.; Weng, L.-H.; Guo, H.-B.; Gao, S.; Zhao, D. Y. *Inorg. Chem.* **2004**, *43*, 4631.
(29) Huang, X.-C.; Lin, Y.-Y.; Zhang, J.-P.; Chen, X.-M. *Angew. Chem., Int. Ed.* **2006**, *45*, 1557.
(30) Fang, Q.; Zhu, G.; Xue, M.; Sun, J.; Wei, Y.; Qiu, S.; Xu, R. *Angew. Chem., Int. Ed.* **2005**, *44*, 3845.
(31) Tian, Y.-Q.; Cai, C.-X.; Ji, Y.; You, X.-Z.; Peng, S.-M.; Lee, G.-H. *Angew. Chem., Int. Ed.* **2002**, *41*, 1384.
(32) Hayashi, H.; Côté, A. P.; Furukawa, H.; O'Keeffe, M.; Yaghi, O. M. *Nat. Mater.* **2007**, *6*, 501.
(33) Wang, B.; Côté, A. P.; Furukawa, H.; O'Keeffe, M.; Yaghi, O. M. *Nature* **2008**, *453*, 207.
(34) Klimakow, M.; Klobes, P.; Thünemann, A. F.; Rademann, K.; Emmerling, F. *Chem. Mater.* **2010**, *22*, 5216.
(35) Braga, D.; Grepioni, F.; Maini, L.; Mazzeo, P. P.; Ventura, B. *New J. Chem.* **2011**, *35*, 339.
(36) Yuan, W.; Friščić, T.; Apperley, D.; James, S. L. *Angew. Chem., Int. Ed.* **2010**, *49*, 3916.
(37) Friščić, T.; Reid, D. G.; Halasz, I.; Stein, R. S.; Dinnebier, R. E.; Duer, M. J. *Angew. Chem., Int. Ed.* **2009**, *49*, 712.
(38) Son, W.-J.; Kim, J.; Kim, J.; Ahn, W.-S. *Chem. Commun.* **2008**, 6336.
(39) Jung, D.-W.; Yang, D.-A.; Kim, J.; Kim, J.; Ahn, W.-S. *Dalton Trans.* **2010**, *39*, 2883.
(40) Ni, Z.; Masel, R. I. *J. Am. Chem. Soc.* **2006**, *128*, 12394.
(41) Centrone, A.; Harada, T.; Speakman, S.; Hatton, T. A. *Small* **2010**, *6*, 1598.
(42) Stein, A.; Keller, S. W.; Mallouk, T. E. *Science* **1993**, *259*, 1558.
(43) Buckingham, A. D.; Fowler, P. W. *J. Chem. Phys.* **1983**, *79*, 6426.
(44) Eddaoudi, M.; Kim, J.; Rosi, N.; Vodak, D.; Wachter, J.; O'Keeffe, M.; Yaghi, O. M. *Science* **2002**, *295*, 469.
(45) Chen, B. L.; Ma, S. Q.; Zapata, F.; Fronczek, F. R.; Lobkovsky, E. B.; Zhou, H. C. *Inorg. Chem.* **2007**, *46*, 1233.
(46) Chen, B. L.; Liang, C. D.; Yang, J.; Contreras, D. S.; Clancy, Y. L.; Lobkovsky, E. B.; Yaghi, O. M.; Dai, S. *Angew. Chem., Int. Ed.* **2006**, *45*, 1390.
(47) O'Keeffe, M.; Peskov, M. A.; Ramsden, S. J.; Yaghi, O. M. *Acc. Chem. Res.* **2008**, *41*, 1782.
(48) Carné, A.; Carbonell, C.; Imaz, I.; Maspoch, D. *Chem. Soc. Rev.* **2011**, *40*, 291.
(49) Lin, W.; Rieter, W. J.; Taylor, K. M. L. *Angew. Chem., Int. Ed.* **2009**, *48*, 650.
(50) Huxford, R. C.; Della Rocca, J.; Lin, W. *Curr. Opin. Chem. Biol.* **2010**, *14*, 262.
(51) Zhao, B.; Chen, X.-Y.; Cheng, P.; Liao, D.-Z.; Yan, S.-P.; Jiang, Z.-H. *J. Am. Chem. Soc.* **2004**, *126*, 15394.
(52) Liu, W.; Jiao, T.; Li, Y.; Liu, Q.; Tan, M.; Wang, H.; Wang, L. *J. Am. Chem. Soc.* **2004**, *126*, 2280.
(53) Chen, B.; Wang, L.; Zapata, F.; Qian, G.; Lobkovsky, E. B. *J. Am. Chem. Soc.* **2008**, *130*, 6718.
(54) Chen, B.; Wang, L.; Xiao, Y.; Fronczek, F. R.; Xue, M.; Cui, Y.; Qian, G. *Angew. Chem., Int. Ed.* **2009**, *48*, 500.
(55) Wong, K. L.; Law, G. L.; Yang, Y. Y.; Wong, W. T. *Adv. Mater.* **2006**, *18*, 1051.
(56) Harbuzaru, B. V.; Corma, A.; Rey, F.; Atienzar, P.; Jordá, J. L.; García, H.; Ananias, D.; Carlos, L. D.; Rocha, J. *Angew. Chem., Int. Ed.* **2008**, *47*, 1080.
(57) Chen, B.; Yang, Y.; Zapata, F.; Lin, G.; Qian, G.; Lobkovsky, E. B. *Adv. Mater.* **2007**, *19*, 1693.
(58) Jiang, H.-L.; Tatsu, Y.; Lu, Z.-H.; Xu, Q. *J. Am. Chem. Soc.* **2010**, *132*, 5586.
(59) Takashima, Y.; Martínez, V. M.; Furukawa, S.; Kondo, M.; Shimomura, S.; Uehara, H.; Nakahama, M.; Sugimoto, K.; Kitagawa, S. *Nat. Comms.* **2011**, *2*, 168.
(60) Xu, H.; Liu, F.; Cui, Y.; Chen, B.; Qian, G. *Chem. Commun.* **2011**, *47*, 3153.
(61) Taylor, K. M. L.; Rieter, W. J.; Lin, W. *J. Am. Chem. Soc.* **2008**, *130*, 14358.
(62) Rieter, W. J.; Taylor, K. M. L.; Lin, W. *J. Am. Chem. Soc.* **2007**, *129*, 9852.
(63) Rieter, W. J.; Taylor, K. M. L.; An, H.; Lin, W.; Lin, W. *J. Am. Chem. Soc.* **2006**, *128*, 9024.
(64) Taylor, K. M. L.; Jin, A.; Lin, W. *Angew. Chem., Int. Ed.* **2008**, *47*, 7722.

(65) Ma, L.; Evans, O. R.; Foxman, B. M.; Lin, W. *Inorg. Chem.* **1999**, *38*, 5837.
(66) Bauer, C. A.; Timofeeva, T. V.; Settersten, T. B.; Patterson, B. D.; Liu, V. H.; Simmons, B. A.; Allendorf, M. D. *J. Am. Chem. Soc.* **2007**, *129*, 7136.
(67) Zhang, L.-Z.; Gu, W.; Li, B.; Liu, X.; Liao, D.-Z. *Inorg. Chem.* **2007**, *46*, 622.
(68) Fang, Q.; Zhu, G.; Xue, M.; Sun, J.; Sun, F.; Qiu, S. *Inorg. Chem.* **2006**, *45*, 3582.
(69) Chelebaeva, E.; Larionova, J.; Guari, Y.; Sá Ferreira, R. A.; Carlos, L. D.; Almeida Paz, F. A.; Trifonov, A.; Guérin, C. *Inorg. Chem.* **2008**, *47*, 775.
(70) Wang, G.-H.; Li, Z.-G.; Jia, H.-Q.; Hu, N.-H.; Xu, J.-W. *CrystEngComm* **2009**, *11*, 292.
(71) Pan, Z.-R.; Xu, J.; Yao, X.-Q.; Li, Y.-Z.; Guo, Z.-J.; Zheng, H.-G. *CrystEngComm* **2011**, *13*, 1617.
(72) Yang, E.-C.; Zhao, H.-K.; Ding, B.; Wang, X.-G.; Zhao, X.-J. *Cryst. Growth Des.* **2007**, *7*, 2009.
(73) Xue, M.; Zhu, G.; Zhang, Y.; Fang, Q.; Hewitt, I. J.; Qiu, S. *Cryst. Growth Des.* **2008**, *8*, 427.
(74) Wang, Z.-W.; Ji, C.-C.; Li, J.; Guo, Z.-J.; Li, Y.-Z.; Zheng, H.-G. *Cryst. Growth Des.* **2009**, *9*, 475.
(75) Wang, X. W.; Chen, J.-Z.; Liu, J.-H. *Cryst. Growth Des.* **2007**, *7*, 1227.
(76) Wang, H.-S.; Zhao, B.; Zhai, B.; Shi, W.; Cheng, P.; Liao, D.-Z.; Yan, S.-P. *Cryst. Growth Des.* **2007**, *7*, 1851.
(77) Su, Z.; Xu, J.; Fan, J.; Liu, D.-J.; Chu, Q.; Chen, M.-S.; Chen, S.-S.; Liu, G.-X.; Wang, X.-F.; Sun, W.-Y. *Cryst. Growth Des.* **2009**, *9*, 2801.
(78) Liu, M.-S.; Yu, Q.-Y.; Cai, Y.-P.; Su, C.-Y.; Lin, X.-M.; Zhou, X.-X.; Cai, J.-W. *Cryst. Growth Des.* **2008**, *8*, 4083.
(79) Liu, H.-J.; Tao, X.-T.; Yang, J.-X.; Yan, Y.-X.; Ren, Y.; Zhao, H.-P.; Xin, Q.; Yu, W.-T.; Jiang, M.-H. *Cryst. Growth Des.* **2008**, *8*, 259.
(80) Huang, W.; Wu, D.; Zhou, P.; Yan, W.; Guo, D.; Duan, C.; Meng, Q. *Cryst. Growth Des.* **2009**, *9*, 1361.
(81) He, J.; Zhang, J.-X.; Tan, G.-P.; Yin, Y.-G.; Zhang, D.; Hu, M.-H. *Cryst. Growth Des.* **2007**, *7*, 1508.
(82) Guo, H.-D.; Guo, X.-M.; Batten, S. R.; Song, J.-F.; Song, S.-Y.; Dang, S.; Zheng, G.-L.; Tang, J.-K.; Zhang, H.-J. *Cryst. Growth Des.* **2009**, *9*, 1394.
(83) Cui, P.; Chen, Z.; Gao, D.; Zhao, B.; Shi, W.; Cheng, P. *Cryst. Growth Des.* **2010**, *10*, 4370.
(84) Tanaka, D.; Horike, S.; Kitagawa, S.; Ohba, M.; Hasegawa, M.; Ozawa, Y.; Toriumi, K. *Chem. Commun.* **2007**, 3142.
(85) Chandler, B. D.; Yu, J. O.; Cramb, D. T.; Shimizu, G. K. H. *Chem. Mater.* **2007**, *19*, 4467.
(86) Chang, Z.; Zhang, A.-S.; Hu, T.-L.; Bu, X.-H. *Cryst. Growth Des.* **2009**, *9*, 4840.
(87) Zhang, L.-P.; Ma, J.-F.; Yang, J.; Pang, Y.-Y.; Ma, J.-C. *Inorg. Chem.* **2010**, *49*, 1535.
(88) Wei, G.; Shen, Y.-F.; Li, Y.-R.; Huang, X.-C. *Inorg. Chem.* **2010**, *49*, 9191.
(89) Wang, S.-N.; Yang, Y.; Bai, J.; Li, Y.-Z.; Scheer, M.; Pan, Y.; You, X.-Z. *Chem. Commun.* **2007**, 4416.
(90) Lin, Z. J.; Xu, B.; Liu, T. F.; Cao, M. N.; Lu, J. A.; Cao, R. *Eur. J. Inorg. Chem.* **2010**, 3842.
(91) Zucchi, G. l.; Maury, O.; Thuéry, P.; Ephritikhine, M. *Inorg. Chem.* **2008**, *47*, 10398.
(92) Shestopalov, M. A.; Cordier, S. p.; Hernandez, O.; Molard, Y.; Perrin, C.; Perrin, A.; Fedorov, V. E.; Mironov, Y. V. *Inorg. Chem.* **2009**, *48*, 1482.
(93) Hou, L.; Lin, Y.-Y.; Chen, X.-M. *Inorg. Chem.* **2008**, *47*, 1346.
(94) Eliseeva, S. V.; Pleshkov, D. N.; Lyssenko, K. A.; Lepnev, L. S.; Bünzli, J.-C. G.; Kuzmina, N. P. *Inorg. Chem.* **2010**, *49*, 9300.
(95) Rodríguez-Diéguez, A.; Salinas-Castillo, A.; Sironi, A.; Seco, J. M.; Colacio, E. *CrystEngComm* **2010**, *12*, 1876.
(96) Li, X.; Wang, X.-W.; Zhang, Y.-H. *Inorg. Chem. Commun.* **2008**, *11*, 832.
(97) de Lill, D. T.; de Bettencourt-Dias, A.; Cahill, C. L. *Inorg. Chem.* **2007**, *46*, 3960.
(98) Lin, Z.-J.; Xu, B.; Liu, T.-F.; Cao, M.-N.; Lü, J.; Cao, R. *Eur. J. Inorg. Chem.* **2010**, *2010*, 3842.
(99) Prasad, T. K.; Rajasekharan, M. V. *Inorg. Chem.* **2009**, *48*, 11543.
(100) Sun, C.-Y.; Zheng, X.-J.; Chen, X.-B.; Li, L.-C.; Jin, L.-P. *Inorg. Chim. Acta* **2009**, *362*, 325.
(101) Müller, M.; Devaux, A.; Yang, C.-H.; De Cola, L.; Fischer, R. A. *Photochem. Photobiol. Sci.* **2010**, *9*, 846.
(102) Liu, J.-Q.; Jia, Z.-B.; Wang, Y.-Y. *J. Mol. Struct.* **2011**, *987*, 126.
(103) Yuan, W.; Li, H.; Guo, Z.; Cao, R. *Inorg. Chem. Commun.* **2011**, *14*, 366.
(104) Sun, Y.-G.; Yu, W.; Wang, L.; Rong, S.-T.; Wu, Y.-L.; Ding, F.; Zhang, W.-Z.; Gao, E.-J. *Inorg. Chem. Commun.* **2010**, *13*, 479.
(105) Peng, G.; Qiu, Y.-C.; Liu, Z.-H.; Li, Y.-H.; Liu, B.; Deng, H. *Inorg. Chem. Commun.* **2008**, *11*, 1409.
(106) Lill, D. T. d.; Tareila, A. M.; Cahill, C. L. *Inorg. Chem. Commun.* **2009**, *12*, 191.
(107) Liao, J.-H.; Tsai, C.-S.; Lin, T.-K. *Inorg. Chem. Commun.* **2010**, *13*, 286.
(108) Bai, Y.-Y.; Huang, Y.; Yan, B.; Song, Y.-S.; Weng, L.-H. *Inorg. Chem. Commun.* **2008**, *11*, 1030.
(109) Pham, B. T. N.; Lund, L. M.; Song, D. *Inorg. Chem.* **2008**, *47*, 6329.
(110) Lin, Y.-W.; Jian, B.-R.; Huang, S.-C.; Huang, C.-H.; Hsu, K.-F. *Inorg. Chem.* **2010**, *49*, 2316.
(111) Kerbellec, N.; Kustaryono, D.; Haquin, V.; Etienne, M.; Daiguebonne, C.; Guillou, O. *Inorg. Chem.* **2009**, *48*, 2837.
(112) Rocha, J. o.; Almeida Paz, F. A.; Shi, F.-N.; Ferreira, R. A. S.; Trindade, T.; Carlos, L. s. D. *Eur. J. Inorg. Chem.* **2009**, *2009*, 4931.
(113) Liu, W.-T.; Ou, Y.-C.; Xie, Y.-L.; Lin, Z.; Tong, M.-L. *Eur. J. Inorg. Chem.* **2009**, *2009*, 4213.
(114) Jiang, H.; Ma, J.-F.; Zhang, W.-L.; Liu, Y.-Y.; Yang, J.; Ping, G.-J.; Su, Z.-M. *Eur. J. Inorg. Chem.* **2008**, *2008*, 745.
(115) Chen, X.-L.; Gou, L.; Hu, H.-M.; Fu, F.; Han, Z.-X.; Shu, H.-M.; Yang, M.-L.; Xue, G.-L.; Du, C.-Q. *Eur. J. Inorg. Chem.* **2008**, *2008*, 239.
(116) Chen, F.; Wu, M.-F.; Liu, G.-N.; Wang, M.-S.; Zheng, F.-K.; Yang, C.; Xu, Z.-N.; Liu, Z.-F.; Guo, G.-C.; Huang, J.-S. *Eur. J. Inorg. Chem.* **2010**, *2010*, 4982.
(117) Yang, X.; Jones, R. A.; Rivers, J. H.; Wong, W.-K. *Dalton Trans.* **2009**, 10505.
(118) Rueff, J.-M.; Barrier, N.; Boudin, S.; Dorcet, V.; Caignaert, V.; Boullay, P.; Hix, G. B.; Jaffrès, P.-A. *Dalton Trans.* **2009**, 10614.
(119) Liu, H.-C.; Chen, I. H.; Huang, A.; Huang, S.-C.; Hsu, K.-F. *Dalton Trans.* **2009**, 3447.
(120) Xiong, S.; Wang, S.; Tang, X.; Wang, Z. *CrystEngComm* **2011**, *13*, 1646.
(121) Saha, R.; Biswas, S.; Mostafa, G. *CrystEngComm* **2011**, *13*, 1018.
(122) Liu, W.; Li, Z.; Wang, N.; Li, X.; Wei, Z.; Yue, S.; Liu, Y. *CrystEngComm* **2011**, *13*, 138.
(123) Chen, M.-S.; Su, Z.; Chen, M.; Chen, S.-S.; Li, Y.-Z.; Sun, W.-Y. *CrystEngComm* **2010**, *12*, 3267.
(124) Zhang, J.-P.; Qi, X.-L.; Liu, Z.-J.; Zhu, A.-X.; Chen, Y.; Wang, J.; Chen, X.-M. *Cryst. Growth Des.* **2011**, *11*, 796.
(125) Yan, L.; Yue, Q.; Jia, Q.-X.; Lemercier, G.; Gao, E.-Q. *Cryst. Growth Des.* **2009**, *9*, 2984.
(126) Xue, M.; Zhu, G.; Li, Y.; Zhao, X.; Jin, Z.; Kang, E.; Qiu, S. *Cryst. Growth Des.* **2008**, *8*, 2478.
(127) Wen, L.-L.; Wang, F.; Feng, J.; Lv, K.-L.; Wang, C.-G.; Li, D.-F. *Cryst. Growth Des.* **2009**, *9*, 3581.
(128) Kustaryono, D.; Kerbellec, N.; Calvez, G.; Freslon, S. p.; Daiguebonne, C.; Guillou, O. *Cryst. Growth Des.* **2010**, *10*, 775.
(129) Wang, P.; Ma, J.-P.; Dong, Y.-B. *Chem.-Eur. J.* **2009**, *15*, 10432.
(130) Braga, D.; Maini, L.; Mazzeo, P. P.; Ventura, B. *Chem.-Eur. J.* **2010**, *16*, 1553.
(131) Feng, P. L.; Perry Iv, J. J.; Nikodemski, S.; Jacobs, B. W.; Meek, S. T.; Allendorf, M. D. *J. Am. Chem. Soc.* **2010**, *132*, 15487.

(132) Li, Y.; Song, D. *CrystEngComm* **2011**, *13*, 1821.
(133) Yang, X.; Rivers, J. H.; McCarty, W. J.; Wiester, M.; Jones, R. A. *New J. Chem.* **2008**, *32*, 790.
(134) Li, X.; Xie, Z.; Lin, J.; Cao, R. *J. Solid State Chem.* **2009**, *182*, 2290.
(135) Shi, F. N.; Cunha-Silva, L.; Mafra, L.; Trindade, T.; Carlos, L. D.; Almeida Paz, F. A.; Rocha, J. *J. Am. Chem. Soc.* **2008**, *130*, 150.
(136) Chai, X.-C.; Sun, Y.-Q.; Lei, R.; Chen, Y.-P.; Zhang, S.; Cao, Y.-N.; Zhang, H.-H. *Cryst. Growth Des.* **2010**, *10*, 658.
(137) Rodrigues, M. O.; Paz, F. A. A.; Freire, R. O.; de Sá, G. F.; Galembeck, A.; Montenegro, M. C. B. S. M.; Araújo, A. N.; Alves, S. *J. Phys. Chem. B* **2009**, *113*, 12181.
(138) Yan, X.; Cai, Z.; Yi, C.; Liu, W.; Tan, M.; Tang, Y. *Inorg. Chem.* **2011**, 2346.
(139) Chandler, B. D.; Cramb, D. T.; Shimizu, G. K. H. *J. Am. Chem. Soc.* **2006**, *128*, 10403.
(140) Chelebaeva, E.; Larionova, J.; Guari, Y.; Ferreira, R. A. S.; Carlos, L. D.; Paz, F. A. A.; Trifonov, A.; Guérin, C. *Inorg. Chem.* **2009**, *48*, 5983.
(141) Fang, Z.-L.; Yu, R.-M.; He, J.-G.; Zhang, Q.-S.; Zhao, Z.-G.; Lu, C.-Z. *Inorg. Chem.* **2009**, *48*, 7691.
(142) Zhu, Q.; Sheng, T.; Fu, R.; Tan, C.; Hu, S.; Wu, X. *Chem. Commun.* **2010**, *46*, 9001.
(143) Feng, R.; Jiang, F.-L.; Chen, L.; Yan, C.-F.; Wu, M.-Y.; Hong, M.-C. *Chem. Commun.* **2009**, 5296.
(144) He, J.; Yin, Y.-G.; Wu, T.; Li, D.; Huang, X.-C. *Chem. Commun.* **2006**, 2845.
(145) Xu, X.; Zhang, X.; Liu, X.; Sun, T.; Wang, E. *Cryst. Growth Des.* **2010**, *10*, 2272.
(146) Bassett, A. P.; Van Deun, R.; Nockemann, P.; Glover, P. B.; Kariuki, B. M.; Van Hecke, K.; Van Meervelt, L.; Pikramenou, Z. *Inorg. Chem.* **2005**, *44*, 6140.
(147) Zou, J.-P.; Peng, Q.; Wen, Z.; Zeng, G.-S.; Xing, Q.-J.; Guo, G.-C. *Cryst. Growth Des.* **2010**, *10*, 2613.
(148) Ding, S.-B.; Wang, W.; Qiu, L.-G.; Yuan, Y.-P.; Peng, F.-M.; Jiang, X.; Xie, A.-J.; Shen, Y.-H.; Zhu, J.-F. *Mater. Lett.* **2011**, *65*, 1385.
(149) Kent, C. A.; Mehl, B. P.; Ma, L.; Papanikolas, J. M.; Meyer, T. J.; Lin, W. *J. Am. Chem. Soc.* **2010**, *132*, 12767.
(150) Wang, Y.; Ding, B.; Cheng, P.; Liao, D.-Z.; Yan, S.-P. *Inorg. Chem.* **2007**, *46*, 2002.
(151) Viswanathan, S.; de Bettencourt-Dias, A. *Inorg. Chem.* **2006**, *45*, 10138.
(152) Rodrigues, M. O.; da Costa Júnior, N. B.; de Simone, C. A.; Araújo, A. A. S.; Brito-Silva, A. M.; Paz, F. A. A.; de Mesquita, M. E.; Júnior, S. A.; Freire, R. O. *J. Phys. Chem. B* **2008**, *112*, 4204.
(153) McManus, G. J.; Perry; Perry, M.; Wagner, B. D.; Zaworotko, M. J. *J. Am. Chem. Soc.* **2007**, *129*, 9094.
(154) Sapchenko, S. A.; Samsonenko, D. G.; Dybtsev, D. N.; Melgunov, M. S.; Fedin, V. P. *Dalton Trans.* **2011**, *40*, 2196.
(155) Berezin, M. Y.; Achilefu, S. *Chem. Rev.* **2010**, *110*, 2641.
(156) Jayaramulu, K.; Kanoo, P.; George, S. J.; Maji, T. K. *Chem. Commun.* **2010**, *46*, 7906.
(157) Moore, E. G.; Samuel, A. P. S.; Raymond, K. N. *Acc. Chem. Res.* **2009**, *42*, 542.
(158) Escribano, P.; Julián-López, B.; Planelles-Aragó, J.; Cordoncillo, E.; Viana, B.; Sanchez, C. *J. Mater. Chem.* **2008**, *18*, 23.
(159) Eliseeva, S. V.; Bünzli, J.-C. G. *Chem. Soc. Rev.* **2010**, *39*, 189.
(160) Bünzli, J.-C. G. *Chem. Rev.* **2010**, *110*, 2729.
(161) Sabbatini, N.; Guardigli, M.; Lehn, J.-M. *Coord. Chem. Rev.* **1993**, *123*, 201.
(162) Weissman, S. I. *J. Chem. Phys.* **1942**, *10*, 214.
(163) de Lill, D. T.; Gunning, N. S.; Cahill, C. L. *Inorg. Chem.* **2005**, *44*, 258.
(164) Soares-Santos, P. C. R.; Cunha-Silva, L.; Paz, F. A. A.; Ferreira, R. A. S.; Rocha, J.; Trindade, T.; Carlos, L. D.; Nogueira, H. I. S. *Cryst. Growth Des.* **2008**, *8*, 2505.
(165) Zhu, X.; Lü, J.; Li, X.; Gao, S.; Li, G.; Xiao, F.; Cao, R. *Cryst. Growth Des.* **2008**, *8*, 1897.
(166) Mahata, P.; Ramya, K. V.; Natarajan, S. *Chem.-Eur. J.* **2008**, *14*, 5839.
(167) Xu, J.; Su, W.; Hong, M. *Cryst. Growth Des.* **2011**, *11*, 337.
(168) Wei, Y.; Yu, Y.; Wu, K. *Cryst. Growth Des.* **2008**, *8*, 2087.
(169) Li, M.-X.; Wang, H.; Liang, S.-W.; Shao, M.; He, X.; Wang, Z.-X.; Zhu, S.-R. *Cryst. Growth Des.* **2009**, *9*, 4626.
(170) An, J.; Shade, C. M.; Chengelis-Czegan, D. A.; Petoud, S. p.; Rosi, N. L. *J. Am. Chem. Soc.* **2011**, *133*, 1220.
(171) Luo, F.; Batten, S. R. *Dalton Trans.* **2010**, *39*, 4485.
(172) Fang, Q.-R.; Zhu, G.-S.; Jin, Z.; Ji, Y.-Y.; Ye, J.-W.; Xue, M.; Yang, H.; Wang, Y.; Qiu, S.-L. *Angew. Chem., Int. Ed.* **2007**, *46*, 6638.
(173) Jung, S.; Kim, Y.; Kim, S.-J.; Kwon, T.-H.; Huh, S.; Park, S. *Chem. Commun.* **2011**, *47*, 2904.
(174) Marchal, C.; Filinchuk, Y.; Imbert, D.; Bünzli, J.-C. G.; Mazzanti, M. *Inorg. Chem.* **2007**, *46*, 6242.
(175) Guo, X.; Zhu, G.; Sun, F.; Li, Z.; Zhao, X.; Li, X.; Wang, H.; Qiu, S. *Inorg. Chem.* **2006**, *45*, 2581.
(176) Yang, X.-P.; Jones, R. A.; Rivers, J. H.; Pen-jen Lai, R. *Dalton Trans.* **2007**, 3936.
(177) Feng, X.; Wang, L.-Y.; Zhao, J.-S.; Wang, J.-G.; Weng, N. S.; Liu, B.; Shi, X.-G. *CrystEngComm* **2010**, *12*, 774.
(178) Ma, S.; Wang, X.-S.; Yuan, D.; Zhou, H.-C. *Angew. Chem., Int. Ed.* **2008**, *47*, 4130.
(179) Ma, S.; Yuan, D.; Wang, X.-S.; Zhou, H.-C. *Inorg. Chem.* **2009**, *48*, 2072.
(180) Jiang, H.-L.; Tsumori, N.; Xu, Q. *Inorg. Chem.* **2010**, *49*, 10001.
(181) Luo, J.; Xu, H.; Liu, Y.; Zhao, Y.; Daemen, L. L.; Brown, C.; Timofeeva, T. V.; Ma, S.; Zhou, H.-C. *J. Am. Chem. Soc.* **2008**, *130*, 9626.
(182) Daiguebonne, C.; Kerbellec, N.; Guillou, O.; Bünzli, J.-C.; Gumy, F.; Catala, L.; Mallah, T.; Audebrand, N.; Gérault, Y.; Bernot, K.; Calvez, G. *Inorg. Chem.* **2008**, *47*, 3700.
(183) Han, Y.; Li, X.; Li, L.; Ma, C.; Shen, Z.; Song, Y.; You, X. *Inorg. Chem.* **2010**, *49*, 10781.
(184) Gándara, F.; Andrés, A. d.; Gómez-Lor, B.; Gutiérrez-Puebla, E.; Iglesias, M.; Monge, M. A.; Proserpio, D. M.; Snejko, N. *Cryst. Growth Des.* **2008**, *8*, 378.
(185) Li, C.; Lin, J. *J. Mater. Chem.* **2010**, *20*, 6831.
(186) Yang, J.; Yue, Q.; Li, G.-D.; Cao, J.-J.; Li, G.-H.; Chen, J.-S. *Inorg. Chem.* **2006**, *45*, 2857.
(187) Weng, D.; Zheng, X.; Jin, L. *Eur. J. Inorg. Chem.* **2006**, *2006*, 4184.
(188) Jiang, H.-L.; Liu, B.; Xu, Q. *Cryst. Growth Des.* **2010**, *10*, 806.
(189) Qiu, Y.; Li, Y.; Peng, G.; Cai, J.; Jin, L.; Ma, L.; Deng, H.; Zeller, M.; Batten, S. R. *Cryst. Growth Des.* **2010**, *10*, 1332.
(190) Yue, Q.; Sun, Q.; Cheng, A.-L.; Gao, E.-Q. *Cryst. Growth Des.* **2010**, *10*, 44.
(191) Liu, X.-G.; Wang, L.-Y.; Zhu, X.; Li, B.-L.; Zhang, Y. *Cryst. Growth Des.* **2009**, *9*, 3997.
(192) Su, Y.; Zang, S.; Li, Y.; Zhu, H.; Meng, Q. *Cryst. Growth Des.* **2007**, *7*, 1277.
(193) Lin, J.-D.; Cheng, J.-W.; Du, S.-W. *Cryst. Growth Des.* **2008**, *8*, 3345.
(194) Xia, J.; Zhang, Z.-j.; Shi, W.; Wei, J.-f.; Cheng, P. *Cryst. Growth Des.* **2010**, *10*, 2323.
(195) Winter, S.; Weber, E.; Eriksson, L.; CsÖregh, I. *New J. Chem.* **2006**, *30*, 1808.
(196) Liu, X.; Huang, K.-L. *Inorg. Chem.* **2009**, *48*, 8653.
(197) Zhang, T.; Ji, C.; Wang, K.; Fortin, D.; Harvey, P. D. *Inorg. Chem.* **2010**, *49*, 11069.
(198) Wu, H.-C.; Thanasekaran, P.; Tsai, C.-H.; Wu, J.-Y.; Huang, S.-M.; Wen, Y.-S.; Lu, K.-L. *Inorg. Chem.* **2006**, *45*, 295.
(199) Song, L.; Du, S.-W.; Lin, J.-D.; Zhou, H.; Li, T. *Cryst. Growth Des.* **2007**, *7*, 2268.
(200) Bai, Y.; Gao, H.; Dang, D.-B.; Guo, X.-Y.; An, B.; Shang, W.-L. *CrystEngComm* **2010**, *12*, 1422.
(201) Sun, Y.-Q.; Zhang, J.; Yang, G.-Y. *Chem. Commun.* **2006**, 4700.
(202) Gu, X.; Xue, D. *CrystEngComm* **2007**, *9*, 471.

(203) Zhao, B.; Chen, X.-Y.; Chen, Z.; Shi, W.; Cheng, P.; Yan, S.-P.; Liao, D.-Z. *Chem. Commun.* **2009**, 3113.
(204) Zhao, B.; Zhao, X. Q.; Chen, Z.; Shi, W.; Cheng, P.; Yan, S. P.; Liao, D. Z. *CrystEngComm* **2008**, *10*, 1144.
(205) Zhao, X.-Q.; Zhao, B.; Shi, W.; Cheng, P. *CrystEngComm* **2009**, *11*, 1261.
(206) Zou, J.-P.; Zhou, G.-W.; Zhang, X.; Wang, M.-S.; Lu, Y.-B.; Zhou, W.-W.; Zhang, Z.-J.; Guo, G.-C.; Huang, J.-S. *CrystEngComm* **2009**, *11*, 972.
(207) Bo, Q.-B.; Sun, G.-X.; Geng, D.-L. *Inorg. Chem.* **2010**, *49*, 561.
(208) Jin, J.; Niu, S.; Han, Q.; Chi, Y. *New J. Chem.* **2010**, *34*, 1176.
(209) Wibowo, A. C.; Vaughn, S. A.; Smith, M. D.; zur Loye, H.-C. *Inorg. Chem.* **2010**, *49*, 11001.
(210) Stylianou, K. C.; Heck, R.; Chong, S. Y.; Bacsa, J.; Jones, J. T. A.; Khimyak, Y. Z.; Bradshaw, D.; Rosseinsky, M. J. *J. Am. Chem. Soc.* **2010**, *132*, 4119.
(211) Yang, E.-C.; Li, J.; Ding, B.; Liang, Q.-Q.; Wang, X.-G.; Zhao, X.-J. *CrystEngComm* **2008**, *10*, 158.
(212) Hu, R.; Cai, H.; Luo, J. *Inorg. Chem. Commun.* **2011**, *14*, 433.
(213) Lu, W.-G.; Jiang, L.; Feng, X.-L.; Lu, T.-B. *Inorg. Chem.* **2009**, *48*, 6997.
(214) Kozlowski, H.; Janicka-Klos, A.; Brasun, J.; Gaggelli, E.; Valensin, D.; Valensin, G. *Coord. Chem. Rev.* **2009**, *253*, 2665.
(215) Que, E. L.; Domaille, D. W.; Chang, C. J. *Chem. Rev.* **2008**, *108*, 1517.
(216) Xiao, Y.; Cui, Y.; Zheng, Q.; Xiang, S.; Qian, G.; Chen, B. *Chem. Commun.* **2010**, *46*, 5503.
(217) Mahajan, R. K.; Kaur, I.; Kaur, R.; Uchida, S.; Onimaru, A.; Shinoda, S.; Tsukube, H. *Chem. Commun.* **2003**, 2238.
(218) Curiel, D.; Cowley, A.; Beer, P. D. *Chem. Commun.* **2005**, 236.
(219) Chow, C.-F.; Lam, M. H. W.; Wong, W.-Y. *Inorg. Chem.* **2004**, *43*, 8387.
(220) Xu, H.; Xiao, Y.; Rao, X.; Dou, Z.; Li, W.; Cui, Y.; Wang, Z.; Qian, G. *J. Alloys Compd.* **2011**, *509*, 2552.
(221) Qiu, Y.; Deng, H.; Mou, J.; Yang, S.; Zeller, M.; Batten, S. R.; Wu, H.; Li, J. *Chem. Commun.* **2009**, 5415.
(222) Lee, E. Y.; Jang, S. Y.; Suh, M. P. *J. Am. Chem. Soc.* **2005**, *127*, 6374.
(223) Bai, Y.; He, G.-J.; Zhao, Y.-G.; Duan, C.-Y.; Dang, D.-B.; Meng, Q.-J. *Chem. Commun.* **2006**, 1530.
(224) Guo, Z.; Xu, H.; Su, S.; Cai, J.; Dang, S.; Xiang, S.; Qian, G.; Zhang, H.; O'Keeffe, M.; Chen, B. *Chem. Commun.* **2011**, *47*, 5551.
(225) Ma, D.; Wang, W.; Li, Y.; Li, J.; Daiguebonne, C.; Calvez, G.; Guillou, O. *CrystEngComm* **2010**, *12*, 4372.
(226) Xiao, Y.; Wang, L.; Cui, Y.; Chen, B.; Zapata, F.; Qian, G. *J. Alloys Compd.* **2009**, *484*, 601.
(227) Zhu, W.-H.; Wang, Z.-M.; Gao, S. *Inorg. Chem.* **2007**, *46*, 1337.
(228) Zhang, Z.; Xiang, S.; Zheng, Q.; Rao, X.; Mondal, J. U.; Arman, H. D.; Qian, G.; Chen, B. *Cryst. Growth Des.* **2010**, *10*, 2372.
(229) Zhang, Z.; Xiang, S.; Rao, X.; Zheng, Q.; Fronczek, F. R.; Qian, G.; Chen, B. *Chem. Commun.* **2010**, *46*, 7205.
(230) Katz, M. J.; Ramnial, T.; Yu, H.-Z.; Leznoff, D. B. *J. Am. Chem. Soc.* **2008**, *130*, 10662.
(231) Habibagahi, A.; Mébarki, Y.; Sultan, Y.; Yap, G. P. A.; Crutchley, R. J. *ACS Appl. Mater. Interfaces* **2009**, *1*, 1785.
(232) Xie, Z.; Ma, L.; deKrafft, K. E.; Jin, A.; Lin, W. *J. Am. Chem. Soc.* **2010**, *132*, 922.
(233) Lan, A.; Li, K.; Wu, H.; Olson, D. H.; Emge, T. J.; Ki, W.; Hong, M.; Li, J. *Angew. Chem., Int. Ed.* **2009**, *121*, 2370.
(234) Zhang, C.; Che, Y.; Zhang, Z.; Yang, X.; Zang, L. *Chem. Commun.* **2011**, *47*, 2336.
(235) Harbuzaru, B. V.; Corma, A.; Rey, F.; Jordá, J. L.; Ananias, D.; Carlos, L. D.; Rocha, J. *Angew. Chem., Int. Ed.* **2009**, *48*, 6476.
(236) Doty, F. P.; Bauer, C. A.; Skulan, A. J.; Grant, P. G.; Allendorf, M. D. *Adv. Mater.* **2009**, *21*, 95.
(237) Park, Y. K.; Choi, S. B.; Kim, H.; Kim, K.; Won, B.-H.; Choi, K.; Choi, J.-S.; Ahn, W.-S.; Won, N.; Kim, S.; Jung, D. H.; Choi, S.-H.; Kim, G.-H.; Cha, S.-S.; Jhon, Y. H.; Yang, J. K.; Kim, J. *Angew. Chem., Int. Ed.* **2007**, *46*, 8230.
(238) D'Andrade, B. W.; Forrest, S. R. *Adv. Mater.* **2004**, *16*, 1585.
(239) Guo, H.; Zhu, Y.; Qiu, S.; Lercher, J. A.; Zhang, H. *Adv. Mater.* **2010**, *22*, 4190.
(240) Liu, K.; You, H.; Zheng, Y.; Jia, G.; Song, Y.; Huang, Y.; Yang, M.; Jia, J.; Guo, N.; Zhang, H. *J. Mater. Chem.* **2010**, *20*, 3272.
(241) Jiang, Y.-Y.; Ren, S.-K.; Ma, J.-P.; Liu, Q.-K.; Dong, Y.-B. *Chem.-Eur. J.* **2009**, *15*, 10742.
(242) Wang, P.; Ma, J.-P.; Dong, Y.-B.; Huang, R.-Q. *J. Am. Chem. Soc.* **2007**, *129*, 10620.
(243) Huang, Y.-Q.; Ding, B.; Song, H.-B.; Zhao, B.; Ren, P.; Cheng, P.; Wang, H.-G.; Liao, D.-Z.; Yan, S.-P. *Chem. Commun.* **2006**, 4906.
(244) Fu, R.; Hu, S.; Wu, X. *Dalton Trans.* **2009**, 9440.
(245) Wang, M.-S.; Guo, S.-P.; Li, Y.; Cai, L.-Z.; Zou, J.-P.; Xu, G.; Zhou, W.-W.; Zheng, F.-K.; Guo, G.-C. *J. Am. Chem. Soc.* **2009**, *131*, 13572.
(246) Kim, J. H.; Holloway, P. H. *Adv. Mater.* **2005**, *17*, 91.
(247) Zhang, J.; Shade, C. M.; Chengelis, D. A.; Petoud, S. *J. Am. Chem. Soc.* **2007**, *129*, 14834.
(248) Lu, X. Q.; Feng, W. X.; Hui, Y. N.; Wei, T.; Song, J. R.; Zhao, S. S.; Wong, W. Y.; Wong, W. K.; Jones, R. A. *Eur. J. Inorg. Chem.* **2010**, 2714.
(249) Cui, X. X.; She, J. B.; Gao, C.; Cui, K.; Hou, C. Q.; Wei, W.; Peng, B. *Chem. Phys. Lett.* **2010**, *494*, 60.
(250) Cheng, C. H.; Wang, J.; Du, Z. J.; Shi, S. H.; Fan, Z. Q.; Geng, D. F.; Shen, R. S.; Luo, Y. M.; Du, G. T. *J. Lumin.* **2010**, *130*, 2293.
(251) Li, X. L.; Zhang, K. J.; Li, J. J.; Cheng, X. X.; Chen, Z. N. *Eur. J. Inorg. Chem.* **2010**, 3449.
(252) Sun, L. N.; Yu, J. B.; Zheng, G. L.; Zhang, H. J.; Meng, Q. G.; Peng, C. Y.; Fu, L. S.; Liu, F. Y.; Yu, Y. N. *Eur. J. Inorg. Chem.* **2006**, 3962.
(253) Khalil, G. E.; Thompson, E. K.; Gouterman, M.; Callis, J. B.; Dalton, L. R.; Turro, N. J.; Jockusch, S. *Chem. Phys. Lett.* **2007**, *435*, 45.
(254) Jin, J.; Niu, S. Y.; Han, Q.; Chi, Y. X. *New J. Chem.* **2010**, *34*, 1176.
(255) Bi, W. Y.; Wei, T.; Lu, X. Q.; Hui, Y. I.; Song, J. R.; Zhao, S. S.; Wong, W. K.; Jones, R. A. *New J. Chem.* **2009**, *33*, 2326.
(256) Sun, L. N.; Zhang, H. J.; Yu, J. B.; Yu, S. Y.; Peng, C. Y.; Dang, S.; Guo, X. M.; Feng, J. *Langmuir* **2008**, *24*, 5500.
(257) Dang, S.; Sun, L. N.; Zhang, H. J.; Guo, X. M.; Li, Z. F.; Feng, J.; Guo, H. D.; Guo, Z. Y. *J. Phys. Chem. C* **2008**, *112*, 13240.
(258) Pellegatti, L.; Zhang, J.; Drahos, B.; Villette, S.; Suzenet, F.; Guillaumet, G.; Petoud, S.; Toth, E. *Chem. Commun.* **2008**, 6591.
(259) Nonat, A. M.; Allain, C.; Faulkner, S.; Gunnlaugsson, T. *Inorg. Chem.* **2010**, *49*, 8449.
(260) Feng, J.; Zhang, H. J.; Song, S. Y.; Li, Z. F.; Sun, L. N.; Xing, Y.; Guo, X. M. *J. Lumin.* **2008**, *128*, 1957.
(261) Glover, P. B.; Bassett, A. P.; Nockemann, P.; Kariuki, B. M.; Van Deun, R.; Pikramenou, Z. *Chem.-Eur. J.* **2007**, *13*, 6308.
(262) Sun, L. N.; Yu, J. B.; Zhang, H. J.; Meng, Q. G.; Ma, E.; Peng, C. Y.; Yang, K. Y. *Microporous Mesoporous Mater.* **2007**, *98*, 156.
(263) Li, H. Y.; Wu, J.; Huang, W.; Zhou, Y. H.; Li, H. R.; Zheng, Y. X.; Zuo, J. L. *J. Photochem. Photobiol., A* **2009**, *208*, 110.
(264) Bünzli, J. C. G.; Eliseeva, S. V. *J. Rare Earths* **2010**, *28*, 824.
(265) Tallec, G.; Imbert, D.; Fries, P. H.; Mazzanti, M. *Dalton Trans.* **2010**, *39*, 9490.
(266) Guo, X.; Zhu, G.; Fang, Q.; Xue, M.; Tian, G.; Sun, J.; Li, X.; Qiu, S. *Inorg. Chem.* **2005**, *44*, 3850.
(267) White, K. A.; Chengelis, D. A.; Zeller, M.; Geib, S. J.; Szakos, J.; Petoud, S.; Rosi, N. L. *Chem. Commun.* **2009**, 4506.
(268) Chen, B.; Yang, Y.; Zapata, F.; Qian, G.; Luo, Y.; Zhang, J.; Lobkovsky, E. B. *Inorg. Chem.* **2006**, *45*, 8882.
(269) White, K. A.; Chengelis, D. A.; Gogick, K. A.; Stehman, J.; Rosi, N. L.; Petoud, S. *J. Am. Chem. Soc.* **2009**, *131*, 18069.
(270) Xamena, F.; Corma, A.; Garcia, H. *J. Phys. Chem. C* **2007**, *111*, 80.
(271) Rowe, M. D.; Thamm, D. H.; Kraft, S. L.; Boyes, S. G. *Biomacromolecules* **2009**, *10*, 983.

(272) McKinlay, A. C.; Morris, R. E.; Horcajada, P.; Férey, G.; Gref, R.; Couvreur, P.; Serre, C. *Angew. Chem., Int. Ed.* **2010**, *49*, 6260.
(273) Keskin, S.; Kızılel, S. *Ind. Eng. Chem. Res.* **2011**, *50*, 1799.
(274) Taylor-Pashow, K. M. L.; Rocca, J. D.; Xie, Z.; Tran, S.; Lin, W. *J. Am. Chem. Soc.* **2009**, *131*, 14261.
(275) Zhang, P.; Steelant, W.; Kumar, M.; Scholfield, M. *J. Am. Chem. Soc.* **2007**, *129*, 4526.
(276) Celli, J. P.; Spring, B. Q.; Rizvi, I.; Evans, C. L.; Samkoe, K. S.; Verma, S.; Pogue, B. W.; Hasan, T. *Chem. Rev.* **2010**, *110*, 2795.